1990-12

Analysis of thick composite plates using higher order three dimensional finite elements

Alon, Yair

Monterey, California: Naval Postgraduate School

NAVAL POSTGRADUATE SCHOOL
Monterey, California

THESIS

STATIC ANALYSIS OF THICK COMPOSITE PLATES USING HIGHER ORDER THREE DIMENSIONAL FINITE ELEMENTS

BY

YAIR ALON

December 1990

Thesis Advisor: Prof. Ramesh Kolar

Unclassified
SECURITY CLASSIFICATION OF THIS PAGE

REPORT DOCUMENTATION PAGE

Form Approved
OMB No 0704-0188

1a REPORT SECURITY CLASSIFICATION Unclassified	1b RESTRICTIVE MARKINGS
2a SECURITY CLASSIFICATION AUTHORITY	3 DISTRIBUTION / AVAILABILITY OF REPORT Approved for public release: distribution is unlimited
2b DECLASSIFICATION / DOWNGRADING SCHEDULE	
4 PERFORMING ORGANIZATION REPORT NUMBER(S)	5 MONITORING ORGANIZATION REPORT NUMBER(S)
6a NAME OF PERFORMING ORGANIZATION Naval Postgraduate School 6b OFFICE SYMBOL (If applicable) 31	7a NAME OF MONITORING ORGANIZATION Naval Postgraduate School
6c ADDRESS (City, State, and ZIP Code) Monterey, CA 93943-5000	7b ADDRESS (City, State, and ZIP Code) Monterey, CA 93943-5000
8a NAME OF FUNDING / SPONSORING ORGANIZATION 8b OFFICE SYMBOL (If applicable)	9 PROCUREMENT INSTRUMENT IDENTIFICATION NUMBER
8c ADDRESS (City, State, and ZIP Code)	10 SOURCE OF FUNDING NUMBERS PROGRAM ELEMENT NO / PROJECT NO / TASK NO / WORK UNIT ACCESSION NO

11 TITLE (Include Security Classification)
STATIC ANALYSIS OF THICK COMPOSITE PLATES USING HIGHER ORDER THREE DIMENSIONAL FINITE ELEMENTS

12 PERSONAL AUTHOR(S)
Yair Alon

13a TYPE OF REPORT	13b TIME COVERED	14 DATE OF REPORT (Year, Month, Day)	15 PAGE COUNT
Engineers/thesis	FROM _____ TO _____	1990, December	100

16 SUPPLEMENTARY NOTATION The views expressed in this thesis are those of the author and do not reflect the official policy or position of the Department of Defense or the U.S. Government.

17 COSATI CODES			18 SUBJECT TERMS (Continue on reverse if necessary and identify by block number)
FIELD	GROUP	SUB-GROUP	Finite Element, nonlinear analysis, plate bending thick plates, laminated composites, buckling, constant arc length three dimensional element.

19 ABSTRACT (Continue on reverse if necessary and identify by block number)

A triquadratic isoparametric sold element is developed to study the behavior of thick isotropic and laminated composite plates. The element is a 27 noded Lagrangian element based on three dimensional elasticity. Material characterisics are accounted by either using laminate plate theory or three dimensional anisotropic theory. Element matrices for nonlinear stability analysis are derived based on total Lagrangian formulation.
Results are presented to compare with analytical solutions to validate the elements behavior. The effects of various integration schemes on the element performance are presented. Convergence studies for laminated composits for different fiber orientations are provided to illustrate application An analysis for thin plated is carried out and results for thick plates are compared with available higher order plate theories. One row of elements in the thickness directions gives satisfactory results for thick laminates.

20 DISTRIBUTION / AVAILABILITY OF ABSTRACT	21 ABSTRACT SECURITY CLASSIFICATION	
☒ UNCLASSIFIED/UNLIMITED ☐ SAME AS RPT ☐ DTIC USERS	UNCLASSIFIED	
22a NAME OF RESPONSIBLE INDIVIDUAL Prof. Ramesh Kolar	22b TELEPHONE (Include Area Code) x2936	22c OFFICE SYMBOL AA/Kj

DD Form 1473, JUN 86 *Previous editions are obsolete*
S/N 0102-LF-014-6603

SECURITY CLASSIFICATION OF THIS PAGE
Unclassified

Approved for public release; distribution is unlimited

Analysis of Thick Composite Plates Using Higher Order Three Dimensional Finite Elements

by

Alon Yair
Captain, Israeli Air Force
B.S.C., Israel Technion Institute of Technology, 1983

Submitted in partial fulfillment of the
requirements for the degree of

MASTER OF SCIENCE IN
AERONAUTICAL ENGINEERING
and
AERONAUTICS AND ASTRONAUTICS ENGINEERS DEGREE

from the

NAVAL POSTGRADUATE SCHOOL

December 1990

Author: [redacted]

Approved by: [redacted]
Ramesh Kolar, Thesis Advisor

[redacted]
G. H. Lindsey, Second Reader

[redacted]
E. Roberts Wood
Department of Aeronautics and Astronautics

[redacted]
Gordon E. Schacher
Dean of Faculty and Graduate Studies

ABSTRACT

A triquadratic isoparametric solid element is developed to study the behavior of thick isotropic and laminated composite plates. The element is a 27 noded Lagrangian element based on three dimensional elasticity. Material characteristics are accounted by either using laminate plate theory or three-dimensional anisotropic theory. Element matrices for nonlinear stability analyses are derived based on total Lagrangian formulation.

Results are presented to compare with analytical solutions to validate the elements behavior. The effects of various integration schemes on the element performance are presented. Convergence studies for laminated composites for different fiber orientations are provided to illustrate applications. An analysis of thin plates is carried out and results for thick plates are compared with available higher order plate theories. One row of elements in the thickness directions gives satisfactory results for thick laminates.

TABLE OF CONTENTS

LIST OF TABLES

LIST OF FIGURES

I. INTRODUCTION

A. OVERVIEW

The finite element method provides a general tool to solve problems of continua such as heat conduction and fluid flow, but it is most widely used in structural mechanics. In structural mechanics, the methodology is applicable for static and dynamic response of structures and in predicting the elastic stability limits.

The focus of the present study is to develop tools to analyze thick laminated composite plates and validate the model by comparing with known solutions. More specifically, the objective of the present study is to develop a finite element for both linear and nonlinear analysis using three dimensional elasticity relations.

By adopting such theory for thick plates, both isotropic and composite, the solutions account for transverse shear stresses. This approach eliminates the limitations imposed by classical plate theory based on Kirchoff-Love hypothesis [Batoz, 1950] or higher order shear deformation theories [Reddy, 1984, Lo et al., 1977].

B. LITERATURE REVIEW

In this section, some literature pertaining to the analysis of thick composite plates is reviewed. The finite element method has been increasingly used as a research tool, as well as a design analysis tool, and the methodology is rapidly evolving along with the development of faster and more efficient computers. Basic concepts of the theory of finite element analysis are well documented [Cook, et al., 1989]. Yang (1987) describes various two dimensional higher order elements as well as three dimensional solid elements. Bathe (1982) discusses the general formulation of finite elements in nonlinear analysis for one, two and three dimensional elements.

based on the total Lagrangian formulation and the principle of virtual displacements. A good source for continuum formulation may be found in Malvern (1969).

Tsai and Pagano (1968) establish a notation in which composite lamina properties are invariant with respect to lamina direction. The laminate theory is well documented by Vinson (1987), where the elasticity solution for "structures composed of composite materials" is given for various cases, such as bending of thin plates. Based on laminate theory, Hoskin, et al. (1986) outline procedures involved in manufacturing composite components and presents some of its applications.

A higher order shear deformation theory of laminated composite plates was developed by Lo, et al. (1977). A higher order nonlinear theory of thick plates was suggested by Reddy (1984a, 1984b, and 1985) and presented solutions (Reddy, 1987) and compared numerical results to Pagano's (1969) elasticity solution for the case of cylindrical bending. Other elasticity solutions are given by Timoshenko (1951 and 1959) and Eisley (1989) who discusses the elasticity solutions. The Heterosis finite element was suggested by Hughes, et al. (1978) for thick and thin plate bending problems. The effect of reduced integration in isoparametric finite elements was presented by Zienkiewicz, et al. (1971).

In recent years, much work is concentrated on the analysis of buckling and post-buckling response of laminated plates and shells using nonlinear analysis. Ramm (1982) applies degenerate finite elements to solve buckling of thin shells. Arnold, et al. (1983) presents a theoretical analysis procedure for prediction of buckling and post-buckling in laminated composite plates and compares the results to experimental results. A combined numerical and experimental study of the post-buckling behavior of composite panel is performed by Natsiavas, et al. (1987). Gujbir et al. (1989) use an eight noded biquadratic element to study the effects of transverse shear on the stability of laminated plates. Some solution algorithms for nonlinear

analysis of structures by adapting modified Newton-Raphson and arc-length methods are given by Kolar et al (1985) and Ford et al (1987). In the literature reviewed, there appears to be no discussion on the higher-order solid element for the analysis of thick laminated plates.

This research addresses the problem of using a tri-quadratic displacement field based finite element based on three-dimensional elasticity equations. A total Lagrangian formulation is used to derive relevant element nonlinear matrices, and numerical examples are included to validate the linear portion of the development.

Analysis of typical examples include slender bars under traction and bending loads, thin and thick plates under bending loads and effects of various integration schemes.

C. THESIS OUTLINE

This section provides an overview of various chapters of the thesis. The total Lagrangian formulation for analyzing structures composed of three-dimensional elements is presented in Chapter II. Element matrices are derived for both linear and nonlinear static analysis using the incremental load method. The material characteristics account for both linear isotropic and anisotropic behavior. Formulas are provided to obtain work-equivalent loads for distributed body and surface forces.

Chapter III addresses aspects of computational implementation of the problem formulated in Chapter II. Test cases, example calculations and comparison with classical solutions and other high order theories are given in Chapter IV. Finally, Chapter V summarizes the results and reflects some suggestions for future work.

II. THEORETICAL FORMULATION

A. INTRODUCTION

In this chapter, using the principle of virtual displacements, the stiffness matrix will be developed for static equilibrium of triquadratic isoparametric solid elements. In the total formulation presented, both small and large displacements are permissible for linear and nonlinear structural analysis. For both cases, small strains and linearly elastic material will be assumed.

The element is developed for analysis of both isotropic and composite structures.

B. GENERAL DERIVATION OF FINITE ELEMENT EQUILIBRIUM EQUATIONS

The principle of virtual work is invoked for the general formulation of equilibrium [Bathe, 1982; Cook, 1989]. The principle of virtual work states that a body is in equilibrium, if and only if, the total virtual work done by the internal forces is equal to the total virtual work done by the external forces. That is,

$$\delta W_{int} = \delta W_{ext} \tag{2.1}$$

This principle is equivalent to the minimum total potential energy principle [$\delta \Pi_p = 0$], and holds at any given time.

Consider a three-dimensional body under arbitrary loads as shown in Figure 2.1. Using a Cartesian system, let the loads be given by

$$\{f^s\} = \left[f_x^s \; f_y^s \; f_z^s\right]^T \tag{2.2}$$

$$\{f^B\} = \left[f_x^B \; f_y^B \; f_z^B\right]^T \tag{2.3}$$

$$\{F^i\} = \left[F_x^i \; F_y^i \; F_z^i\right]^T \tag{2.4}$$

where $\{f^s\}$, $\{f^B\}$ and $\{F^i\}$ are surface tractions, body forces, and concentrated applied forces respectively.

The displacements of a finite element in the body due to external load is denoted by $\{d\}$, where

$$\{d\} = [u \; v \; w]^T \tag{2.5}$$

and the corresponding strains are given by,

$$\{\epsilon\} = [\epsilon_{xx} \; \epsilon_{yy} \; \epsilon_{zz} \; \epsilon_{yz} \; \epsilon_{xz} \; \epsilon_{xy}]^T \tag{2.6}$$

for which the corresponding stresses are,

$$\{\sigma\} = [\sigma_{xx} \; \sigma_{yy} \; \sigma_{zz} \; \sigma_{yz} \; \sigma_{xz} \; \sigma_{xy}]^T \tag{2.7}$$

The total internal virtual work for a finite element in the body is $\{\delta\epsilon\}^T\{\sigma\}dv$ and for the whole body,

$$\delta W_{int} = \int_v \{\delta\epsilon\}^T\{\sigma\}dv \tag{2.8}$$

where the virtual strains, $\{\delta\epsilon\}$, are

$$\{\delta\epsilon\} = [\delta\epsilon_{xx} \; \delta\epsilon_{yy} \; \delta\epsilon_{zz} \; \delta\epsilon_{yz} \; \delta\epsilon_{xz} \; \delta\epsilon_{xy}]^T \tag{2.9}$$

The total external virtual work is given by:

$$\delta W_{ext} = \int_v \{\delta d\}^T\{f^B\}dv + \int_s \{\delta d^s\}^T\{f^s\}ds + \{\delta d^i\}^T\{F^i\} \tag{2.10}$$

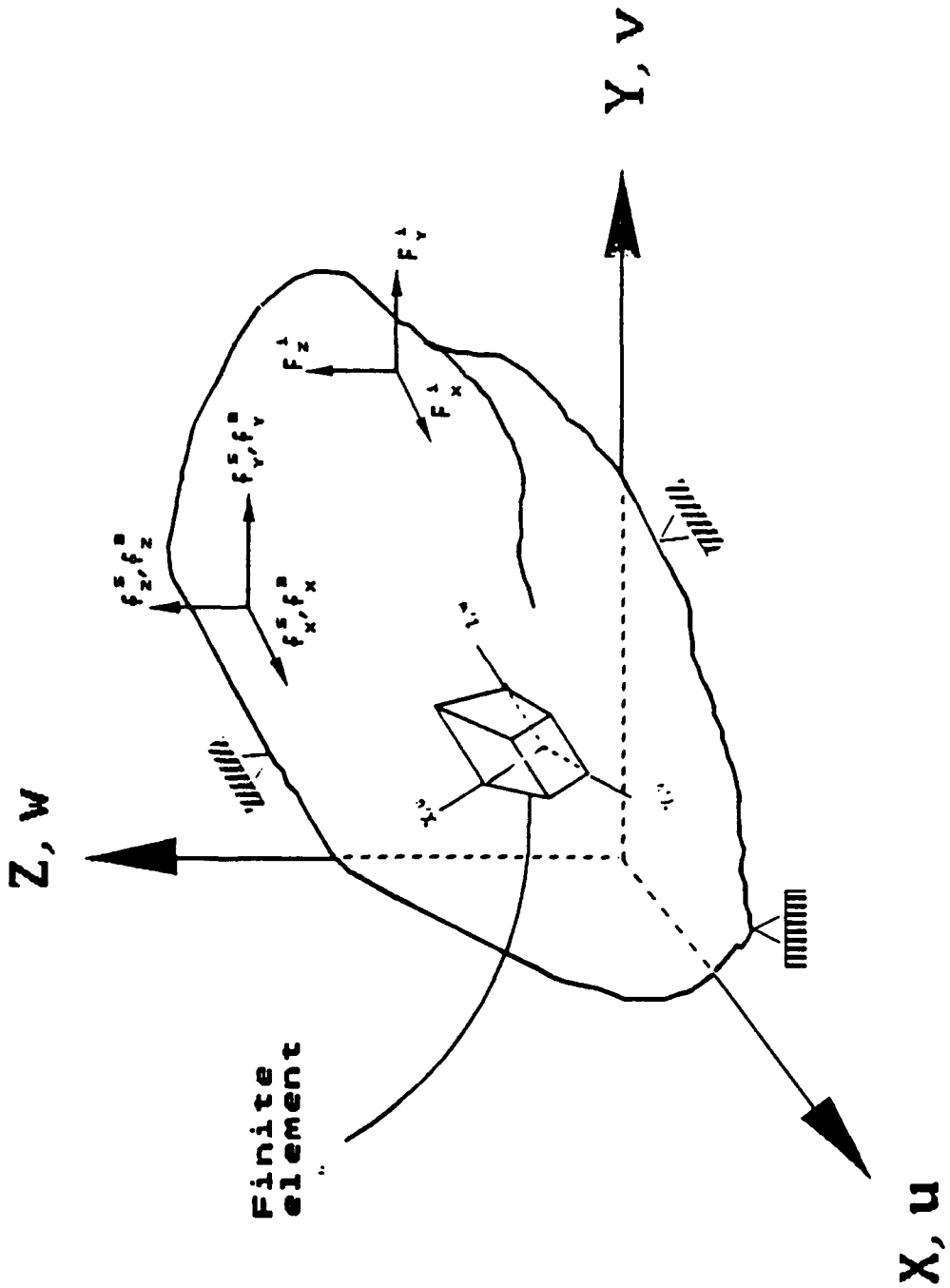

Fig. 2.1; General 3-D body

Figure 2.1: General 3-D Body

where $\{\delta d^s\}$ denotes a surface displacements and $\{\delta d^i\}$ represents point (nodal) displacements corresponding to the applied loads, and the virtual displacements $\{\delta d\}$ are

$$\{\delta d\}^T = [\delta u \ \delta v \ \delta w] \tag{2.11}$$

On substituting equations 2.8 and 2.10 into 2.1, we get,

$$\int_v \{\delta\epsilon\}^T \{\sigma\} dv = \int_v \{\delta d\}^T \{f^B\} dv + \int_s \{\delta d^s\}^T \{f^s\} ds + \{\delta d^i\}^T \{F^i\} \tag{2.12}$$

It may be noted that the principle of complementary virtual work may have been undertaken, assuming small virtual stresses with true displacements, yielding in an analogous expression for equation 2.12.

Introducing the generalized Hooke's law for material constitutive relations,

$$\{\sigma\} = [E]\{\epsilon\} + \{\sigma_o\} \tag{2.13}$$

where $\{\sigma_o\}$ denotes the element initial stresses and $[E]$ denotes the elasticity matrix of the element material.

In general, the strain-displacement relations are given by

$$\{\epsilon\} = [B]\{d\} \tag{2.14}$$

while the virtual strains are given by

$$\{\delta\epsilon\} = [B]\{\delta d\} \tag{2.15}$$

Substituting equations 2.13 and 2.15 into equation 2.12 and simplifying, we have,

$$\begin{aligned} \int_v \{\delta d\}^T \left([B]^T [E] [B]\right) \{d\} dv \ &= \ \int_v \{\delta d\}^T \{f^B\} dv + \int_s \{\delta d^s\}^T \{f^s\} ds \\ &- \ \int_v \{\delta d\}^T [B]^T \{\sigma_o\} dv + \{\delta d^i\}^T \{F^i\} \end{aligned} \tag{2.16}$$

The integrations in equation 2.16 are performed over the element volume and surface, i.e., we can evaluate every integral using the element local coordinates and

assemble tor the global system coordinates. Thus, we define the global displacement vector and the global virtual displacement vector as follows:

$$\{D\} = [u_1 v_1 w_1 \; u_2 v_2 w_2 \; \ldots u_n v_n w_n]^T \tag{2.17}$$

and

$$\{\delta D\} = [\delta u_1 \delta v_1 \delta w_1 \; \ldots \delta u_n \delta v_n \delta w_n]^T \tag{2.18}$$

where n is the total number of nodal points in the body. Now we define, for m elements,

$$[K] = \sum_{j=1}^{m} \int_v [B]^T [E] [B] \, dv \tag{2.19}$$

$$[k_j] = \int_v [B]^T [E] [B] \, dv \tag{2.20}$$

where $[K]$ and $[k_j]$ are the global and local stiffness matrices respectively. In addition, we define,

$$\{R_B\} = \sum_{j=1}^{m} \int_v [N]^T \{f^B\} dv \tag{2.21}$$

$$\{r_B\}_j = \int_v [N]^T \{f^B\} dv \tag{2.22}$$

$$\{R_s\} = \sum_{j=1}^{m} \int_s [N^s]^T \{f^s\} ds \tag{2.23}$$

$$\{r_s\}_j = \int_s [N^s]^T \{f^s\} ds \tag{2.24}$$

$$\{R_I\} = \sum_{j=1}^{m} \int_v [B]^T \{\sigma_o\} dv \tag{2.25}$$

$$\{r_I\}_j = \int_v [B]^T \{\sigma_o\} dv \tag{2.26}$$

where $\{R\}$ and $\{r\}$ denote the global and local load vectors and $[N]$ and $[N^s]$ are the displacement interpolation (shape functions) matrices for the volume and surface where traction is prescribed. Using these definitions, we obtain

$$\{\delta D\}^T [K] [D] = \{\delta D\}^T \left(\{R_B\} + \{R_s\} - \{R_I\} + \{F^i\} \right) \tag{2.27}$$

$$\{R\} = \{R_B\} + \{R_s\} - \{R_I\} + \{F^i\} \tag{2.28}$$

By invoking the principle of virtual displacements and noting that $\{\delta D\}$ is arbitrary, we get the equilibrium equations in the following form:

$$[K]\{D\} = \{R\} \tag{2.29}$$

Equation 2.29 is the basic equation for static equilibrium, which also gives the general form for nonlinear analysis with large displacements and strains.

C. INTERPOLATION SCHEME

1. Shape Functions (Displacement Interpolation Functions)

In this section, the interpolation scheme for a triquadratic isoparametric solid element will be developed.

The one-dimensional Lagrange interpolation function based on parameters is given by

$$P = \sum_{i=1}^{q} N_i P_i = N_1 P_1 + N_2 P_2 + \ldots + N_q P_q \tag{2.30}$$

where N_i, also called the shape functions, are given by

$$N_i(x) = \prod_{\substack{j=1 \\ i \neq j}}^{M} \frac{x - x_j}{x_i - x_j} \tag{2.31}$$

A triquadratic solid element is a three dimensional element in which the displacements u, v, and w are interpolated by quadratic langrangian interpolation functions with 27 nodes. Figure 2.2 depicts an element in the local non-dimensional coordinates (r, s, t).

For an isoparametric element, the geometry may be interpolated as,

$$x = \sum_{i=1}^{27} N_i x_i$$

$$y = \sum_{i=1}^{27} N_i y_i$$

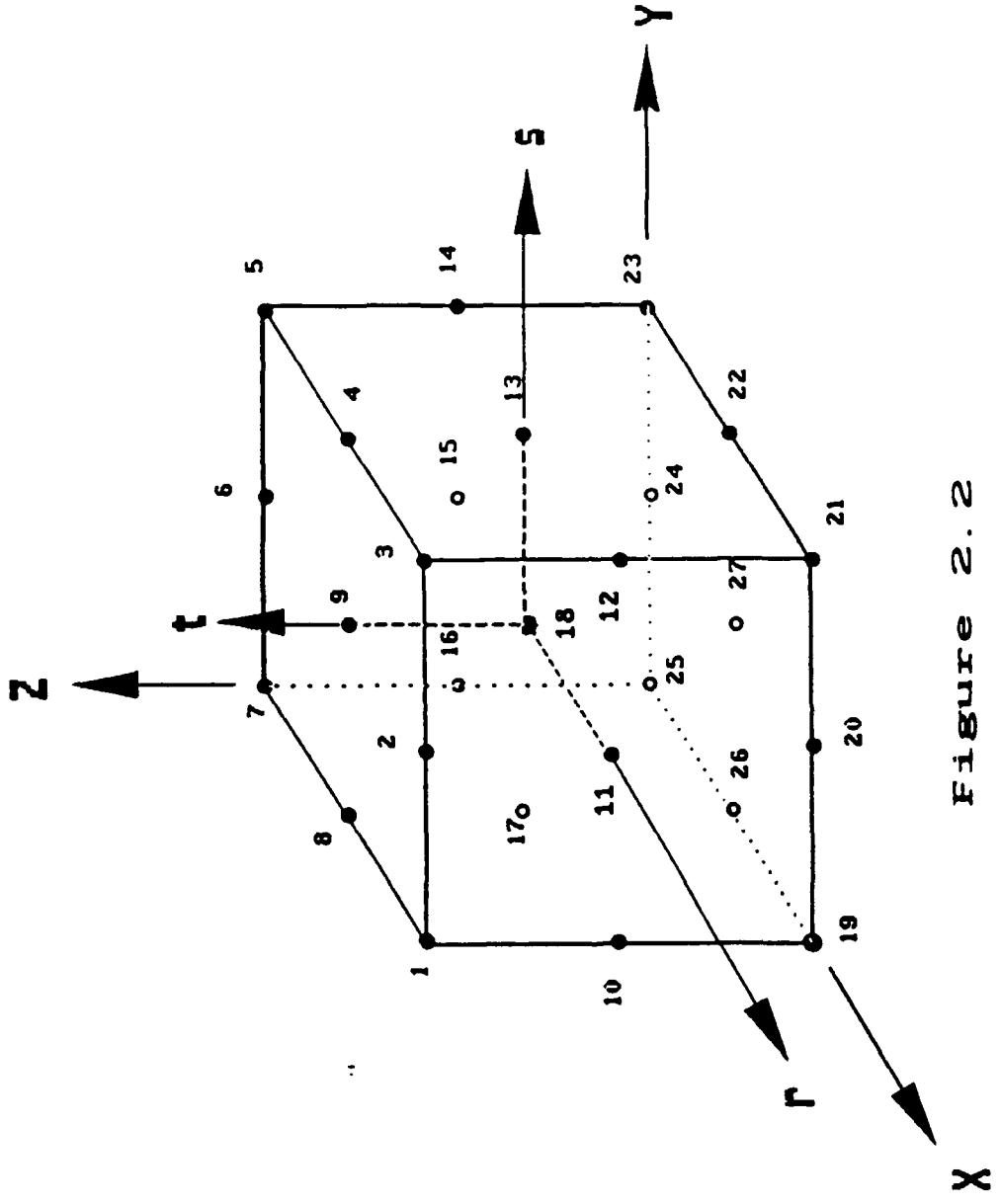

Figure 2.2: Lagrangian Solid Element – 27 nodes

$$z = \sum_{i=1}^{27} N_i z_i \tag{2.32}$$

or, in a matrix form,

$$\begin{Bmatrix} x \\ y \\ z \end{Bmatrix} = [N]\,[x_1 y_1 z_1 \ \ldots x_{27} y_{27} z_{27}]^T \tag{2.33}$$

where the shape function matrix is given by

$$[N] = \begin{bmatrix} N_1 & 0 & 0 & N_2 & 0 & 0 & \ldots & N_{27} & 0 & 0 \\ 0 & N_1 & 0 & 0 & N_2 & 0 & \ldots & 0 & N_{27} & 0 \\ 0 & 0 & N_1 & 0 & 0 & N_2 & \ldots & 0 & 0 & N_{27} \end{bmatrix} \tag{2.34}$$

The shape functions and their derivatives in local coordinates are presented in Appendix A.

2. Jacobian Transformation Matrix

To obtain equilibrium equations in the global coordinate system and construct stiffness matrices, we need the derivatives of the shape functions in cartesian system. Using the chain rule for differentiation, we obtain,

$$\begin{Bmatrix} N_{i,r} \\ N_{i,s} \\ N_{i,t} \end{Bmatrix} = \begin{bmatrix} x_{,r} & y_{,r} & z_{,r} \\ x_{,s} & y_{,s} & z_{,s} \\ x_{,t} & y_{,t} & z_{,t} \end{bmatrix} \begin{Bmatrix} N_{i,x} \\ N_{i,y} \\ N_{i,z} \end{Bmatrix} \tag{2.35}$$

where $[J]$, the Jacobian matrix is given by,

$$[J] = \begin{bmatrix} x_{,r} & y_{,r} & z_{,r} \\ x_{,s} & y_{,s} & z_{,s} \\ x_{,t} & y_{,t} & z_{,t} \end{bmatrix} \tag{2.36}$$

A comma denotes differentiation, where for example, $N_{i,r} = \frac{\partial N_i}{\delta r}$ etc. Using the shape function derivatives, the elements of the Jacobian matrix may be calculated and is given in Appendix B. The global cartesian derivatives may now be obtained as,

$$\begin{Bmatrix} N_{i,x} \\ N_{i,y} \\ N_{i,z} \end{Bmatrix} = [J]^{-1} \begin{Bmatrix} N_{i,r} \\ N_{i,s} \\ N_{i,t} \end{Bmatrix} \tag{2.37}$$

where the inverse of the Jacobian,

$$[\Gamma] = [J]^{-1} \tag{2.38}$$

is given explicitly in Appendix B.

D. STRAIN DISPLACEMENT RELATIONS - $[B]$

1. Basic Formulation

In this section, the basic formulation for nonlinear analysis of a general solid body is presented [Refs. Bathe (1982), and Malvern (1969)]. First, some definitions and notations will be introduced concerning the coordinate system, displacement, stress and strain measures and later on the linearized equilibrium equation will be developed based on section II/B.

Consider the motion of a body, or an element within, in a fixed cartesian coordinate system as shown in Figure 2.3. We have the body at time $0, t$ and $t + \Delta t$ for which the upper left superscript corresponds. The displacements at time t and $t + \Delta t$ are given as

$$^{t}u_i = {}^{t}x_i - {}^{0}x_i \tag{2.39}$$

$$^{t+\Delta t}u_i = {}^{t+\Delta t}x_i - {}^{0}x_i \tag{2.40}$$

so that the incremental displacements are

$$u_i = {}^{t+\Delta t}u_i - {}^{t}u_i \tag{2.41}$$

where,

$$\begin{aligned} u_1 &= u \quad u_2 = v \quad u_3 = w \\ x_1 &= r \quad x_2 = s \quad x_3 = t \end{aligned} \tag{2.42}$$

we use the following notation for derivatives at time, say $t + \Delta t$, with respect to coordinate at time 0 as,

$$ {}^{t+\Delta t}_{0}u_{i,j} = \frac{\partial^{t+\Delta t} u_i}{\partial^0 x_j} \tag{2.43} $$

In the present approach, we use the total Lagrangian formulation, referencing all variables to the undeformed configuration at time 0, [Ref. Bathe, 1982; Malvern, 1969]. It is assumed that at time 0 and t the equilibrium configuration is known. Basically, equation 2.12 needs to be solved corresponding to time $t + \Delta t$. Since we assume large displacements, and nonlinear constitutive relations [equation 2.14], equation 2.12 may be solved by incremental load methods [Ref. Ford & Stiemer, 1987].

On introducing the 2nd Piola-Kirchhoff stress, it may be shown that the 2nd Piola-Kirchhoff stress tensor is energentically conjugate to the Green-Lagrange strain tensor [Ref. Bathe, 1982; Malvern, 1969].

$$ \int_{{}^0v} \{\delta^{t+\Delta t}\epsilon\}^T \{{}^{t+\Delta t}S\}^0 dv = \int_{{}^{t+\Delta t}v} \{\delta e\}^T \{{}^{t+\Delta t}\sigma\}^{t+\Delta t} dv \tag{2.44} $$

where the 2nd Piola-Kirchhoff stress at time t is defined as,

$$ \{{}^t\sigma\} = \left[{}^t\chi\right]^T \{{}^tS\} \left[{}^t\chi\right] \det[\chi] \tag{2.45} $$

such that $[{}^t\chi]$, the deformation-gradient tensor is a tranformation operator from the coordinates at time 0 to time t. Note that in the equation 2.44, the right hand side represents internal virtual work at time $t + \Delta t$ over the volume at that time while the left hand side has the virtual work integrated over known configuration at the reference volume.

Assuming linear material behaviour, we may use the linear stress-strain relations (Generalized Hooke's Law) for the 2nd Piola-Kirchhoff stress tensor.

$$ \left[{}^tS\right] = [E] \left[{}^t\epsilon\right] \tag{2.46} $$

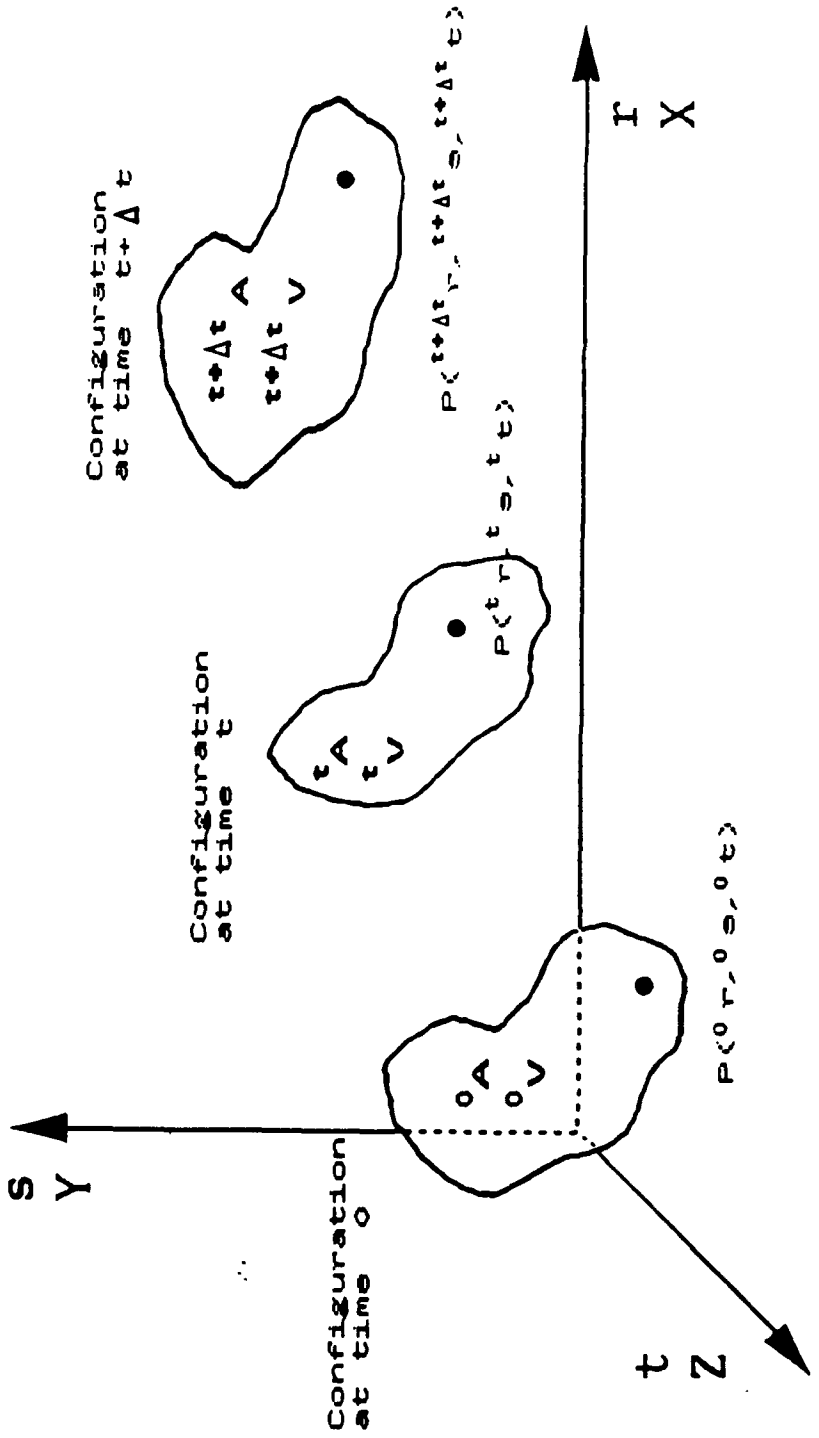

Fig. 2.3; Motion of a body in fixed cartezian coord. system

Figure 2.3: Motion of a body in a fixed Cartesian coordinate system

where the Green-Lagrange strain tensor at time t is defined as,

$$ {}^{t}\epsilon_{ij} = \frac{1}{2}\left({}^{t}u_{i,j} + {}^{t}u_{j,i} + {}^{t}u_{k,i}\,{}^{t}u_{k,j}\right) \tag{2.47} $$

with $i,\ j,\ k\ =\ 1,\ 2,$ and 3. On subs ..uting ${}^{t+\Delta t}u = {}^{t}u_i + u_i$, we obtain at time $t + \Delta t$,

$$ \begin{aligned} {}^{t+\Delta t}\epsilon_{ij} &= \frac{1}{2}\left({}^{t}u_{i,j} + {}^{t}u_{j,i} + {}^{t}u_{k,i}\,{}^{t}u_{k,j}\right) \\ &+ \frac{1}{2}\left(u_{i,j} + u_{j,i} + {}^{t}u_{k,i}\,u_{k,j} + u_{k,i}\,{}^{t}u_{k,j}\right) \\ &+ \frac{1}{2}u_{k,i}\,u_{k,j} \end{aligned} \tag{2.48} $$

which may be written as,

$$ {}^{t+\Delta t}\epsilon_{ij} = {}^{t}\epsilon_{ij} + \epsilon_{ij} \tag{2.49} $$

where, ${}^{t}\epsilon_{ij}$ is defined earlier and the incremental strain ϵ_{ij} is given by

$$ \epsilon_{ij} = e_{ij} + \eta_{ij} \tag{2.50} $$

In matrix notation,

$$ \{\epsilon\} = \{e\} + \{\eta\} \tag{2.51} $$

The linear incremental strain is identified as

$$ e_{ij} = \frac{1}{2}\left(u_{i,j} + u_{j,i} + {}^{t}u_{k,i}\,u_{k,j} + u_{k,i}\,{}^{t}u_{k,j}\right) \tag{2.52} $$

in which ${}^{t}u_{k,i}$ and ${}^{t}u_{k,j}$ are the known displacement gradients at time t. The non-linear incremental strains, then, are given by

$$ \eta_{ij} = \frac{1}{2}u_{k,i}\,u_{k,j} \tag{2.53} $$

Rewriting the equilibrium equation as stated in equation 2.12, using the total Lagrangian approach, we have,

$$ \int_{{}^{t+\Delta t}v} \{\delta e\}^{T}\{{}^{t+\Delta t}\sigma\}\,{}^{t+\Delta t}dv = {}^{t+\Delta t}R \tag{2.54} $$

where ${}^{t+\Delta t}R$, the external virtual work, is assumed to be deformation independent. Using the identity form equation 2.44, we may write the equilibrium equation in the undeformed configuration as

$$\int_{{}^0v} \{\delta^{t+\Delta t}\epsilon\}^T \{{}^{t+\Delta t}s\}^0 dv = {}^{t+\Delta t}R \tag{2.55}$$

Noting that $\{{}^t\epsilon\}$ is displacement invariant,

$$\{\delta^{t+\Delta t}\epsilon\} = \{\delta\epsilon\} \tag{2.56}$$

The 2nd Piola-Kirchhoff stress at time $t + \Delta t$ may be expressed as

$$\{{}^{t+\Delta t}s\} = \{{}^ts\} + \{s\} \tag{2.57}$$

where $\{s\}$ is the incremental 2nd Piola-Kirchhoff stress. On substituting Equations 2.56, 2.51, and 2.57 into 2.55 yields,

$$\int_{{}^0v} \{\delta\epsilon\}^T \{s\}^0 dv + \int_{{}^0v} \{\delta e\}^T \{{}^ts\}^0 dv + \int_{{}^0v} \{\delta\eta\}^T \{{}^ts\}^0 dv \tag{2.58}$$

The incremental stresses are expressed using equations 2.47 and 2.57 as

$$\{s\} = [E]\{{}^{t+\Delta t}\epsilon\} - [E]\{{}^t\epsilon\} \tag{2.59}$$

which in view of Equation 2.50 yields

$$\{s\} = [E]\{\epsilon\} \tag{2.60}$$

Referring to Equation 2.51 and neglecting the nonlinear strain contribution, we get the linearized approximation as

$$\{s\} = [E]\{e\} \tag{2.61}$$

and

$$\{\delta\epsilon\}^T = \{\delta e\}^T \tag{2.62}$$

On substituting these into Equation 2.58 and rearranging yields the linearized incremental equilibrium equation,

$$\int_{0_v} \{\delta e\}^T [E] \{e\}^0 dv + \int_{0_v} \{\delta \eta\}^T \{{}^t s\}^0 dv = {}^{t+\Delta t} R - \int_{0_v} \{\delta e\}^T \{{}^t s\}^0 dv \qquad (2.63)$$

2. General Nonlinear Discretization

The general nonlinear finite element discretization for the 27-noded element is presented based on the total Lagrangian formulation discussed in the previous section. Equation 2.52 for the linear incremental strain in cartesian form yields

$$\begin{aligned}
e_{xx} &= u_{,x} + {}^t u_{,x}\, u_{,x} + {}^t v_{,x}\, v_{,x} + {}^t w_{,x}\, w_{,x} \\
e_{yy} &= u_{,y} + {}^t u_{,y}\, u_{,y} + {}^t v_{,y}\, v_{,y} + {}^t w_{,y}\, w_{,y} \\
e_{zz} &= u_{,z} + {}^t u_{,z}\, u_{,z} + {}^t v_{,z}\, v_{,z} + {}^t w_{,z}\, w_{,z} \\
2e_{yz} &= v_{,z} + w_{,y} + {}^t u_{,y}\, u_{,z} + u_{,y}\, {}^t u_{,z} + {}^t v_{,y}\, v_{,z} + v_{,y}\, {}^t v_{,z} + {}^t w_{,y}\, w_{,z} + w_{,y}\, {}^t w_{,z} \\
2e_{xz} &= u_{,z} + w_{,x} + {}^t u_{,x}\, u_{,z} + u_{,x}\, {}^t u_{,z} + {}^t v_{,x}\, v_{,z} + v_{,x}\, {}^t v_{,z} + {}^t w_{,x}\, v_{,z} + w_{,x}\, {}^t w_{,z} \\
2e_{xy} &= u_{,y} + v_{,x} + {}^t u_{,x}\, u_{,y} + u_{,x}\, {}^t u_{,y} + {}^t v_{,x}\, v_{,y} + v_{,x}\, {}^t v_{,y} + {}^t w_{,x}\, w_{,y} + w_{,x}\, {}^t w_{,y}
\end{aligned} \qquad (2.64)$$

which in matrix form is given by

$$\{e\} = \{e_{L0}\} + \{e_{L1}\} \qquad (2.65)$$

The first term on the right hand side is displacement independent while the second term is displacement dependent with the engineering strains $\{\epsilon\}$ represented by

$$\{e\} = [e_{xx}\ e_{yy}\ e_{zz}\ 2e_{yz}\ 2e_{xz}\ 2e_{xy}]^T \qquad (2.66)$$

We define the incremental displacement gradient in the global coordinates by

$$\{U_G\} = [u_{,x}\ u_{,y}\ u_{,z}\ v_{,x}\ v_{,y}\ v_{,z}\ w_{,x}\ w_{,y}\ w_{,z}]^T \qquad (2.67)$$

Equations 2.64, 2.65, 2.66, and 2.67 result in

$$\{e_{L0}\} = [A_{L0}]\{U_G\} \tag{2.68}$$

$$\{e_{L1}\} = [A_{L1}]\{U_G\} \tag{2.69}$$

so that $[A_{L0}]$ and $[A_{L1}]$ are given by,

$$[A_{L0}] = \begin{bmatrix} 1 & 0 & 0 & 0 & 0 & 0 & 0 & 0 & 0 \\ 0 & 0 & 0 & 0 & 1 & 0 & 0 & 0 & 0 \\ 0 & 0 & 0 & 0 & 0 & 0 & 0 & 0 & 1 \\ & & & & & & & & \\ 0 & 0 & 0 & 0 & 0 & 1 & 0 & 1 & 0 \\ 0 & 0 & 1 & 0 & 0 & 0 & 1 & 0 & 0 \\ 0 & 1 & 0 & 1 & 0 & 0 & 0 & 0 & 0 \end{bmatrix} \tag{2.70}$$

$$[A_{L1}] = \begin{bmatrix} {}^{t}u_{,x} & 0 & 0 & {}^{t}v_{,x} & 0 & 0 & {}^{t}w_{,x} & 0 & 0 \\ 0 & {}^{t}u_{,y} & 0 & 0 & {}^{t}v_{,y} & 0 & 0 & {}^{t}w_{,y} & 0 \\ 0 & 0 & {}^{t}u_{,z} & 0 & 0 & {}^{t}v_{,z} & 0 & 0 & {}^{t}w_{,z} \\ & & & & & & & & \\ 0 & {}^{t}u_{,z} & {}^{t}u_{,y} & 0 & {}^{t}v_{,z} & {}^{t}v_{,y} & 0 & {}^{t}w_{,z} & {}^{t}w_{,y} \\ {}^{t}u_{,z} & 0 & {}^{t}u_{,x} & {}^{t}v_{,z} & 0 & {}^{t}v_{,x} & {}^{t}w_{,z} & 0 & {}^{t}w_{,x} \\ {}^{t}u_{,y} & {}^{t}u_{,x} & 0 & {}^{t}v_{,y} & {}^{t}v_{,x} & 0 & {}^{t}w_{,y} & {}^{t}w_{,x} & 0 \end{bmatrix} \tag{2.71}$$

It may be noted that the values of ${}^{t}u_{i,j}$ are known at the new configuration at time $t + \Delta t$. With the displacements interpolated by

$$\begin{aligned} u &= \sum_{k=1}^{27} N_k u_k \\ v &= \sum_{k=1}^{27} N_k v_k \\ w &= \sum_{k=1}^{27} N_k w_k \end{aligned} \tag{2.72}$$

the local displacement gradients are obtained from

$$\begin{aligned} u_{,r} &= \sum_{k=1}^{27} N_{k,r}\, u_k \\ u_{,s} &= \sum_{k=1}^{27} N_{k,s}\, u_k \\ u_{,t} &= \sum_{k=1}^{27} N_{k,t}\, u_k \end{aligned} \tag{2.73}$$

and similar expressions may be attributed to v and w. These gradients may be represented as

$$\begin{Bmatrix} u_{,r} \\ u_{,s} \\ u_{,t} \\ v_{,r} \\ v_{,s} \\ v_{,t} \\ w_{,r} \\ w_{,s} \\ w_{,t} \end{Bmatrix} = \begin{bmatrix} N_{1,r} & 0 & 0 & N_{2,r} & 0 & 0 & \cdots & N_{27,r} & 0 & 0 \\ N_{1,s} & 0 & 0 & N_{2,s} & 0 & 0 & & N_{27,s} & 0 & 0 \\ N_{1,t} & 0 & 0 & N_{2,t} & 0 & 0 & & N_{27,t} & 0 & 0 \\ 0 & N_{1,r} & 0 & 0 & N_{2,r} & 0 & & 0 & N_{27,r} & 0 \\ 0 & N_{1,s} & 0 & 0 & N_{2,s} & 0 & & 0 & N_{27,s} & 0 \\ 0 & N_{1,t} & 0 & 0 & N_{2,t} & 0 & & 0 & N_{27,t} & 0 \\ 0 & 0 & N_{1,r} & 0 & 0 & N_{2,r} & & 0 & 0 & N_{27,r} \\ 0 & 0 & N_{1,s} & 0 & 0 & N_{2,s} & & 0 & 0 & N_{27,s} \\ 0 & 0 & N_{1,t} & 0 & 0 & N_{2,t} & & 0 & 0 & N_{27,t} \end{bmatrix} \begin{Bmatrix} u_1 \\ v_1 \\ w_1 \\ u_2 \\ v_2 \\ w_2 \\ \cdot \\ \cdot \\ \cdot \\ u_{27} \\ v_{27} \\ w_{27} \end{Bmatrix} \tag{2.74}$$

or alternatively,

$$\{U_L\} = [DH]\{d\} \tag{2.75}$$

where the nodal displacement vector is given by,

$$\{d\} = [u_1\ v_1\ w_1\ u_2\ v_2\ \cdots\ w_{27}]^T \tag{2.76}$$

and the local incremental displacements gradient are given by

$$\{U_L\} = [u_{,r}\ u_{,s}\ u_{,t}\ v_{,r}\ v_{,s}\ v_{,t}\ w_{,r}\ w_{,s}\ w_{,t}]^T \tag{2.77}$$

As previously mentioned, in isoparametric finite elements, the same interpolation functions are used for approximating the geometry and the displacements. Using these definitions, we may transform the displacement in global and local coordinates by similar transformations used for the geometry. Furthermore, we can define arbitrarily the global and local coordinates to coincide at time 0 configuration, thereby, the transformation from local coordinates at time 0 to local coordinates at any other time, say t or $t + \Delta t$ is identical to the transformation that relates the global coordinates to the local coordinates at any configuration. In other words, we

can use the same jacobian matrix defined previously for all configurations. Writing the relation in accordance to equations 2.37 and 2.38 we have,

$$\{U_G\} = [\Gamma_3]\{u_L\} \tag{2.78}$$

such that,

$$[\Gamma_3] = \begin{bmatrix} [\Gamma] & [0] & [0] \\ [0] & [\Gamma] & [0] \\ [0] & [0] & [\Gamma] \end{bmatrix} \tag{2.79}$$

and substituting equation 2.75 into 2.78 yields,

$$\{U_G\} = [\Gamma_3][DH]\{d\} \tag{2.80}$$

The incremental strains, then, may be expressed in terms of nodal displacements, and substituting equation 2.77 in 2.68 and 2.69

$$\{e_{L0}\} = [A_{L0}][\Gamma_3][DH]\{d\} \tag{2.81}$$

$$\{e_{L1}\} = [A_{L1}][\Gamma_3][DH]\{d\} \tag{2.82}$$

The strain displacement operator may be identified as

$$[B_{L0}] = [A_{L0}][\Gamma_3][DH] \tag{2.83}$$

$$[B_{L1}] = [A_{L1}][\Gamma_3][DH] \tag{2.84}$$

such that,

$$[B_L] = [B_{L0}] + [B_{L1}] \tag{2.85}$$

and,

$$\{e\} = [B_L]\{d\} \tag{2.86}$$

It should be underscored that using only the displacement independent strains in equations 2.63 and 2.64 results in the linearized problem (same as linear small

displacement - small strain formulation) with

$$[B_{L0}] = \begin{bmatrix} N_{1,x} & 0 & 0 & N_{2,x} & 0 & 0 & \cdots & N_{27,x} & 0 & 0 \\ 0 & N_{1,y} & 0 & 0 & N_{2,y} & 0 & & 0 & N_{27,y} & 0 \\ 0 & 0 & N_{1,z} & 0 & 0 & N_{27,z} & & 0 & 0 & N_{27,y} \\ 0 & N_{1,z} & N_{1,y} & 0 & N_{2,z} & N_{2,y} & & 0 & N_{27,z} & N_{27,y} \\ N_{1,z} & 0 & N_{1,x} & N_{2,z} & 0 & N_{2,x} & & N_{27,z} & 0 & N_{27,x} \\ N_{1,y} & N_{1,x} & 0 & N_{2,y} & N_{2,x} & 0 & & N_{27,y} & N_{27,x} & 0 \end{bmatrix} \tag{2.87}$$

The displacement dependent contribution to the strain-displacement operator is given by

$$[B_{L1}] = \begin{bmatrix} {}'u_{,x} N_{1,x} & {}'v_{,x} N_{1,x} & {}'w_{,x} N_{1,x} & {}'u_{,x} N_{2,x} & \cdots & {}'w_{,x} N_{27,x} \\ {}'u_{,y} N_{1,y} & {}'v_{,y} N_{1,y} & {}'w_{,y} N_{1,y} & {}'u_{,y} N_{2,y} & & {}'w_{,y} N_{27,y} \\ {}'u_{,z} N_{1,z} & {}'v_{,z} N_{1,z} & {}'w_{,z} N_{1,z} & {}'u_{,z} N_{2,z} & & {}'w_{,z} N_{27,z} \\ {}'u_{,y} N_{1,x} + {}'u_{,x} N_{1,y} & {}'v_{,y} N_{1,x} + {}'v_{,x} N_{1,y} & {}'w_{,y} N_{1,x} + {}'w_{,x} N_{1,y} & {}'u_{,y} N_{2,x} + {}'u_{,x} N_{2,y} & & {}'w_{,y} N_{27,x} + {}'w_{,x} N_{27,y} \\ {}'u_{,z} N_{1,x} + {}'u_{,x} N_{1,z} & {}'v_{,z} N_{1,x} + {}'v_{,x} N_{1,z} & {}'w_{,z} N_{1,x} + {}'w_{,x} N_{1,z} & {}'u_{,z} N_{2,x} + {}'u_{,x} N_{2,z} & & {}'w_{,z} N_{27,x} + {}'w_{,x} N_{27,z} \\ {}'u_{,z} N_{1,y} + {}'u_{,y} N_{1,z} & {}'v_{,z} N_{1,y} + {}'v_{,y} N_{1,z} & {}'w_{,z} N_{1,y} + {}'w_{,y} N_{1,z} & {}'u_{,z} N_{2,y} + {}'u_{,y} N_{2,z} & & {}'w_{,z} N_{27,y} + {}'w_{,y} N_{27,z} \end{bmatrix}$$

(2.88)

To obtain the incremental nonlinear strain contribution, consider equation 2.53, which has the cartesian components,

$$\begin{aligned} \eta_{xx} &= \frac{1}{2}(u_{,x}^2 + v_{,x}^2 + w_{,x}^2) \\ \eta_{yy} &= \frac{1}{2}(u_{,y}^2 + v_{,y}^2 + w_{,y}^2) \\ \eta_{zz} &= \frac{1}{2}(u_{,z}^2 + v_{,z}^2 + w_{,z}^2) \\ \eta_{yz} &= \frac{1}{2}(u_{,y}u_{,z} + v_{,y}v_{,z} + w_{,y}w_{,z}) \\ \eta_{xz} &= \frac{1}{2}(u_{,x}u_{,z} + v_{,x}v_{,z} + w_{,x}w_{,z}) \\ \eta_{xy} &= \frac{1}{2}(u_{,x}u_{,y} + v_{,x}v_{,y} + w_{,x}w_{,y}) \end{aligned} \tag{2.89}$$

With the variations at time t given by,

$$
\begin{aligned}
\delta\eta_{xx} &= \delta u_{1,x}\,{}^{t}u_{,x} + \delta v_{,x}\,{}^{t}v_{,x} + \delta w_{,x}\,{}^{t}w_{,x} \\
\delta\eta_{yy} &= \delta u_{1,y}\,{}^{t}u_{,y} + \delta v_{,y}\,{}^{t}v_{,y} + \delta w_{,y}\,{}^{t}w_{,y} \\
\delta\eta_{zz} &= \delta u_{1,z}\,{}^{t}u_{,z} + \delta v_{,z}\,{}^{t}v_{,z} + \delta w_{,z}\,{}^{t}w_{,z} \\
2\delta\eta_{yz} &= \delta u_{,y}\,{}^{t}u_{,z} + {}^{t}u_{,y}\delta u_{,z} + \delta v_{,y}\,{}^{t}v_{,z} + {}^{t}v_{,y}\delta v_{,z} + \delta w_{,y}\,{}^{t}w_{,z} + {}^{t}w_{,y}\delta w_{,z} \\
2\delta\eta_{xz} &= \delta u_{,x}\,{}^{t}u_{,z} + {}^{t}u_{,x}\delta u_{,z} + \delta v_{,x}\,{}^{t}v_{,z} + {}^{t}v_{,x}\delta v_{,z} + \delta w_{,x}\,{}^{t}w_{,z} + {}^{t}w_{,x}\delta w_{,z} \\
2\delta\eta_{xy} &= \delta u_{,x}\,{}^{t}u_{,y} + {}^{t}u_{,x}\delta u_{,y} + \delta v_{,x}\,{}^{t}v_{,y} + {}^{t}v_{,x}\delta v_{,y} + \delta w_{,x}\,{}^{t}w_{,y} + {}^{t}w_{,x}\delta w_{,y} \qquad (2.90)
\end{aligned}
$$

(2.91)

It is worth noting that equations 2.90 are in exactly the same form as the displacement dependent strains $\{\epsilon_{L1}\}$ given in equations 2.64 and 2.65 with the incremental displacements derivatives replaced by their variations. Thus, we may write,

$$\{\delta\eta\} = [A_{L1}]\,\{\delta U_G\} \qquad (2.92)$$

$$\{\eta\} = [A_{L1}]\,\{U_G\} \qquad (2.93)$$

such that the nonlinear incremental strain variation vector is defined as,

$$\{\delta\eta\}^T = [\delta\eta_{xx}\ \delta\eta_{yy}\ \delta\eta_{zz}\ 2\delta\eta_{yz}\ 2\delta\eta_{xz}\ 2\delta\eta_{xy}] \qquad (2.94)$$

and $[A_{L1}]$ is as given in 2.71. Observing relation 2.80 for $\{U_G\}$, we have,

$$\{\delta U_G\} = [\Gamma_3]\,[DH]\,\{\delta d\} \qquad (2.95)$$

and substituting for the global variations into the nonlinear strains in equation 2.90, we get

$$\{\delta\eta\}^T = \{\delta d\}^T\,[DH]^T\,[\Gamma_3]^T\,[A_{L1}]^T \qquad (2.96)$$

Using the strain-displacement relations defined thus far, we formulate the linearized incremental equilibrium equation, given by 2.63 to take the general form as stated in 2.29, to give,

$$\left(\left[{}^{t}k_L\right] + \left[{}^{t}k_{nL}\right]\right)\{d\}^{(i+1)} = \{{}^{t+\Delta t}R\} - \{{}^{t+\Delta t}F\}^{(i)} \tag{2.97}$$

where $[{}^{t}k_L]$, in view of equation 2.85 is seen to be

$$\left[{}^{t}k_L\right] = \int_{{}_0v} [B_L]^T [E] [B_L]^0 \, dv \tag{2.98}$$

which is the linear stiffness matrix, and i is the iteration number. This includes the displacement dependent and independent contributions.

When small displacements are assumed, the $[{}^{t}k_L]$ reduces to standard linear stiffness matrix, given by $\int_{{}_0v}[B_{L0}]^T [E] [B_{L0}]^0 \, dv$. In what follows, the derivation of $[k_{NL}]$ is described.

The 2nd-Piola stress vector at time t is accumulated such that,

$$\{{}^{t}s\} = \{{}^{t+\Delta t}s\} + [E]\{\epsilon\} \tag{2.99}$$

Using equations 2.51, 2.85, 2.86, and 2.91, the incremental strains take the form

$$\{\epsilon\} = (2[A_{L1}] + [A_{L0}])[\Gamma_3][DH]\{d\} \tag{2.100}$$

or alternatively,

$$\{\epsilon\} = (2[B_{L1}] + [B_{L0}])\{d\} \tag{2.101}$$

Noting that equations 2.99 and 2.100 are valid at any time t, and by using equation 2.46, the 2nd Piola-Kirchhoff stress may be written as

$$\{{}^{t}s\} = [E](2[A_{L1}] + [A_{L0}])[\Gamma_3][DH]\{d\} \tag{2.102}$$

and the nonlinear part of equation 2.63 becomes, using the relations 2.95 and 2.101,

$$\begin{aligned}\int_{{}_0v} \{\delta\eta\}^T \{{}^{t}s\}^0 dv \;=\; & \int_{{}_0v} \left(\{\delta d\}^T [DH]^T [\Gamma_3]^T [A_{L1}]^T\right)[E] \\ & (2[A_{L1}] + [A_{L0}])[\Gamma_3][DH]\{d\}^0 dv\end{aligned} \tag{2.103}$$

we define the nonlinear strain contribution, $[k_{NL}]$, as

$$[k_{NL}] = \int_{0_v} [DH]^T [\Gamma_3]^T [A_{L1}]^T [E] (2[A_{L1}] + [A_{L0}]) [\Gamma_3] [DH]^0 dv \qquad (2.104)$$

It may be recognized that $[DH]$ is the strain-displacement relation given by equation 2.74 which corresponds to the linear contribution of the stiffness matrix given in equation 2.97, and the contribution of the non-linear strains results in the 2nd Piola-Kirchhoff matrix, $[s]$, as

$$[s] = [\Gamma_3]^T [A_{L1}]^T [E] (2[A_{L1}] + [A_{L0}]) [\Gamma_3] \qquad (2.105)$$

$[\Gamma_3]$ is given in equation 2.79. It may be shown that the matrix $[s]$ takes the form,

$$[s] = \begin{bmatrix} [s_1] & [0] & [0] \\ [0] & [s_1] & [0] \\ [0] & [0] & [s_1] \end{bmatrix} \qquad (2.106)$$

The expression for the second term in the right hand side of equation 2.63 is evaluated in the same manner as the linear and nonlinear parts. On using equations 2.100 and 2.101, we obtain,

$$\int_{0_v} \{\delta e\}^T \{{}^t s\}^0 dv = \int_{0_v} \{\delta d\}^T (2[B_{L1}]^T + [B_{L0}]^T) [E] (2[B_{L1}] + [B_{L0}]) \{d\}^0 dv \qquad (2.107)$$

It may be seen that by defining

$$\left\{{}^{(t+\Delta t)}F\right\} = \int_{0_v} (2[B_{L1}]^T + [B_{L0}]^T) [E] (2[B_{L1}] + [B_{L0}]) \{d\}^0 dv \qquad (2.108)$$

the expression $\{d\}^T \left\{{}^{t+\Delta t}F\right\}$ represents the work done by the external loads at time $t + \Delta t$. Noting that

$$\{\delta^{t+\Delta t}\epsilon\} = \{\delta e\} \qquad (2.109)$$

We approximate for the second term in the right hand side of equation 2.62 such that

$$\int_{0_v} \{\delta e\}^T \{{}^t s\}^0 dv \cong \int_{0_v} \{\delta^{t+\Delta t}\epsilon\}^T \{{}^{t+\Delta t}s\}^0 dv \qquad (2.110)$$

which represents the internal virtual work, so that the right hand side of the equilibrium equation 2.63 is the difference between the external and internal virtual work. On substitution of relations 2.97, 2.102, 2.103, 2.107, and 2.109 into 2.63 and applying the principle of virtual displacement as shown previously, we arrive at the incremental equilibrium equation 2.96, which may be solved by Newton-type methods. [Ford and Stieman, 1987]

E. STRESS-STRAIN RELATIONS

In this section, the stress-strain relations for a composite material, to be used in the three dimensional analysis is developed. Two approaches, one based on classical laminate theory and the other based on anisotropic material constitutive relations, are presented.

1. Classical and Higher Order Laminate Theories

Typical structures composed of composite materials are built using several number of laminae, forming a laminate. Each lamina consists of, typically, uniaxial fibers embedded in a matrix, such as epoxy-resin, forming a thin plate. Figure 2.4 shows principal material axes, labelled 1 and 2 in directions parallel to and normal to the fibers, respectively. It may be noted that in each lamina, there exists a state of plane stress, as shown in Figure 2.4.

Assuming elastic orthotropic material, (i.e., the lamina possesses a plane of elastic symmetry parallel to the x-y plane), the generalized Hooke's law may be written as

$$\begin{Bmatrix} \sigma_1 \\ \sigma_2 \\ \sigma_3 \\ \sigma_4 \\ \sigma_5 \\ \sigma_6 \end{Bmatrix} = \begin{bmatrix} Q_{11} & Q_{12} & Q_{13} & 0 & 0 & 0 \\ & Q_{22} & Q_{23} & 0 & 0 & 0 \\ & & Q_{33} & 0 & 0 & 0 \\ & & & 2Q_{44} & 0 & 0 \\ & \text{symm} & & & 2Q_{55} & 0 \\ & & & & & 2Q_{66} \end{bmatrix} \begin{Bmatrix} \epsilon_1 \\ \epsilon_2 \\ \epsilon_3 \\ \epsilon_4 \\ \epsilon_5 \\ \epsilon_6 \end{Bmatrix} \tag{2.111}$$

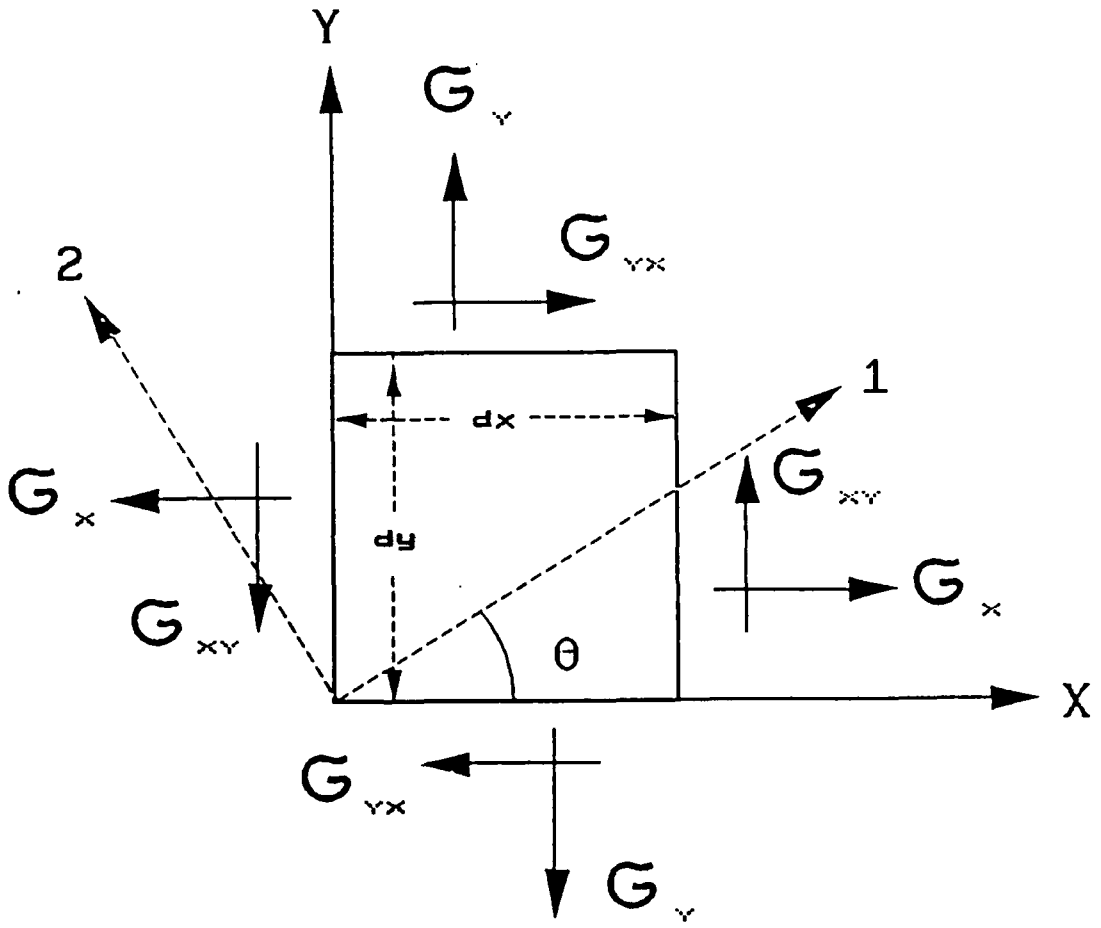

Fig. 2.4; Lamina coordinate system (2-D)

Figure 2.4: Lamina coordinate system (2-D)

where the plane-stress elastic constants are given by:

$$\begin{aligned} Q_{11} &= \frac{E_1}{1-\nu_{12}\,\nu_{21}} \\ Q_{12} &= \frac{\nu_{12}E_2}{1-\nu_{12}\,\nu_{21}} \\ Q_{22} &= Q_{33} = \frac{E_2}{1-\nu_{12}\,\nu_{21}} \\ Q_{44} &= G_{23},\ Q_{55} = G_{13},\ Q_{66} = G_{12} \\ Q_{13} &= Q_{23} = O \end{aligned} \tag{2.112}$$

The subscripts 1, 2, and 3 correspond to normal stresses or normal strains while 4, 5, and 6 correspond to shear stresses or tensorial shearing strains in yz, zx, and xy planes, respectively.

The stresses in the material coordinate axes are transformed to reference coordinate axes (x, y, z) by the following equation:

$$\begin{Bmatrix} \sigma_x \\ \sigma_y \\ \sigma_z \\ \sigma_{yz} \\ \sigma_{xz} \\ \sigma_{xy} \end{Bmatrix} = \begin{bmatrix} m^2 & n^2 & 0 & 0 & 0 & -2mn \\ n^2 & m^2 & 0 & 0 & 0 & 2mn \\ 0 & 0 & 1 & 0 & 0 & 0 \\ 0 & 0 & 0 & m & n & 0 \\ 0 & 0 & 0 & -n & m & 0 \\ mn & -mn & 0 & 0 & 0 & (m^2-n^2) \end{bmatrix} \begin{Bmatrix} \sigma_1 \\ \sigma_2 \\ \sigma_3 \\ \sigma_4 \\ \sigma_5 \\ \sigma_6 \end{Bmatrix} \tag{2.113}$$

where the direction cosines m and n are given by $m = \cos\theta$ and $n = \sin\theta$.

The strains may be transformed in a similar manner. Introducing the strain transformation, along with equation 2.110 into equation 2.112 results in

$$\begin{Bmatrix} \sigma_x \\ \sigma_y \\ \sigma_z \\ \sigma_{yz} \\ \sigma_{xz} \\ \sigma_{xy} \end{Bmatrix}_k = \begin{bmatrix} \bar{Q}_{11} & \bar{Q}_{12} & 0 & 0 & 0 & 2\bar{Q}_{16} \\ \bar{Q}_{12} & \bar{Q}_{22} & 0 & 0 & 0 & 2\bar{Q}_{26} \\ 0 & 0 & \bar{Q}_{33} & 0 & 0 & 0 \\ 0 & 0 & 0 & 2\bar{Q}_{44} & 2\bar{Q}_{45} & 0 \\ 0 & 0 & 0 & 2\bar{Q}_{45} & 2\bar{Q}_{55} & 0 \\ \bar{Q}_{16} & \bar{Q}_{26} & 0 & 0 & 0 & 2\bar{Q}_{66} \end{bmatrix} \begin{Bmatrix} \epsilon_x \\ \epsilon_y \\ \epsilon_z \\ \epsilon_{yz} \\ \epsilon_{xz} \\ \epsilon_{xy} \end{Bmatrix}_k \tag{2.114}$$

where,

$$\bar{Q}_{11} = Q_{11}m^4 + 2\left(Q_{12} + 2Q_{66}\right)m^2n^2 + Q_{22}n^4$$

$$
\begin{aligned}
\bar{Q}_{12} &= (Q_{11} + Q_{22} - 4Q_{66})\, m^2 n^2 + Q_{12}\left(m^4 + n^4\right) \\
\bar{Q}_{22} &= Q_{11} n^4 + 2\,(Q_{12} + 2Q_{66})\, m^2 n^2 + Q_{22} m^4 \\
\bar{Q}_{33} &= Q_{33} \\
\bar{Q}_{16} &= Q_{11} m^3 n - Q_{22} m n^3 - (Q_{12} + 2Q_{66})\, mn\left(m^2 - n^2\right) \\
\bar{Q}_{26} &= Q_{11} m n^3 - Q_{22} m^3 n + (Q_{12} + 2Q_{66})\, mn\left(m^2 - n^2\right) \\
\bar{Q}_{66} &= (Q_{11} + Q_{22} - 2Q_{12})\, m^2 n^2 + Q_{66}\left(m^2 - n^2\right)^2 \\
\bar{Q}_{44} &= Q_{44} m^2 + Q_{55} n^2 \\
\bar{Q}_{45} &= (Q_{55} - Q_{44})\, mn \\
\bar{Q}_{55} &= Q_{44} n^2 + Q_{55} m^2
\end{aligned}
\tag{2.115}
$$

The stress strain relations presented correspond to k^{th} lamina. Now, consider a laminate composed of N laminae for which, each lamina has a different orientation (θ), with respect to the laminate x and y axes. For linear elastic plates, the functional form of the displacement may be assumed to be

$$
\begin{aligned}
u(x,\, y,\, z) &= u_0(x,y) + z u_1(x,y) \\
v(x,\, y,\, z) &= v_0(x,y) + z v_1(x,y) \\
w(x,\, y) &= w_0(x,y)
\end{aligned}
\tag{2.116}
$$

and, the linear strains are given by,

$$
\epsilon_{ij} = \frac{1}{2}(u_{i,j} + u_{j,i}) \tag{2.117}
$$

so that,

$$
\begin{aligned}
\epsilon_{xx} &= u_{0,x} + z u_{1,x} \\
\epsilon_{yy} &= v_{0,y} + z v_{1,y} \\
\epsilon_{zz} &= 0
\end{aligned}
$$

$$\begin{aligned}
\epsilon_{yz} &= \frac{1}{2}(v_1 + w_{0,y}) \\
\epsilon_{xz} &= \frac{1}{2}(u_1 + w_{0,x}) \\
\epsilon_{xy} &= \frac{1}{2}(u_{0,y} + v_{0,x}) + \frac{z}{2}(u_{1,y} + v_{1,x})
\end{aligned} \tag{2.118}$$

where u_0, v_0 and w_0 are the midplane displacements, u_1 and v_1 are related to the rotations of the normals. It may be noted that the in-plane strains,

$$\epsilon_{x0} = u_{0,x},\ \epsilon_{y0} = v_{0,y},\ \epsilon_{xy_0} = \frac{1}{2}(u_{0,y} + v_{0,x}) \tag{2.119}$$

and the curvatures are given by

$$\kappa_x = u_{1,x},\ \kappa_y = v_{1,y},\ \kappa_{xy} = \frac{1}{2}(u_{1,y} + v_{1,x}) \tag{2.120}$$

We define stress resultants for plate/shell type structures in terms of stresses and shears (see Figure 2.5) as follows for the k^{th} layer:

$$\begin{aligned}
N_x &= \int_{-\frac{h}{2}}^{\frac{h}{2}} \sigma_x dz \\
Q_x &= \int_{-\frac{h}{2}}^{\frac{h}{2}} \sigma_{yz} dz \\
M_x &= \int_{-\frac{h}{2}}^{\frac{h}{2}} \sigma_x z dz
\end{aligned} \tag{2.121}$$

Similar expressions are applicable for N_y, N_{xy}, Q_y, M_y and M_{xy}, where h is the lamina thickness.

By summing all laminae over the laminate thickness in the following manner,

$$\begin{Bmatrix} N_x \\ N_y \\ N_{xy} \end{Bmatrix} = \sum_{k=1}^{N} \left\{ \int_{h_{k-1}}^{h_k} \left[\bar{Q}\right]_k \begin{Bmatrix} \epsilon_{x0} \\ \epsilon_{y0} \\ \epsilon_{xy0} \end{Bmatrix} dz + \int_{h_{k-1}}^{h_k} \left[\bar{Q}\right]_k \begin{Bmatrix} \kappa_x \\ \kappa_y \\ \kappa_{xy} \end{Bmatrix} z dz \right\} \tag{2.122}$$

which, in matrix form, may be written as

$$\{N\} = [A]\{\epsilon_0\} + [B]\{\kappa\} \tag{2.123}$$

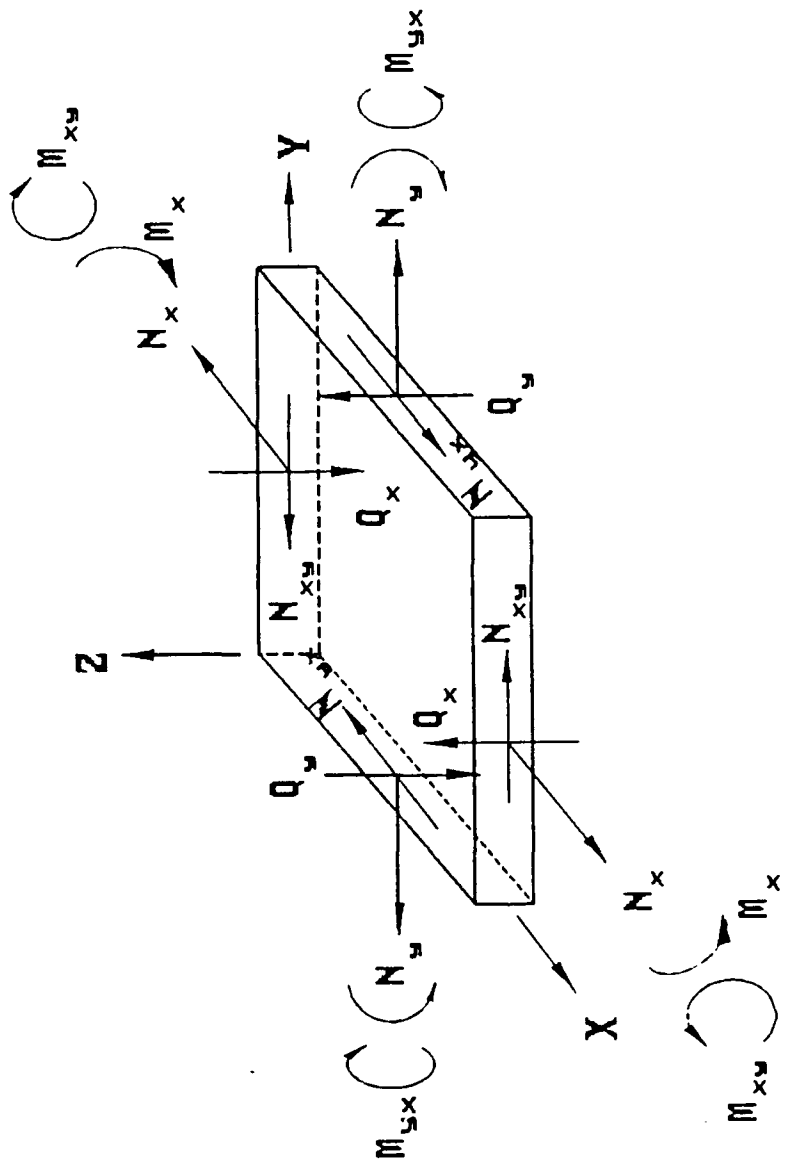

Fig. 2.5; Stress resultants and couples in a lamina

Figure 2.5: Stress resultants and couples in a lamina

where,

$$A_{ij} = \sum_{k=1}^{N} \left(\bar{Q}_{ij}\right)_k (h_k - h_{k-1})$$
$$B_{ij} = \sum_{k=1}^{N} \left(\bar{Q}_{ij}\right)_k \left(h_k^2 - h_{k-1}^2\right) \tag{2.124}$$

with $i, j = 1, 2,$ and 6 and the moment resultants are given by

$$\{M\} = [B]\{\epsilon_0\} + [D]\{\kappa\} \tag{2.125}$$

where,

$$D_{ij} = \frac{1}{3} \sum_{k=1}^{N} \left(\bar{Q}_{ij}\right)_k \left(h_k^3 - h_{k-1}^3\right) \tag{2.126}$$

with $i, j = 1, 2,$ and 6.

The displacement field, as stated in equation 2.105 is linear in the thickness direction, resulting in constant shear stresses. To get better accuracy, a higher order displacement field may be used [Reddy, 1984].

In order to account for the accurate shear distribution, shape factors are used in computing shear energies. These factors are typically obtained by equating the shear energies. The procedure is outlined for linear and cubic variation of displacement fields. The shear energy due to transverse shear stresses is given by,

$$U_s = \frac{1}{2} \int_A \int_{-\frac{h}{2}}^{\frac{h}{2}} \left(\sigma_{xz}\left(2\epsilon_{xz}\right) + \sigma_{yz}\left(2\epsilon_{yz}\right)\right) dz\, dA \tag{2.127}$$

where A is the area bounded by the lamina surface dy. On using Hooke's Law, we get

$$U_s = \frac{1}{2} \int_A \int_{-\frac{h}{2}}^{\frac{h}{2}} \left(G_{xz}\left(2\epsilon_{xz}\right)^2 + G_{yz}\left(2\epsilon_{yz}\right)^2\right) dz\, dA \tag{2.128}$$

Equating this to the linear displacement field and simplifying,

$$U_s = \left(\frac{1}{2} \int_A \left[G_{xz}\left(u_1 + w_{0,x}\right)^2 + G_{yz}\left(v_1 + w_{0,y}\right)^2\right] dA\right) h \tag{2.129}$$

Introducing a higher order displacement field yields a more realistic stress distribution, but in doing so, a shape factor is introduced to yield consistent shear energy.

Assuming a displacement field in which the displacements are expanded as cubic functions of the thickness coordinate, while the transverse displacement is assumed to be constant through the thickness, yields

$$\begin{aligned} u_{(x,y,z)} &= u_{0(x,y)} + z u_{1(x,y)} + z^2 u_{2(x,y)} + z^3 u_{3(x,y)} \\ v_{(x,y,z)} &= v_{0(x,y)} + z v_{1(x,y)} + z^2 v_{2(x,y)} + z^3 v_{3(x,y)} \\ w_{(x,y,z)} &= w_{0(x,y)} \end{aligned} \tag{2.130}$$

With u_0, v_0, and w_0 being the displacements of the midplane, the tensorial shearing strains are evaluated as,

$$\begin{aligned} 2\epsilon_{xz} &= \left[u_{1(x,y)} + 2u_{2(x,y)} z + 3u_{3(x,y)} z^3 + w_{0,x}\right] \\ 2\epsilon_{yz} &= \left[v_{1(x,y)} + 2v_{2(x,y)} z + 3u_{3(x,y)} z^3 + w_{0,y}\right] \end{aligned} \tag{2.131}$$

Using the condition that the transverse shear stresses vanish on the plate top and bottom surfaces, we have,

$$\sigma_{xz}\left(x,\, y,\, \pm\frac{h}{2}\right) = \sigma_{yz}\left(x,\, y,\, \pm\frac{h}{2}\right) = 0 \tag{2.132}$$

or,

$$\epsilon_{xz}\left(x,\, y,\, \pm\frac{h}{2}\right) = \epsilon_{yz}\left(x,\, y,\, \pm\frac{h}{2}\right) = 0 \tag{2.133}$$

Substituting relations 2.132 into 2.130, we obtain,

$$\begin{aligned} u_2 &= v_2 = 0 \\ u_3 &= -\frac{4}{3h^2}\left(w_{0,x} + u_1\right) \\ v_3 &= -\frac{4}{3h^2}\left(w_{0,y} + v_1\right) \end{aligned} \tag{2.134}$$

The displacement field then becomes

$$\begin{aligned} u &= u_0 + zu_1 - z^3\frac{4}{3h^2}(w_{0,x} + u_1) \\ v &= v_0 + zv_1 - z^3\frac{4}{3h^2}(w_{0,y} + v_1) \qquad (2.135) \\ w &= w_0 \qquad (2.136) \end{aligned}$$

and the shearing strains are given by

$$\begin{aligned} \epsilon_{xz} &= \frac{1}{2}(u_1 + w_{0,x})\left[1 - 4\left(\frac{z}{h}\right)^2\right] \\ \epsilon_{yz} &= \frac{1}{2}(v_1 + w_{0,x})\left[1 - 4\left(\frac{z}{h}\right)^2\right] \qquad (2.137) \end{aligned}$$

Yielding

$$U_s = \left(\frac{1}{2}\int_A \left[G_{xz}(u_1 + w_{0,x})^2 + G_{yz}(v_1 + w_{0,y})^2\right] dA\right)\int_{-\frac{h}{2}}^{\frac{h}{2}}\left[1 - 4\left(\frac{z}{h}\right)^2\right]^2 dz \qquad (2.138)$$

The shear energy ratio of the two displacement field is found to be $\frac{8}{15}$, so that the correction factor for constant shear stress using cubic displacements is $\frac{8}{15}$.

It is clear from the discussion that the classical plate theory stiffens the plate by not taking into account the higher order terms. If we use the higher order theory, we need to introduce a correction factor to the shearing strains of the magnitude $\sqrt{\frac{15}{8}}$. Using equation 2.113, the transverse shearing stresses for the k^{th} layer are given by

$$\begin{aligned} \sigma_{xz_k} &= 2\bar{Q}_{55_k}\epsilon_{xz} + 2\bar{Q}_{45_k}\epsilon_{yz} \\ \sigma_{yz_k} &= 2\bar{Q}_{45_k}\epsilon_{xz} + 2\bar{Q}_{44_k}\epsilon_{yz} \qquad (2.139) \end{aligned}$$

and the resultants are obtained using equation 2.122 as

$$\begin{aligned} Q_x &= 2(A_{55}\epsilon_{xz} + A_{45}\epsilon_{yz}) \\ Q_y &= 2(A_{45}\epsilon_{xz} + A_{44}\epsilon_{yz}) \qquad (2.140) \end{aligned}$$

Note, that equations 2.139 and 2.140 are applicable for any displacement field. Hence, for the higher order theory presented,

$$A_{ij} = \sqrt{\frac{15}{8}} \sum_{k=1}^{N} \int_{h_{k-1}}^{h_k} \left(\bar{Q}_{ij}\right)_k \left[1 - 4\left(\frac{z}{h}\right)^2\right] dz \tag{2.141}$$

or,

$$A_{ij} = \sqrt{\frac{15}{8}} \sum_{k=1}^{N} \left(\bar{Q}_{ij}\right)_k \left[h_k - h_{k-1} - \frac{4}{3h^2}\left(h_k^3 - h_{k-1}^3\right)\right] \tag{2.142}$$

with $i, j = 4, 5$.

In the present three dimensional solid element, for which only three translational degrees of freedom per node are defined, resultants are divided by the corresponding thicknesses to obtain the stress-strain relations with

$$[E] = \frac{1}{h}\begin{bmatrix} A_{11} & A_{12} & 0 & 0 & 0 & 2A_{16} \\ A_{12} & A_{22} & 0 & 0 & 0 & 2A_{26} \\ 0 & 0 & 0 & 0 & 0 & 0 \\ 0 & 0 & 0 & 2A_{44} & 2A_{45} & 0 \\ 0 & 0 & 0 & 2A_{45} & 2A_{55} & 0 \\ A_{16} & A_{26} & 0 & 0 & 0 & 2A_{66} \end{bmatrix} \tag{2.143}$$

For the special case of isotropic material, the material stiffness matrix is given by

$$[E] = \begin{bmatrix} \lambda + 2G & \lambda & \lambda & 0 & 0 & 0 \\ \lambda & \lambda + 2G & \lambda & 0 & 0 & 0 \\ \lambda & \lambda & \lambda + 2G & 0 & 0 & 0 \\ 0 & 0 & 0 & G & 0 & 0 \\ 0 & 0 & 0 & 0 & G & 0 \\ 0 & 0 & 0 & 0 & 0 & G \end{bmatrix} \tag{2.144}$$

where

$$\lambda = \frac{\nu E}{(1+\nu)(1-2\nu)} \tag{2.145}$$

2. Three-dimensional Anisotropic Theory

As an alternative to using laminate theories to obtain $[E]$ matrix, we may use anisotropic definition of the laminates.

$$\sigma_i = \left(\bar{Q}_{ij}\right) \epsilon_j \tag{2.146}$$

These relations are approximated by obtaining the $\bar{Q}_{ij}$ in the laminate x-y axes by suitable transformations and transverse properties (thickness direction) correspond to the matrix characteristics.

F. CONSISTENT LOADS

In this section, we consider the element nodal loads vector, due to applied loads. Using the virtual work principle, the distributed loads, such as surface loads and body forces, are converted into discrete loads applied at the element nodal points. Discretizing the distributed loads along these lines are referred to as consistent or work-equivalent loads. Consider a case where a uniform distributed load acts on a prescribed face of the element, as seen in Figure 2.6. The consistent load vector may be written as

$$\{r_s\} = \int_s [N^s]^T \{f^s\} ds \tag{2.147}$$

For uniform distributed surface loads, we have

$$\{f^s\} = p\,\{1\} \tag{2.148}$$

It is worth noting that the interpolation functions on a given surface, say $t = 1$ reduces to that of a plane biquadratic Lagrangian isoparametric element and are presented in Table 2.1. Invoking symmetry, we observe that the forces at nodes 1, 3, 5, and 7 are equal, and similarly, forces at nodes 2, 4, 6, and 8 are equal. On using the shape functions for the $t = 1$ surface, we have,

$$\begin{aligned}
r_9 &= \int_{-1}^{1}\int_{-1}^{1} \left(1-r^2\right)\left(1-s^2\right) p\, dr\, ds = \frac{16}{9}p \\
r_4 &= \int_{-1}^{1}\int_{-1}^{1} \frac{1}{2}\left(1-r^2\right)(1-s)\, p\, dr\, ds - \frac{1}{2}r_9 = \frac{4}{9}p \\
r_1 &= \int_{-1}^{1}\int_{-1}^{1} \frac{1}{4}(1+r)(1-s)\, p\, dr\, ds - \frac{1}{2}r_8 - \frac{1}{2}r_2 - \frac{1}{4}r_9 = \frac{1}{9}p
\end{aligned} \tag{2.149}$$

TABLE 2.1: SHAPE FUNCTIONS FOR 9 NODED BIQUADRATIC ELEMENT

$$
\begin{aligned}
N_1 &= \frac{1}{4}(1+r)(1-s) - \frac{1}{2}N_8 - \frac{1}{2}N_2 - \frac{1}{4}N_9 \\
N_3 &= \frac{1}{4}(1+r)(1+s) - \frac{1}{2}N_2 - \frac{1}{2}N_4 - \frac{1}{4}N_9 \\
N_5 &= \frac{1}{4}(1-r)(1+s) - \frac{1}{2}N_4 - \frac{1}{2}N_6 - \frac{1}{4}N_9 \\
N_7 &= \frac{1}{4}(1-r)(1-s) - \frac{1}{2}N_8 - \frac{1}{2}N_6 - \frac{1}{4}N_9 \\
N_2 &= \frac{1}{2}(1+r)\left(1-s^2\right) - \frac{1}{2}N_9 \\
N_4 &= \frac{1}{2}\left(1-r^2\right)(1+s) - \frac{1}{2}N_9 \\
N_6 &= \frac{1}{2}(1-r)\left(1-s^2\right) - \frac{1}{2}N_9 \\
N_8 &= \frac{1}{2}\left(1-r^2\right)(1-s) - \frac{1}{2}N_9 \\
N_9 &= \left(1-r^2\right)\left(1-s^2\right)
\end{aligned}
$$

Note: Node numbering is referred to Figure 2.2 where $t = 1$, upper plane.

Figure 2.6 gives consistent element nodal loads for a single element. As a check, the total pressure loading on the surface, $2 \times 2 \times p = 4p$, is seen to be equal to the sum of all the discretized nodal point forces. The procedure may be extended for more than one element by summing loads at joint nodes, as illustrated in Figure 2.7 for four elements.

G. INTEGRATION

In this section, we summarize the Gauss method for numerical integration, including a discussion on some aspects of integration schemes.

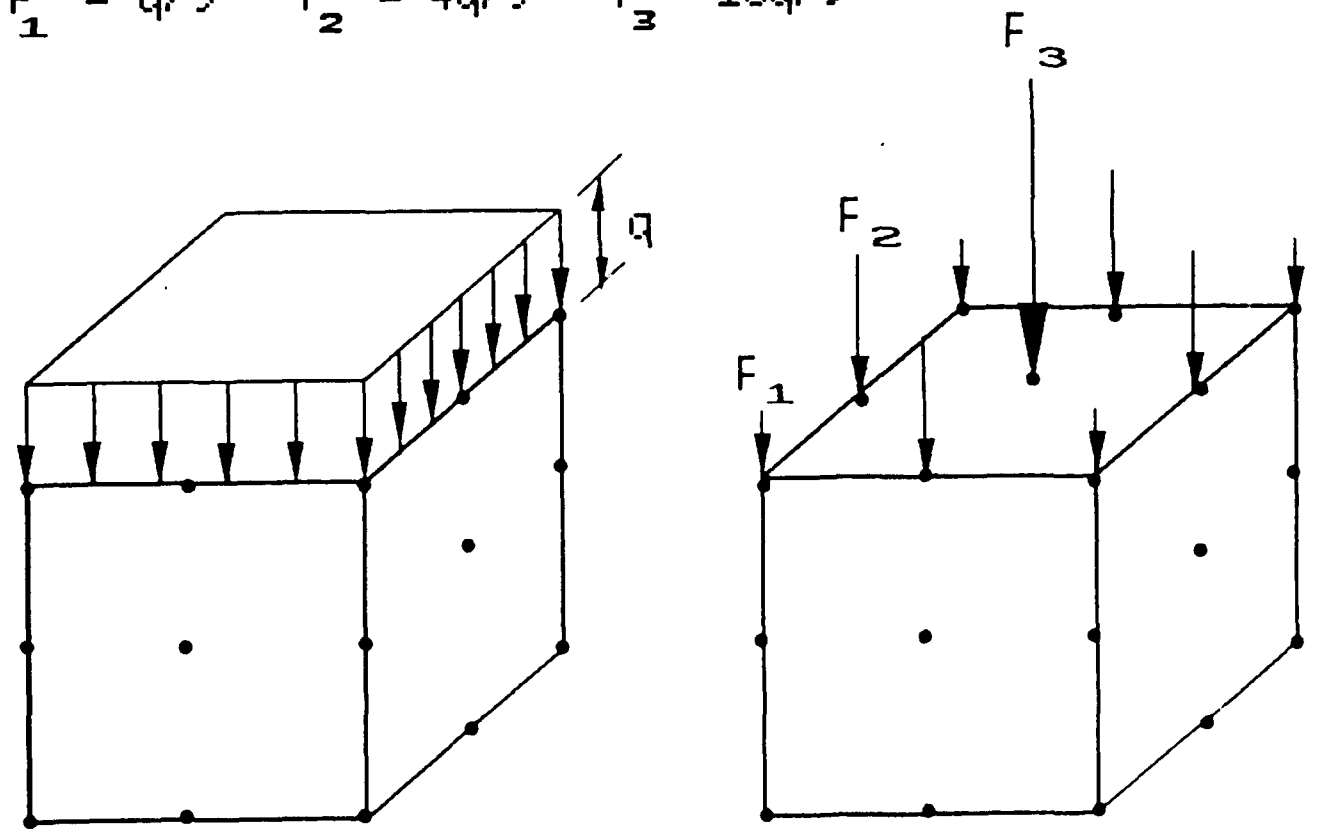

Figure 2.6: Consistent loads

Fig. 2.6; Consistent loads

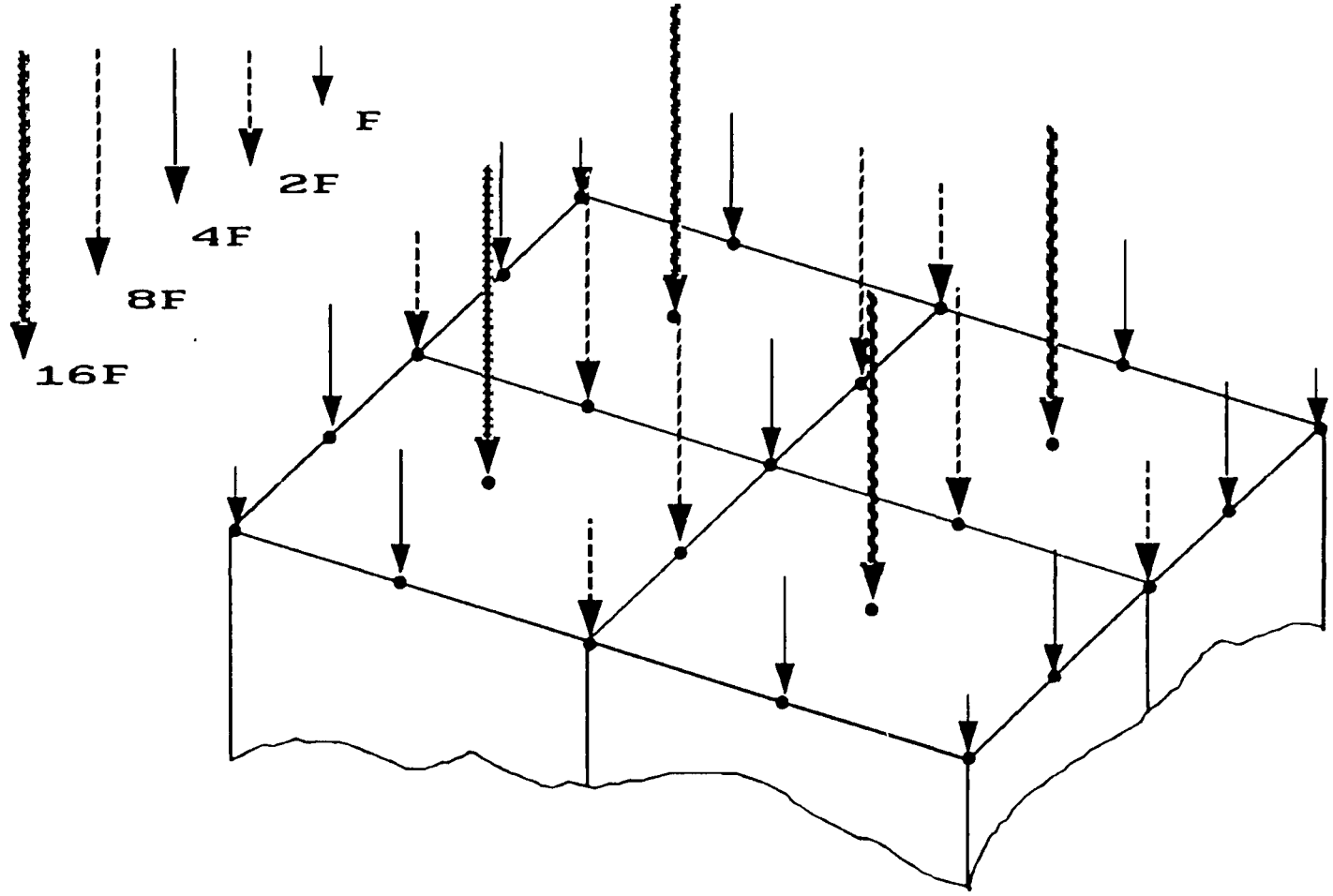

Figure 2.7: Consistent loads on a mesh

Fig. 2.7; Consistent loads on a mesh

1. Gauss Quadrature

The nature of finite element matrices suggests the usage of numerical quadrature. Gauss's integration scheme is the most commonly used approach and is adopted in the present analysis.

The method enables exact evaluation integrals, consisting of polynomials of any order, by using appropriate order of integration. In general, the Gauss quadrature for a function $\phi(r,s,t)$, has the form

$$I = \int_{-1}^{1}\int_{-1}^{1}\int_{-1}^{1} \phi(r,s,t)\, dr\, ds\, dt \approx \sum_i \sum_j \sum_k w_i w_j w_k \phi(r,s,t) \qquad (2.150)$$

The integration limit reflects the limits of non-dimensional 'master' isoparametric elements, while $\phi(r,s,t)$ represents the stiffness contribution.

Figure 2.8 demonstrates the application of the method for a two dimensional biquadratic element. Using the weighting factors as given in Table 2.3, the element stiffness matrix is evaluated, for example, by using a 3rd order integration scheme as follows:

$$[K] = \frac{5}{9}\frac{5}{9}(\phi_1 + \phi_3 + \phi_7 + \phi_9) + \frac{5}{9}\frac{8}{9}(\phi_2 + \phi_4 + \phi_6 + \phi_8) + \frac{8}{9}\frac{8}{9}\phi_5 \qquad (2.151)$$

where

$$\phi_i = h\,[B(r,s)]^T\,[E]\,[B(r,s)]\;|\;J(r,s)\;| \qquad (2.152)$$

as is evaluated at Gauss point i as shown in the Figure.

2. Integration Scheme

The term "full integration" refers to an integration scheme which evaluates the integral exactly as shown in the previous example. In the same manner, a lower order integration is referred to as 'reduced integration'.

In the present analysis, 'full integration' is used to evaluate the stiffness matrices. When a crude mesh is used, a stiffer structure is obtained. In general, there

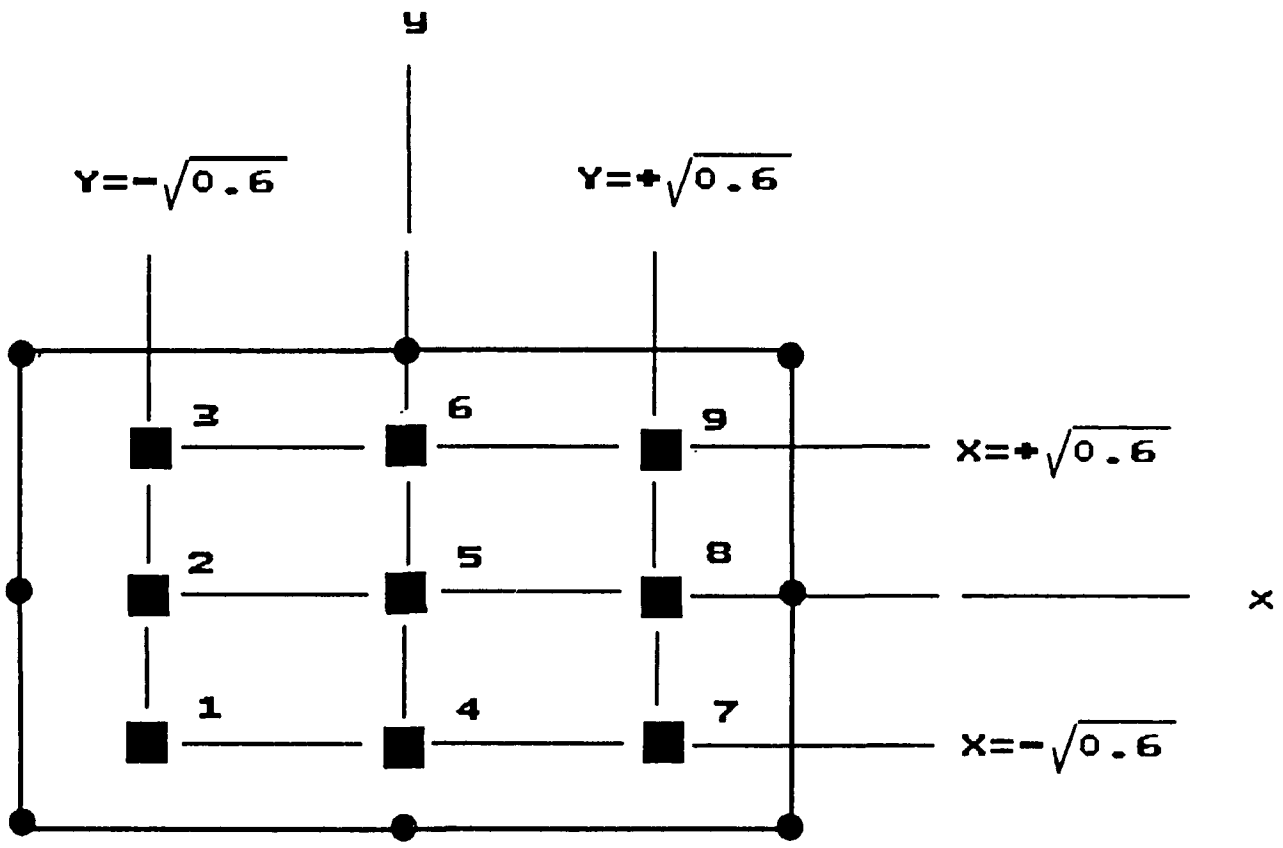

Figure 2.8: Gauss points

Fig. 2.8; Gauss points

TABLE 2.2: SAMPLING POINTS AND WEIGHTS FOR GAUSS QUADRATURE OVER THE INTERVAL -1 to 1

Order n	Location of Sampling Point	Weight Factor W_i
1	0.	2.
2	$\pm 0.57735\ 02691\ 89626 = \pm\frac{1}{\sqrt{3}}$	1.
3	$\pm 0.77459\ 66692\ 41483 = \pm\sqrt{0.6}$	$0.55555\ 55555\ 55555 = \frac{5}{9}$
	0.	$0.88888\ 88888\ 88888 = \frac{8}{9}$
4	$\pm 0.86113\ 63115\ 94053 = \pm\left[\frac{3+2r}{7}\right]^{\frac{1}{2}}$	$0.34785\ 48451\ 37454 = \frac{1}{2} - \frac{1}{6r}$
	$\pm 0.33998\ 10435\ 84856 = \pm\left[\frac{3-2r}{7}\right]^{\frac{1}{2}}$	$0.65214\ 51548\ 62546 = \frac{1}{2} + \frac{1}{6r}$
	where $r = \sqrt{1.2}$	and $(2r-1)$ is the polinom order

are two ways to soften the structure. One way is to refine the mesh and another by using 'reduced integration'. Thus, by using a 'reduced integration' scheme, a faster convergence and more cost-effective, accurate solution may be obtained. However, the method suffers such drawbacks as mesh instabilities or mechanisms, resulting in a singular element stiffness matrix.

H. BUCKLING ANALYSIS

1. Introduction

It is well known that thin columns or plates under axial compression tend to buckle. Elastic buckling occurs when the compressive stress is well below the material stress limit. A flat plate under axial compression shortens in the direction of the applied compressive loads. This shortening results in coupling between in-plane and out-of-plane displacements.

As the applied compressive load increases, there is a configuration at which the plate offers no more resistance to deform, resulting in a state of neutral stability. The load corresponding to this configuration is referred to as the buckling load and constitutes a limit point on the load response curve.

At this critical value, the deflection becomes very sensitive to any change in the configuration. For some structures, beyond the limit point, the load-displacement path may take any of multiple paths. The point where the plate can take any of the different paths is called the Bifurcation point and is illustrated in Figure 2.9. In analyzing for nonlinear response, the incremental load method is adopted, which may be summarized as follows: (a) the tangent stiffness matrix is formed, and solved for displacements for an incremental load. Keeping the stiffness matrix constant, corrections to the incremental displacements are obtained in an iterative manner until equilibrium is achieved, (b) total displacements for this load are obtained, (c) a new tangent stiffness matrix is formed at this new equilibrium position and steps (a) and (b) are repeated. This procedure is continued until the desired load is reached or the critical buckling load is reached.

2. Implementation

In this section, the Finite-Element formulation for buckling will be presented [Bathe, (1982), Kolar, et al., (1985)]. The problem of instability can be approached either by looking at the equilibrium of the structure in the deflected position and transforming all quantities to the initial configuration or by solving the system in the current configuration. The former approach, described earlier as the total Lagrangian formulation, is adopted here. By performing an incremental load analysis, using the nonlinear formulation described earlier, we may write

$$\left(\left[{}^{t}K_L\right] + \left[{}^{t}K_{NL}\right]\right)\{d\}^{(i+1)} = {}^{t+\Delta t}\lambda\{P\} - \{F\}^{(i)} \qquad (2.153)$$

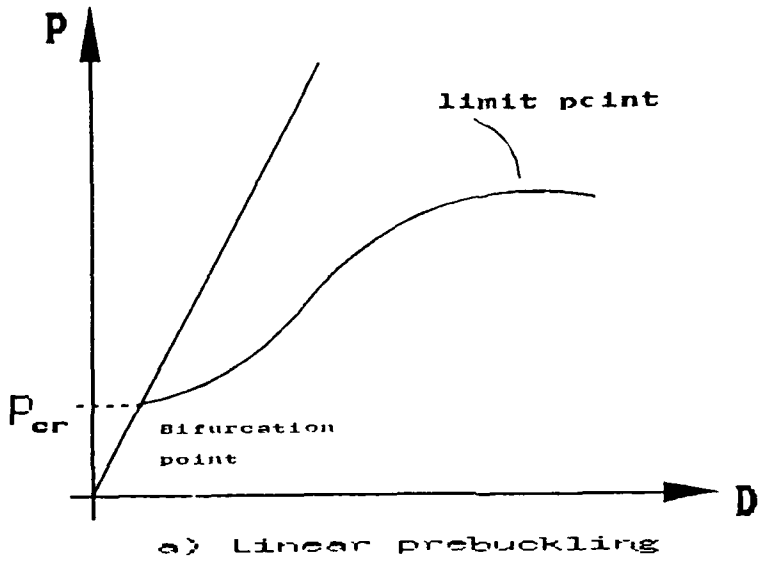

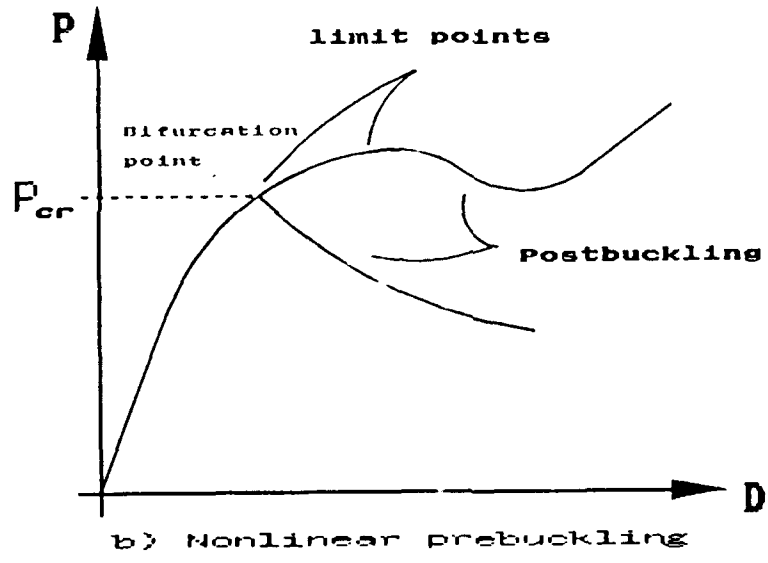

Fig. 2.9; Instability and bifurcation points

Figure 2.9: Instability and bifurcation points

where $\{P\}$ represents the total load applied and ${}^{t+\Delta t}\lambda$ is a scalar, referred to as load parameter. The value λ scales the incremental load and may be treated as a constant or variable during iterations. Buckling load is reached when displacements become large with no increase in the incremental load, i.e., the global stiffness of the structure, as illustrated for a single degree of freedom system in Figure 2.9, becomes small and $[K]$ tend to be singular. Thus, using Newton-Raphson and modified Newton-Raphson methods, convergence difficulties are encountered as buckling load is approached. This is overcome by using arc length methods, described in the next section, where the load parameter is continuously updated to reflect the state of the structure.

3. Constant Arc Length Method [Kolar and Kamel (1985)]

When using the Newton type iteration schemes, the stiffness matrix becomes singular as limit points are approached. In order to obtain post-buckling response, a method to overcome this singularity is needed. This is accomplished by treating the load parameter as a variable and thus have an adaptive load incrementation. This approach differs from the conventional Newton type schemes where the load level is held constant for all iterations at a given load step. Symbolically, at load step m and iteration i, equation 2.153 can be rewritten as follows

$$ {}^{m}[K]\{d\}^{(i+1)} = \left({}^{m}\lambda + \lambda^{(i)} + \Delta\lambda\right)\{P\} - \{F\}^{(i)} \tag{2.154} $$

where ${}^{m}[K]$ is the tangent stiffness matrix at load step m

$$ \lambda^{i+1} = \lambda^{(i)} + \Delta\lambda \tag{2.155} $$

The Arc Length Method (ALM) may easily be visualized for a single degree of freedom as shown in Figure 2.10. The displacements are updated as

$$ \{x\}^{(i+1)} = {}^{m}\{x\} + \{u\}^{(i)} + \Delta u \tag{2.156} $$

such that $x^{(i+1)}$ corresponds to the displacement at the $(i+1)^{th}$ iteration of load step m.

In the constant ALM, the radius of the arc at each load step is constant. It is clear from Figure 2.10 that the ALM is used in conjunction with the modified Newton-Raphson method, and may also be implemented with NR iteration schemes. The method allows one to obtain postbuckling response but bifurcation problems require modification that will seek out multiple paths after a limit point.

4. Convergence Criterion

For a given load step, the iterations on displacements are carried out until a pre-set convergence is achieved. There are three convergence tests most commonly used, (a) Displacement Convergence, (b) Residual Force Convergence, and (c) Strain Energy Convergence. These criterion may be summarized as follows:

$$\begin{aligned} \frac{\{\Delta u^i\}^T\{\Delta u^i\}}{\{\Delta u^1\}^T\{\Delta u^1\}} &\leq \alpha_{DISP} \\ \frac{\{g^i\}^T\{g\}}{(\Delta\lambda^1)^2\{P\}^T\{P\}} &\leq \alpha_{R.F.} \\ \frac{\{\Delta u^i\}^T\{g^i\}}{\Delta\lambda^1\{\Delta u^1\}\{P\}} &\leq \alpha_{DISP}\alpha_{R.F.} \end{aligned} \tag{2.157}$$

It may be noted that $\{\Delta u^i\}$ is the incremental displacement at i^{th} iteration, $\{g^i\}$ is the residual force at i^{th} iteration, $\Delta\lambda^1\{P\}$ is the incremental load at the first iteration, $\{\Delta u^1\}$ is the incremental displacement at the first iteration, and α's are the prescribed convergence parameters, usually in the order of 10^{-2} to 10^{-4}.

It is further noted that the initial load $\{P\}$ used to start the analysis is set arbitrarily and only the load parameter is modified automatically to go from zero load to the desired load level.

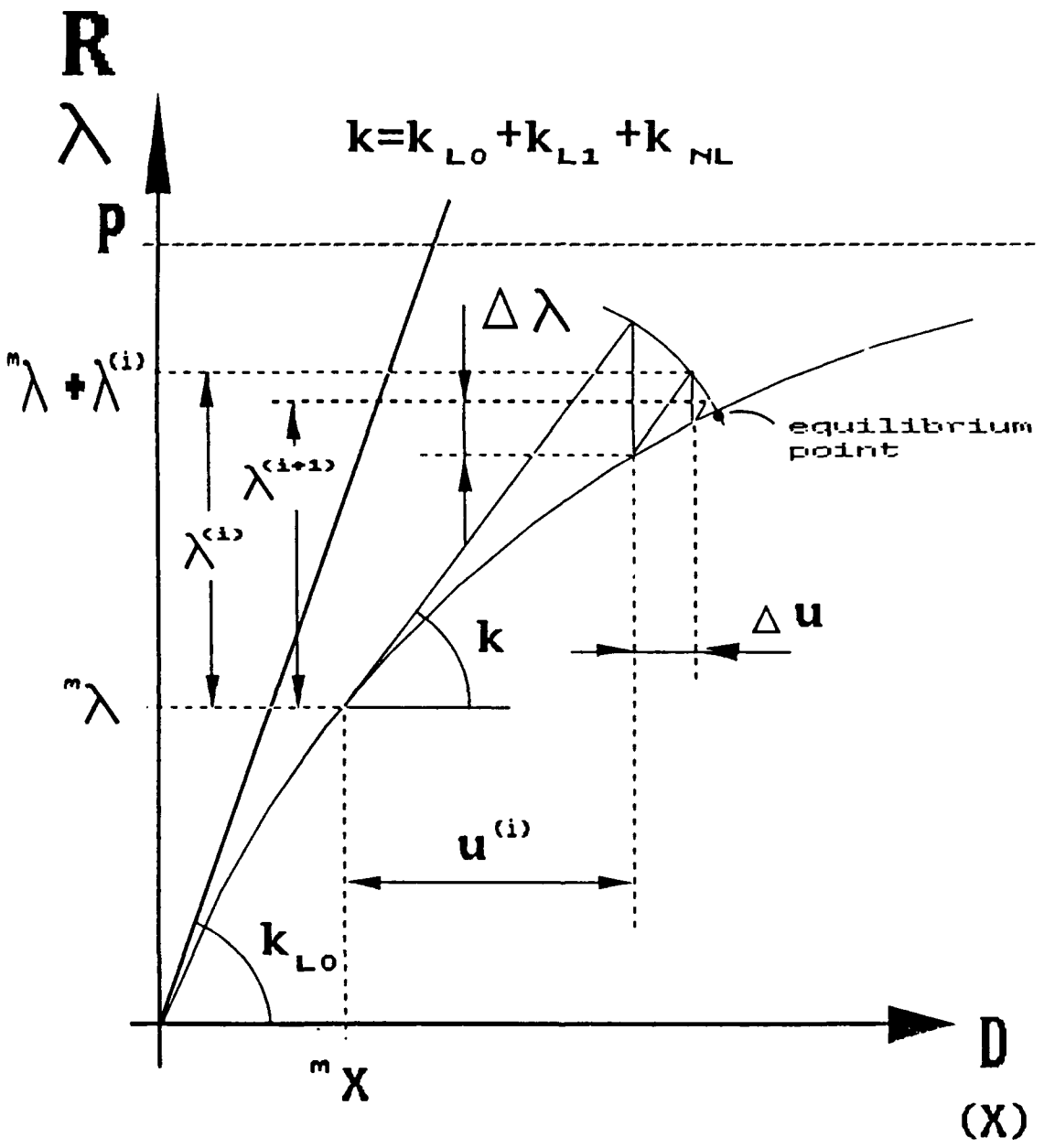

Figure 2.10: Constant Arc Length Method

III. PROGRAM IMPLEMENTATION

A. INTRODUCTION

This chapter presents certain aspects of computer implementation of the elements matrices developed in the previous chapter. As mentioned in Equation 2.25, the general problem to be solved is given by

$$[K]\{d\} = \{r\} \tag{3.1}$$

$$[K]\{D\} = \{R\} \tag{3.2}$$

where equations 3.1 and 3.2 are the static equilibrium equations for the element and structural assemblage respectively. If the stiffness matrix, $[K]$, is independent of displacements, the analysis reduces to solving a set of linear algebraic equations. In the case of the stiffness matrix being displacement independent, the structural behavior is nonlinear, and an incremental load analysis together with a suitable iterative methods has to be adopted.

B. LINEAR ANALYSIS

In the case of linear analysis, we assume small displacements and small strains, and the resulting force-displacement relations are solved only once. Using the displacement independent part in equation 2.61 to get the strain-displacement relations $[B_{Lo}]$, as given by equation 2.80, equation 2.20 is used to form the element stiffness matrix. A series of Fortran subroutines was developed incorporating the element stiffness matrix for this element. The material characteristics may be either isotropic, laminate theory definitions, or anisotropic description. The subroutines are implemented in an existing computer program, FEMCOM, which is capable of

element assembly and subsequently calculation of the displacement solution for both linear and incremental load methods.

C. NONLINEAR ANALYSIS

In this research effort, geometric nonlinearities, namely, large displacements but small strains are considered. Consequently, the element consists of a linear displacement independent stiffness matrix, $[K_{L0}]$, and two other contributions. The first contribution is due to the linear displacement dependent stiffness matrix, $[K_{L1}]$, based on $[B_{L1}]$, as given in equation 2.81. The other contribution comes from nonlinear stiffness matrix, $[K_{NL}]$, as given by equation 2.95.

Note that the stress-strain matrix, $[E]$, may be used both for isotropic as well as composite materials using relations 2.131 and 2.132.

D. SOLUTION PROCEDURE

1. Composite Material

In order to generalize the procedure of implementing the solid element with composite materials, the plate built of solid elements may be stacked in all three directions. Figure 3.1 shows such a stack, where rows of elements are arranged in the thickness direction. For each finite element, the stress-strain matrix is computed in a subroutine separately, though it would be more efficient to compute it for the whole row of elements, taking into account the appropriate layers. In assigning a certain number of layers in each row, a constraint to be noted is that the total number of layers of all rows match the number of layers of the structure being modeled.

2. Linear Case

As mentioned earlier, the matrices corresponding to the linear displacement independent part was coded into several subroutines and implemented into a

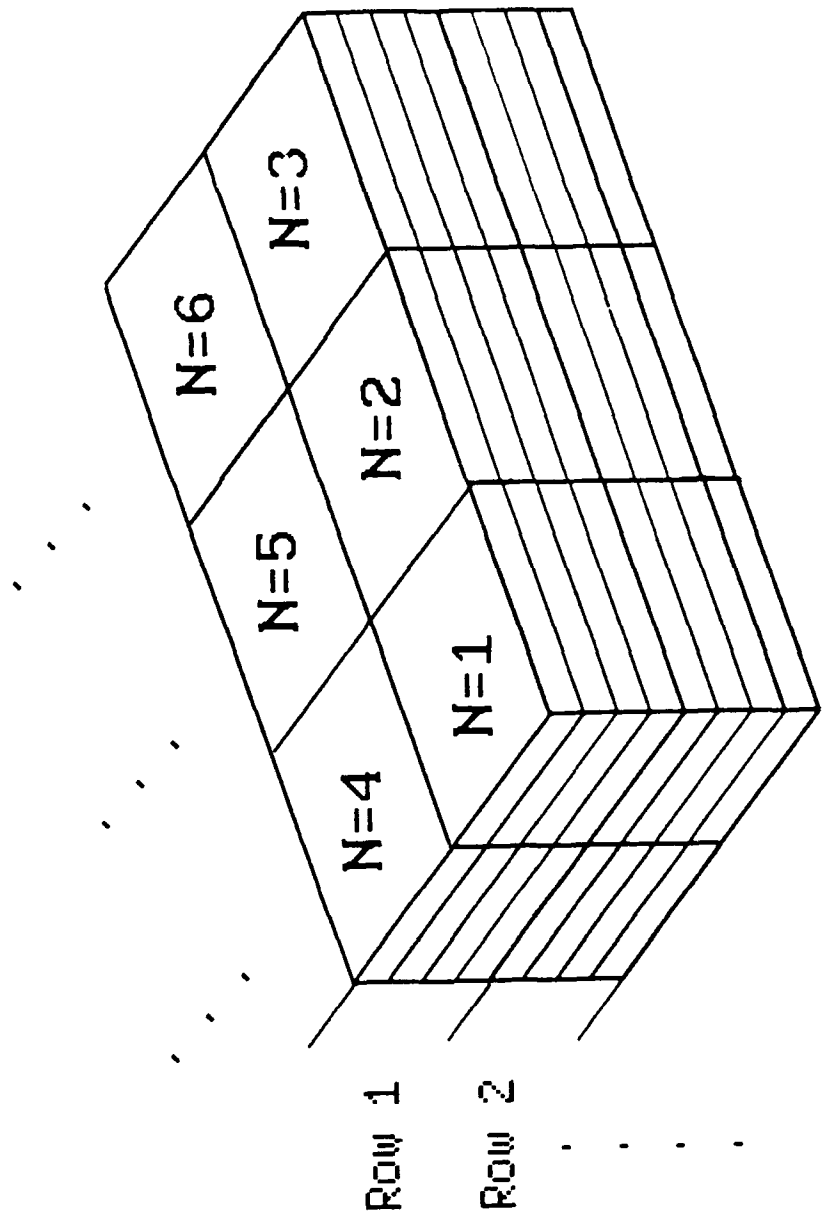

Fig. 3.1; Thick composite plate-element arrangement

Figure 3.1: Thick composite plate-element arrangement

general purpose finite element program, FEMCOM. The program does automatic element assembly and yields solutions to prescribed loads. The flow chart shown in Figure 3.2 shows various steps that may be summarized as follows.

1. The material properties, model geometry, applied loads, integration scheme, boundary conditions and solution parameters are input. The material properties needed for isotropic material are Young's modulus and Poisson ratio. For composites, data needed includes the number of layers, rows of elements, fiber orientations, Young's moduli, shear modulus in three directions, and Poisson ratio.

2. Using the shape function derivatives, the coordinates transformation relations, Jacobian and the strain displacement relations are established.

3. Using the specified Gauss quadrature, the element stiffness matrix is formed in global coordinates.

4. The element global stiffness matrix is assembled.

5. Using Gauss elimination technique, the displacement vector is computed.

6. Stresses may be computed using equations 2.14 and 2.15.

3. Nonlinear Case

In order to obtain nonlinear response, either for studying the extension-twist-flexure coupling or nonlinear buckling and post-buckling, the analysis procedure is termed the incremental load method, and a variation of Newton-type iteration is used. The element formulation, assembly and equation solving proceed as before, except that additional element stiffness contributions have to be taken into account. The assembly and solution to get displacements needs to be done as

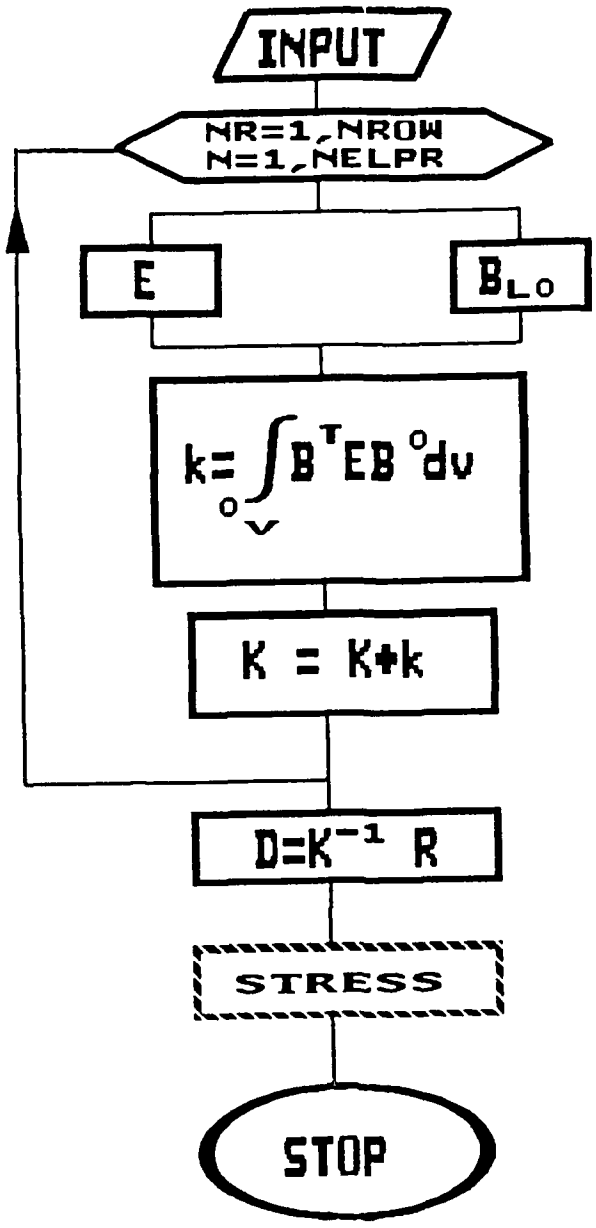

FIG. 3.2; Flow chart-
linear analysis

Figure 3.2: Flow chart – linear analysis

frequently as the load steps increments and iterations continue, depending on the solution strategy selected. A typical flow chart is given in Figure 3.3.

For a given load step, the incremental displacements are computed iteratively until the convergence criterion is satisfied. At that point, equilibrium is achieved and new incremental load is applied and a new tangent stiffness matrix is computed. The iterations continue until the new equilibrium position is obtained. In the modified Newton-Raphson method, the tangent stiffness matrix is kept constant for all iterations for a given load step, while, for the Newton-Raphson method, the stiffness matrix for the whole structure is formed at every iteration. By tracing the load-displacement path, critical points, characterizing buckling, and stable and unstable regions of post-buckling equilibrium states may be identified.

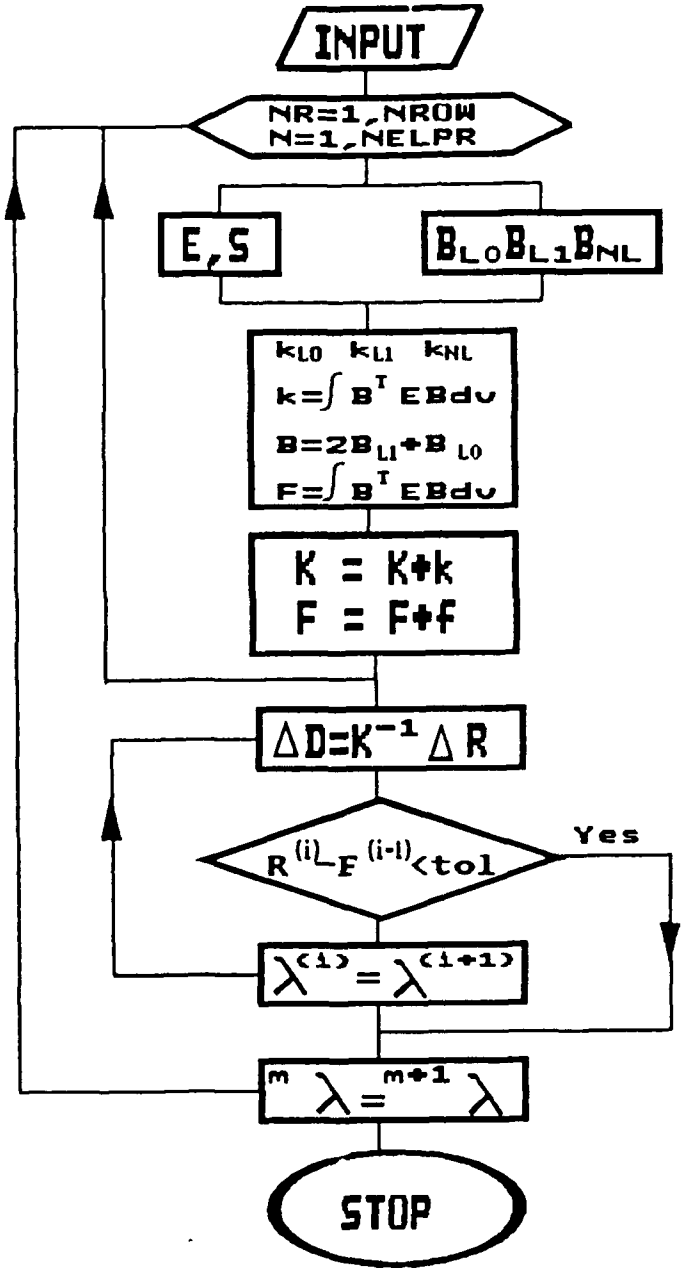

FIG. 3.3; Flow chart-
Nonlinear analysis

Figure 3.3: Flow chart – Nonlinear analysis

IV. NUMERICAL EXAMPLES

A. INTRODUCTION AND NOTATIONS

In this chapter, selected numerical examples are used to evaluate element idiosynchrasies and demonstrate its application in solving critical structural components that use thick composites. Solutions obtained here are compared with available elasticity solutions or other numberical solutions.

1. Material Properties

In all the examples to be discussed, the material characteristics used are as follows. For isotropic materials,

$$E = 30 \times 10^6 \text{ psi}, \ \nu = 0.30$$

and for composite materials used for laminated plates, layer properties are given by

$$\begin{aligned} E_1 &= 40 \times 10^6 \text{ psi} \\ E_2 &= 10^6 \text{ psi} \\ G_{12} &= G_{13} = 0.6 \times 10^6 \text{ psi} \\ G_{23} &= 0.5 \times 10^6 \text{psi} \\ \nu &= 0.25 \end{aligned}$$

An eight-layered symmetric laminate configuration using this material is selected. All the dimensions presented in this chapter are in inches. In the discussion on effects of numerical integration rules, $L \times M \times N$ notation refers to the number of integration points in x, y, and z directions respectively.

B. COLUMNS AND BARS

Two simple cases have been selected as part of the element validation process.

1. Bars

A bar clamped at one end and loaded at the other end with uniformly distributed traction (Figure 4.1a) was studied and compared to the theory of elasticity. In the numerical solution, work-equivalent loads were used. The dimensions of the bar are 10 in. x 1 in. x 1 in., and it is isotropic. The boundary conditions are given by

$$u\left(0,\ \frac{h}{2},\ \pm\frac{h}{2}\right) = v\left(0,\ \frac{h}{2},\ \pm\frac{h}{2}\right) = w\left(0, \pm\frac{h}{2}, \pm\frac{h}{2}\right) = 0 \qquad (4.1)$$

Figure 4.2 depicts the effects of reduced integration and mesh refinement on the maximum deflection. It is obvious that when the mesh is refined in the thickness direction, for instance, one element in each of x and y direction and two in z direction [1 x 1 x 2] mesh, provides a stiffer solution than for the [1 x 1 x 1] mesh. It may be noted that the full (F) and reduced (R) integration schemes converge to about 95% of the classical solution (See Appendix C). It may be noted that the classical elasticity solution does not account for transverse shear stresses. A reduced integration in the axial direction (2 x 3 x 3) gives the same results as the full integration. However, when reduced integration in the thickness directions is performed (3 x 2 x 2), the solution converges slowly. On using (2 x 2 x 3) integration scheme in the thickness direction for (12 x 1 x 1) mesh, spurious mode is observed. Table 4.1 summarizes the effects of various integration schemes and mesh sizes.

2. Beams

The next example considered is a clamped, cantilever beam loaded at the free end by a shear load. Using the clamped boundary conditions, dimensions and material as the previous example, solutions using full and reduced (R) integration are compared with the elasticity solution in Figure 4.3. The comparisons also include the solution obtained using eight noded first order solid element of 'GIFTS' software.

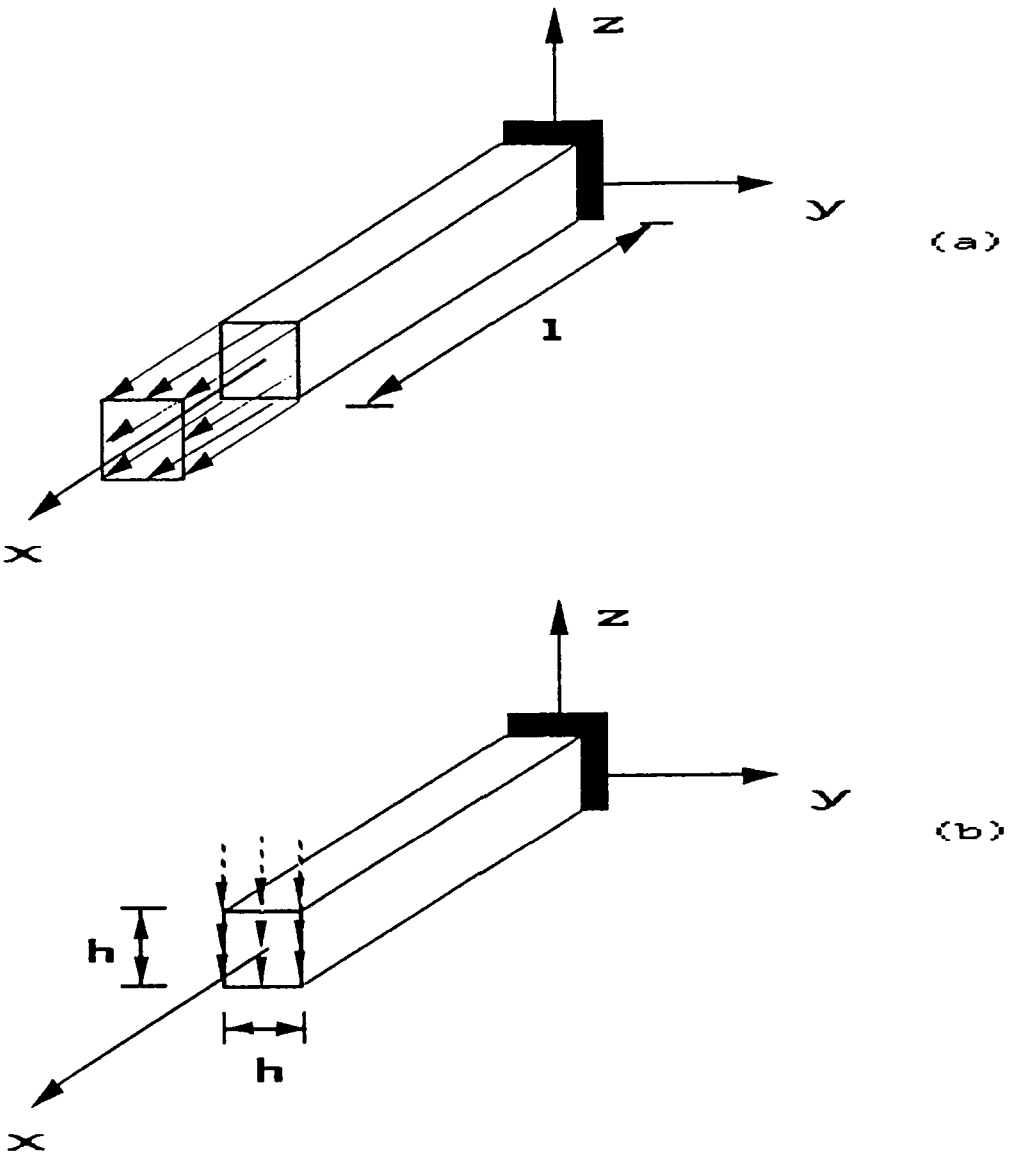

Fig. 4.1; Bar Sample problems

Figure 4.1: Bar Sample Problems

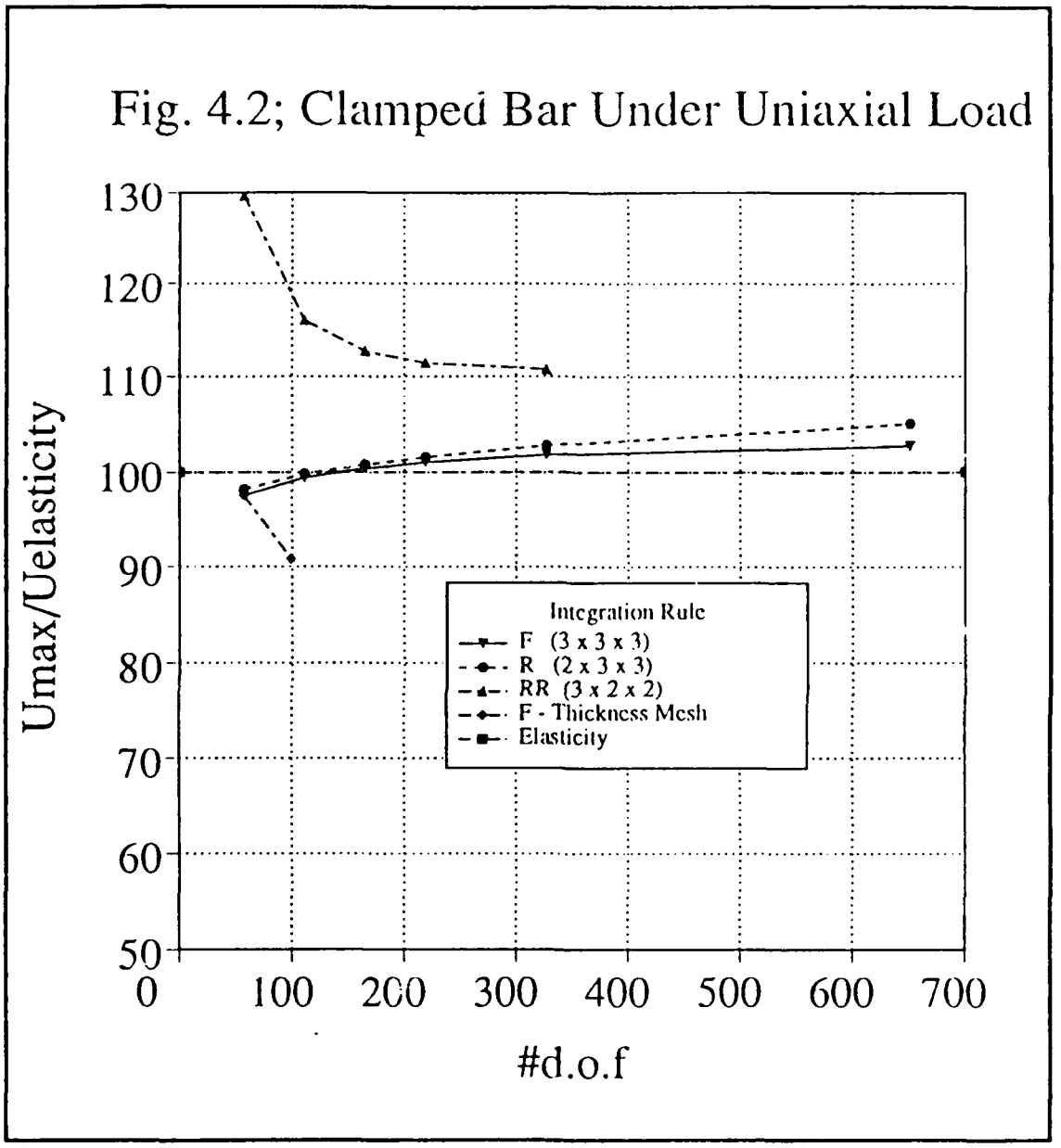

Figure 4.2: Clamped Bar Under Uniaxial Load

TABLE 4.1: EFFECTS OF REDUCED INTEGRATION AND REFINED MESH, ON THE MAXIMUM DEFLECTION OF CLAMPED ISOTROPIC CANTILEVER BAR UNDER UNIAXIAL LOAD

Mesh	# d.o.f.	Integration Rule	$\frac{U_{max}}{U_{elasticity}} \times 100$
1 = 1 x 1 x 1	5.7	F (3 x 3 x 3)	97.49
		R (3 x 3 x 3)	98.17
		RR (2 x 2 x 3)	129.56
2 = 2 x 1 x 1	111	F	99.43
		R	99.84
		RR	115.98
2 = 1 x 1 x 2	99	F	90.77
		R	91.20
		RR	91.83
3 = 3 x 1 x 1	165	F	100.40
		R	100.81
		RR	112.64
4 = 4 x 1 x 1	219	F	101.04
		R	101.59
		RR	111.39
6 = 6 x 1 x 1	327	F	101.83
		R	102.80
		RR	110.74
12 = 12 x 1 x 1	651	F	102.74
		R	105.00
		RR	11,500.00

$$\frac{U_{max}}{U_{elasticity}} = U_{max}\,\frac{AE}{pl}$$

The reduced integration shows a better convergence than both the full integration and the first order solid element. It may be noted that the eight noded solid element converges more rapidly than the full integration scheme of the present element up to about 300 degrees of freedom (d.o.f.).

It can be seen from Table 4.2 that mesh refinement in the thickness direction results in reduced performance and one element in the thickness direction consistently yields good results.

In Figure 4.4, the effect of transverse shear deformation is studied for a 12 x 1 x 1 mesh using reduced integration scheme, and compared to the theory of elasticity solution (See Appendix C). The results are summarized in Table 4.3 versus the aspect $\left(\frac{l}{h}\right)$ ratio.

It is clear that for thin beams where the elasticity solution is adequate, the present element gives stiff solutions, whereas for thick beams ($\frac{l}{h} \leq 10$), better solutions are predicted. The reason for these effects may be attributed to the transverse shear stresses. In the case of thin bars, or beams, the element aspect ratio is very large and the parasitic shear strains appear at Gauss points, resulting in a phenomena called 'shear locking' [Cook, 1989, and Hughes, 1978]. When the beam is thick and the aspect ratio is of the order of 1/10, the transverse shear stresses start to become significant, whereas in the elasticity solution, they are taken into account only to a limited degree together with the restrictions of Saint-Venant's principle.

C. CLAMPED PLATES

An isotropic clamped plate of dimensions 20 in. x 20 in. x 1 in. under a central concentrated load is shown in Figure 4.5a. This problem is studied for mesh sensitivity and the effects of different integration rules. The present solution

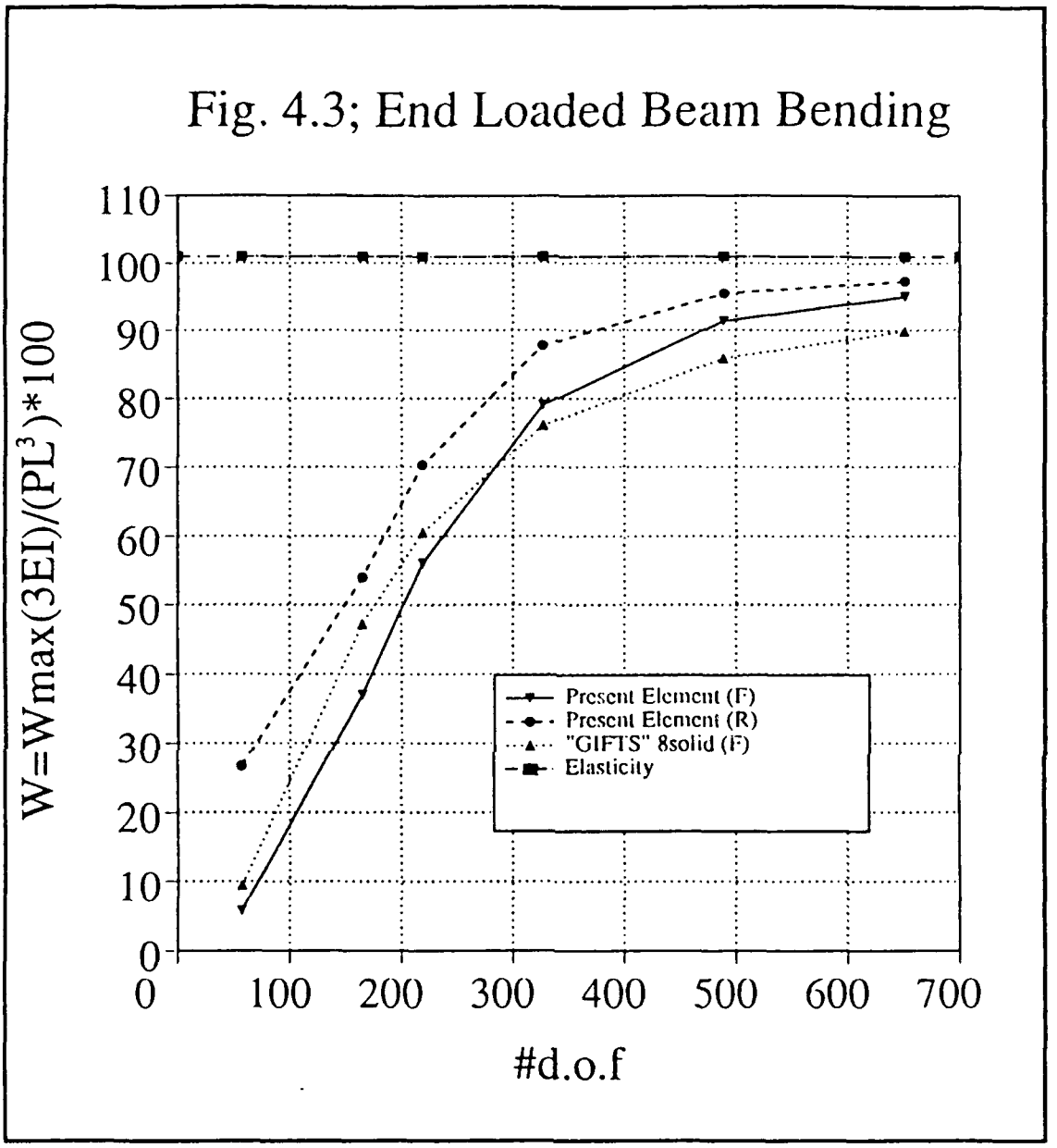

Figure 4.3: End Loaded Beam Bending

TABLE 4.2: EFFECTS OF REDUCED INTEGRATION AND MESH CONFIGURATION ON THE MAXIMUM DEFLECTION OF CLAMPED ISOTROPIC CANTILEVER BEAM LOADED AT THE END

Mesh * (27 solid)	# d.o.f.	$\bar{w} = w_{max} \frac{3EI}{PL^3} 100$		
		27 solid		8 solid †
		F	R	F
1 = 1 x 1 x 1	57	5.7	26.7	9.4
3 = 3 x 1 x 1	165	37.0	54.0	47.2
4 = 4 x 1 x 1	219	56.0	70.3	60.5
9 = 9 x 1 x 1	489	91.3	95.4	85.8
12 = 12 x 1 x 1	651	95.0	97.3	89.8
3 = 1 x 1 x 3	147	5.5		
4 = 2 x 1 x 1	135	16.9		
6 = 2 x 1 x 3	273	17.0	$\bar{w}_{elasticity} = 101.0$	
6 = 3 x 1 x 2	285	36.0		
9 = 3 x 1 x 3	399	39.1		

F: Full integration

- 3 x 3 x 3 for 27 solid
- 2 x 2 x 2 for 8 solid

R: Reduced integration

- 2 x 3 x 3 for 27 solid

† 8 solid is generated in "GIFTS".
* Mesh configuration for 8 solid is twice of 27 solid in each direction, i.e., 2 x 1 x 3 for 27 solid is 4 x 2 x 6 for 8 solid.

TABLE 4.3: CENTER DEFLECTION VS. ASPECT RATIO $\left(\frac{l}{h}\right)$ OF AN ISOTROPIC CANTILEVER CLAMPED BEAM LOADED AT ONE END

$\frac{l}{h}$	$\bar{w}_e$	$\bar{w}$
2	124.38	110.07
5	103.90	99.49
10	100.98	97.07
50	100.04	53.43
100	100.01	17.85

$$\bar{w} = \frac{w\left(l, \frac{1}{2}h, \frac{1}{2}h\right)\ 3EI}{P\ l^2} 10^2$$

$$= \frac{w\left(l, \frac{1}{2}h, \frac{1}{2}h\right)\ Eh}{4P\left(\frac{l}{h}\right)^3}\ 10^2$$

$$\bar{w}_e = \left[1 + \frac{3}{4}(1+\nu)\frac{h}{l}^2\right]\ 10^2$$

See Appendix C.

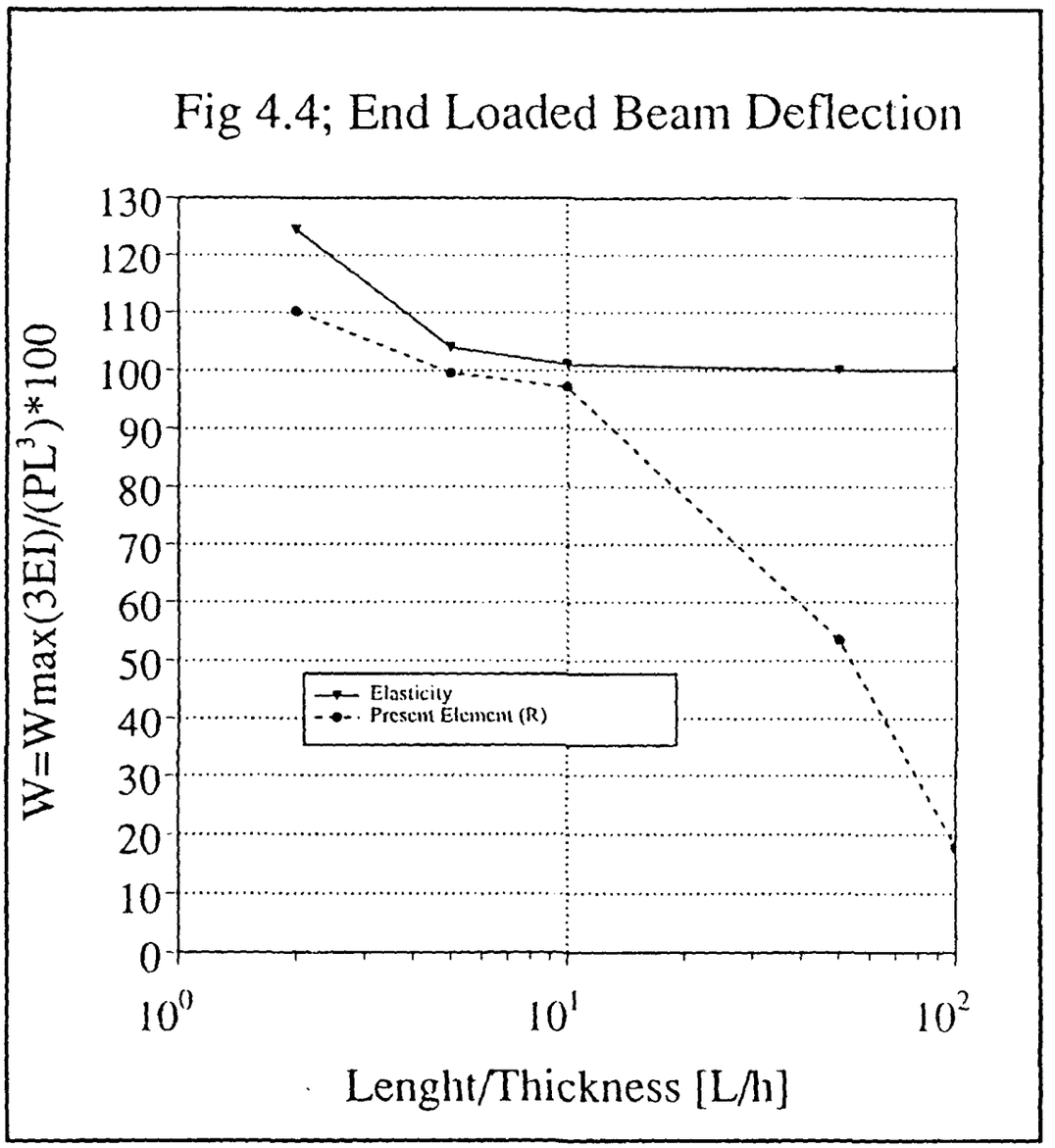

Figure 4.4: End Loaded Beam Deflection

is compared with the elasticity solution (See Appendix C for details on elasticity solutions).

Invoking symmetry conditions of the problem, a quarter of the plate is modeled with the following boundary conditions imposed:

$$u\left(0,\ y,\ \pm\frac{h}{2}\right) = v\left(o,\ y,\ \pm\frac{h}{2}\right) = w\left(0,\ y,\ \pm\frac{h}{2}\right) = 0 \tag{4.2}$$

$$u\left(x,\ 0,\ \pm\frac{h}{2}\right) = v\left(x,\ 0\ \pm\frac{h}{2}\right) = w\left(x,\ 0,\ \pm\frac{h}{2}\right) = 0 \tag{4.3}$$

and the symmetry conditions.

$$u\left(\frac{a}{2},\ y,\ z\right) = v\left(x,\ \frac{a}{2},\ z\right) = 0 \tag{4.4}$$

The load was taken as one quarter of the total load. Figure 4.6 shows the comparison of a mesh composed of elements arranged in one row of elements (N x N x 1) vs. a mesh of the type (2 x 2 x M), composed of M rows of elements arranged in the thickness direction with 2 x 2 elements in each row. Full integration is employed in the computations. Table 4.4 summarizes the resultant deflection and mesh sizes. It is clear from this and the previous examples that one row of elements in the thickness direction is adequate to predict the response of the structures. Figure 4.7 presents the convergence characteristics of three integration schemes. It may be noted that reduced integration (3 x 3 x 2) in the thickness direction yields very close results to that of the full integration scheme. Reduced integration produces good results by compensating for the estimation of finite element approximation. The in-plane reduced integration scheme (3 x 2 x 2) shows divergence in the computed response. It may be mentioned that using one element to model quarter plate resulted in much higher deflection than expected. This implies that a one element model contains spurious modes and a one-element modeling of plate/shell problem should be avoided. On examining the convergence plot, with less than 600 d.o.f., the

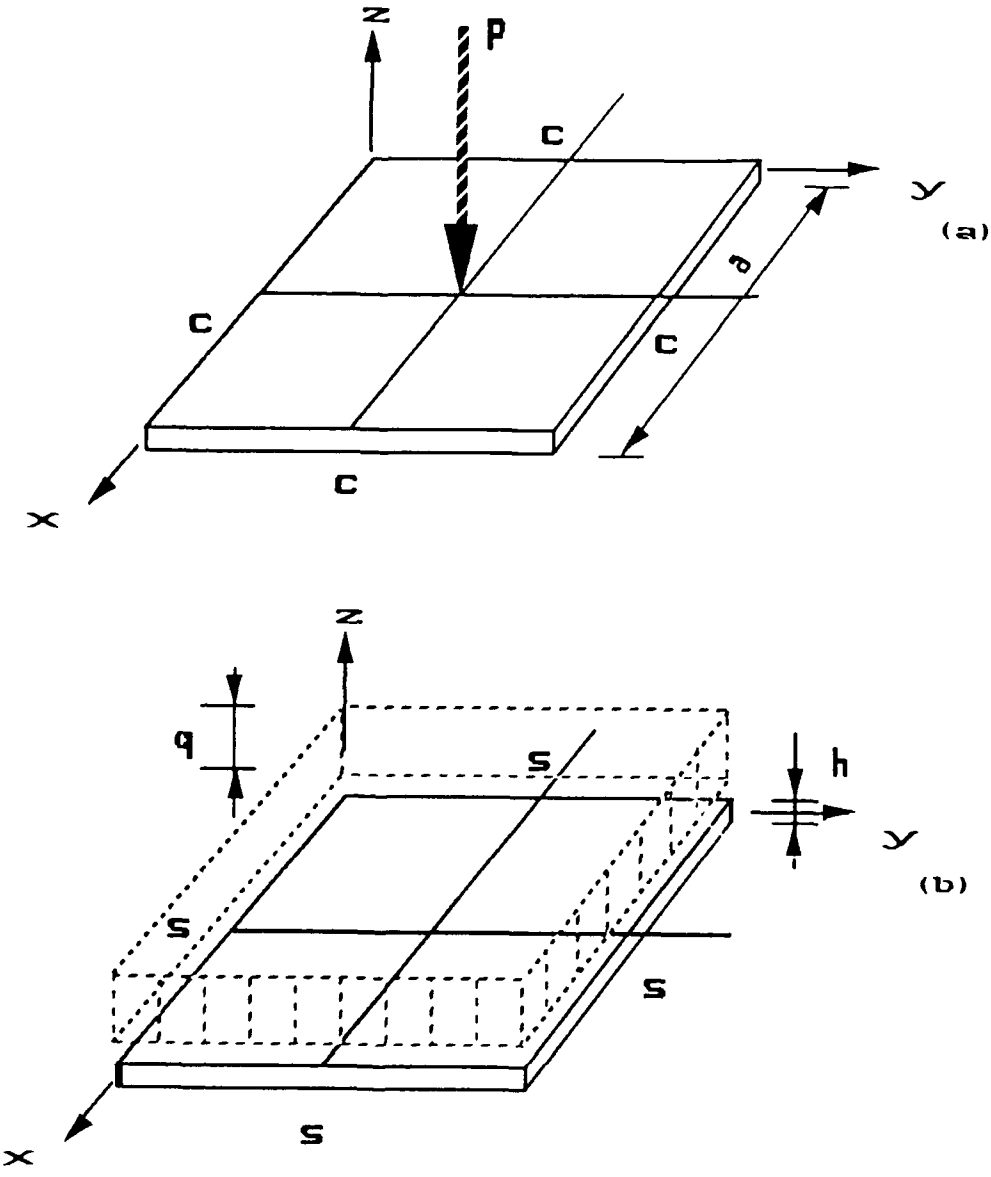

Fig. 4.5; Plate Sample problems

Figure 4.5: Plate Sample Problems

TABLE 4.4: MESH COMPARISON OF AN ALL EDGES CLAMPED RECTANGULAR ISOTROPIC PLATE UNDER CENTRAL LOAD ($\frac{1}{4}$P = 1000 lb.)

Mesh	# d.o.f.	w
1 = 1 x 1 x 1	37	13.8529
4 = 2 x 2 x 1	145	4.2230
9 = 3 x 3 x 1	325	5.0690
16 = 4 x 4 x 1	577	5.6592
8 = 2 x 2 x 2	275	4.0133
12 = 2 x 2 x 3	405	3.9955
16 = 2 x 2 x 4	535	3.9597
18 = 3 x 3 x 2	591	5.0647

$$w = \frac{w\left(\frac{a}{2}, \frac{a}{2}, h\right) Eh^3}{p\, a^2} 100$$

evaluated deflection is within 90% of the elasticity solution. Table 4.5 summarizes the effects of various integration schemes and mesh sizes.

D. SIMPLY SUPPORTED PLATES

Bending of a simply supported rectangular plate under uniformly distributed force is presented herein. (See Figure 4.5b) Both isotropic and laminated plates are investigated using one quarter of the plate, as discussed previously. The results are

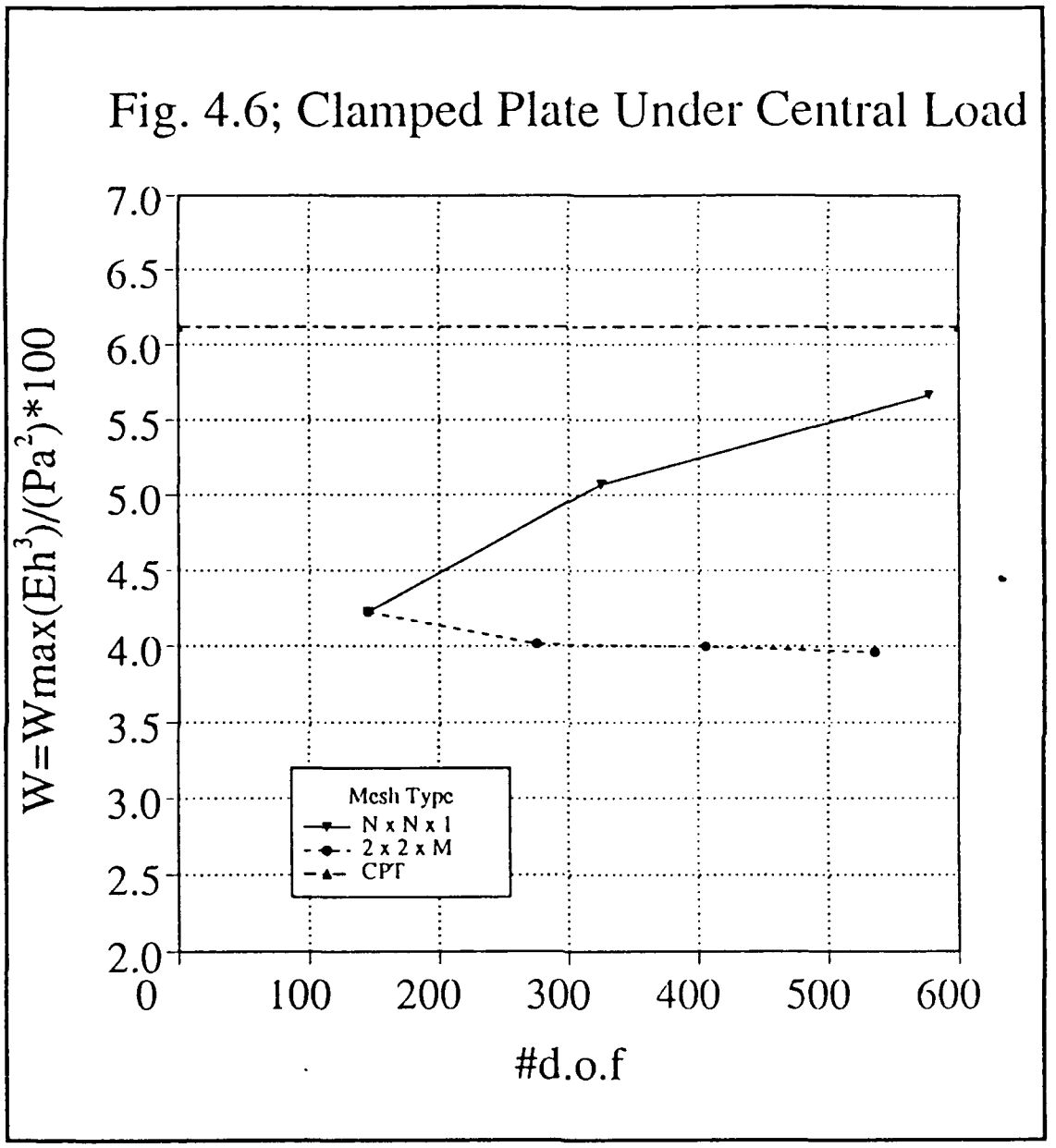

Figure 4.6: Clamped Plate Under Central Load

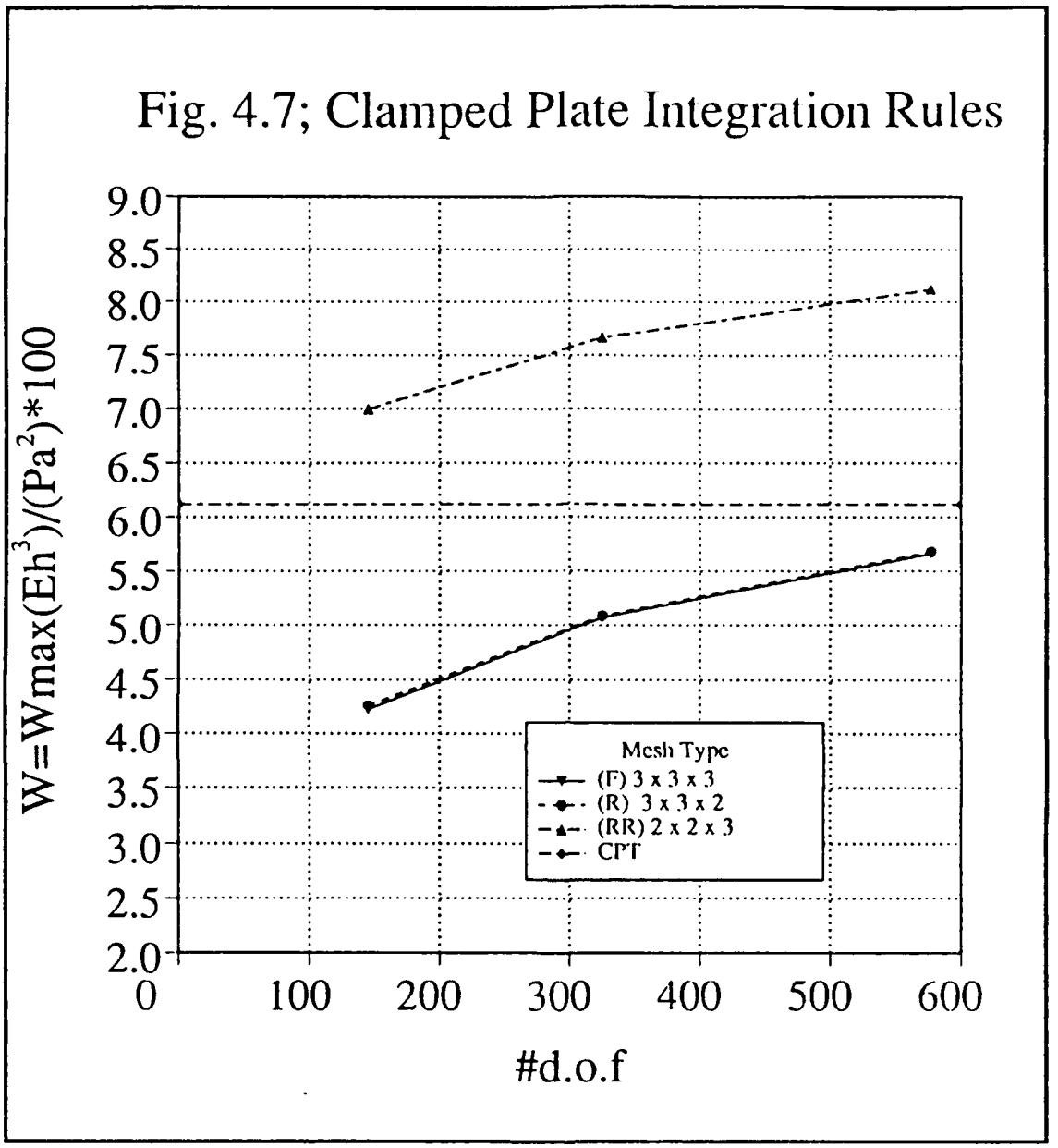

Figure 4.7: Clamped Plate Integration Rules

TABLE 4.5: INTEGRATION RULES COMPARISON OF AN ALL EDGES CLAMPED RECTANGULAR ISOTROPIC PLATE UNDER CENTRAL LOAD ($\frac{1}{4}$P = 1000)

Mesh	# d.o.f.	w for various integration rules		
		(3 x 3 x 3)	(3 x 3 x 2)	(2 x 2 x 3)
4 = 2 x 2 x 1	145	4.2230	4.2575	6.9918
9 = 3 x 3 x 1	325	5.0690	5.0853	7.6576
16 = 4 x 4 x 1	577	5.6592	5.6763	8.1128

$$w = \frac{w\left(\frac{a}{2}, \frac{a}{2}, h\right) Eh^3}{P a^2} 100$$

compared with Classical Plate Theory (CPT) as given in Appendix C and higher order shear-deformation (HSDT) plate theories [Reddy, 1985, Lo et al., 1977].

The following boundary conditions are imposed,

$$w\left(0,\, y,\, \pm\frac{h}{2}\right) = w\left(x,\, 0,\, \pm\frac{h}{2}\right) = 0 \tag{4.5}$$

and the symmetry conditions are as given in equation 4.4. Reduced integration (3 x 3 x 2) is adapted throughout all the computations presented in this section. The convergence characteristics of the element and comparison to CPT is depicted in Figures 4.8 and 4.9 for both isotropic and laminated plates. In the isotropic case, the present element shows convergence within 90% of the elasticity solution for less than 200 d.o.f. In the case of laminated plates, (Figure 4.9), the classical solution [Vinson, 1987] gives a more flexible solution than the present element. Table 4.6 summarizes the deflections of the isotropic and laminated plates and mesh sizes. It may be noted that the classical solution uses laminate theory, which neglects the transverse shear stresses, and hence the contribution of these stresses is not taken into account. This assumes more significance for thick plates $\left(\frac{a}{h} < 10 \text{ to } 15\right)$. Furthermore, when the plate stiffness in the thickness direction is significantly lower than its stiffness in the in-plane direction and when the shear modulus in the thickness direction is significant, the classical laminate theory does not predict the response of the structure accurately. In the present example, $\frac{a}{h} = 20$ and $\frac{E_1}{E_2} = 40$, $G_{13} \approx G_{12}$. It may be concluded that using laminate theory for bending of thick plates yields a nonconservative estimate of deflections and special attention should be given to the stiffness ratio $\left[\frac{E_2}{E_1}\right]$ and shear modulus ratio $\left[\frac{G_{23}}{G_{12}}\right]$ in determining the response of such plates. In Figures 4.10 and 4.11, the maximum deflection is presented for different aspect ratios, $\left(\frac{a}{h}\right)$, of the plate. Both isotropic and laminated plates are analyzed and compared to CPT. In addition, the solution of the laminated plate is

also compared to Higher Order Shear Deformation Theory [Reddy, 1985], as shown in Table 4.7.

As in the beam bending case, shear locking is observed for thin isotropic plates. For thick plates, $\left(\text{say, } \frac{a}{h} = 4\right)$, the computed deflections become significantly larger than predicted by CPT, as expected.

Examining Figure 4.11, it may be deduced that even the HSDT [Reddy, 1985] underpredicts the deflections. For thin laminated plates, the shear locking effect is not as significant as observed for isotropic plates. This may be attributed to the fact the laminated plate has more flexible transverse material stiffness in bending than the coefficients than the isotropic plate, so that shear locking is expected to develop only for thin isotropic plates.

TABLE 4.6: ALL EDGES SIMPLY SUPPORTED RECTANGULAR PLATE, UNDER UNIFORMLY DISTRIBUTED LOAD

Mesh	# d.o.f.	Isotropic w	Composite w
4 = 2 x 2 x 1	186	3.2826	0.3871
9 = 3 x 3 x 1	386	3.6335	0.3878
16 = 4 x 4 x 1	658	4.0541	0.4053
CPT		4.4335	*0.3634

* Neglects G_{13} and G_{23}. See Appendix C.

The uniformly distributed load is taken as the total consistent load over the area of the quarter plate.

$$q = \frac{F}{\left(\frac{1}{2}a\right)^2}$$

The maximum deflection is taken at upper surface.

$$w = \frac{w\left(\frac{a}{2}, \frac{a}{2}, h\right) E_2 h^3}{q\, a^4} 100$$

TABLE 4.7: CENTER DEFLECTION VS. ASPECT RATIO OF SIMPLY SUPPORTED RECTANGULAR PLATE UNDER UNIFORMLY DISTRIBUTED LOAD

$\frac{a}{h}$	Isotropic w	Orthotropic w	Reference* w
4	9.8275	5.1324	1.6340
10	4.9581	0.8221	0.5904
20	4.0541	0.4053	0.4336
100	1.0902	0.2406	0.3769
CPT	4.4335	0.3634	

*Reference: Reddy, 1985.

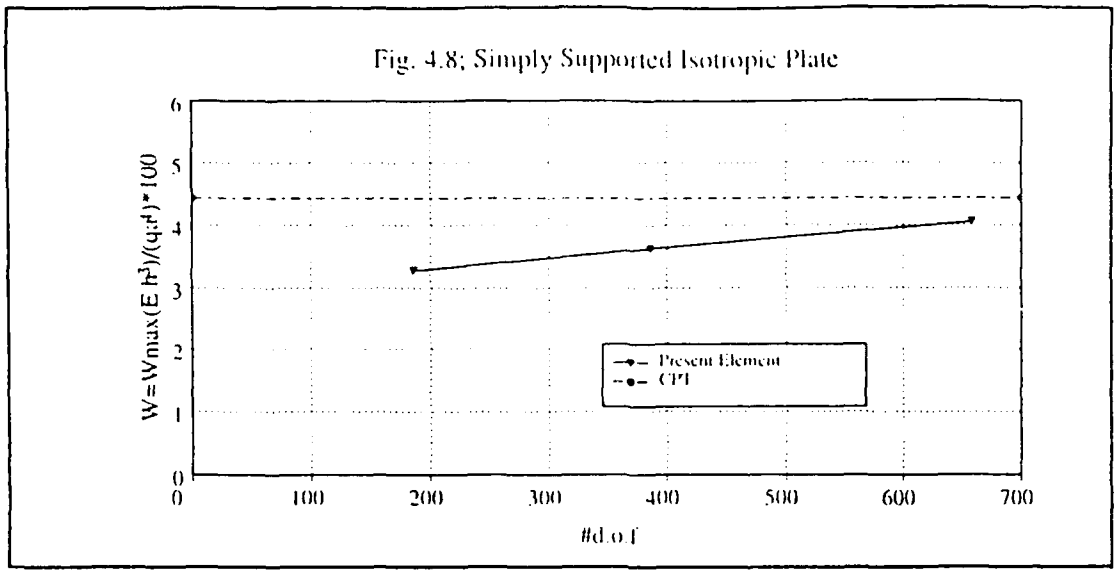

Figure 4.8: Simply Supported Isotropic Plate

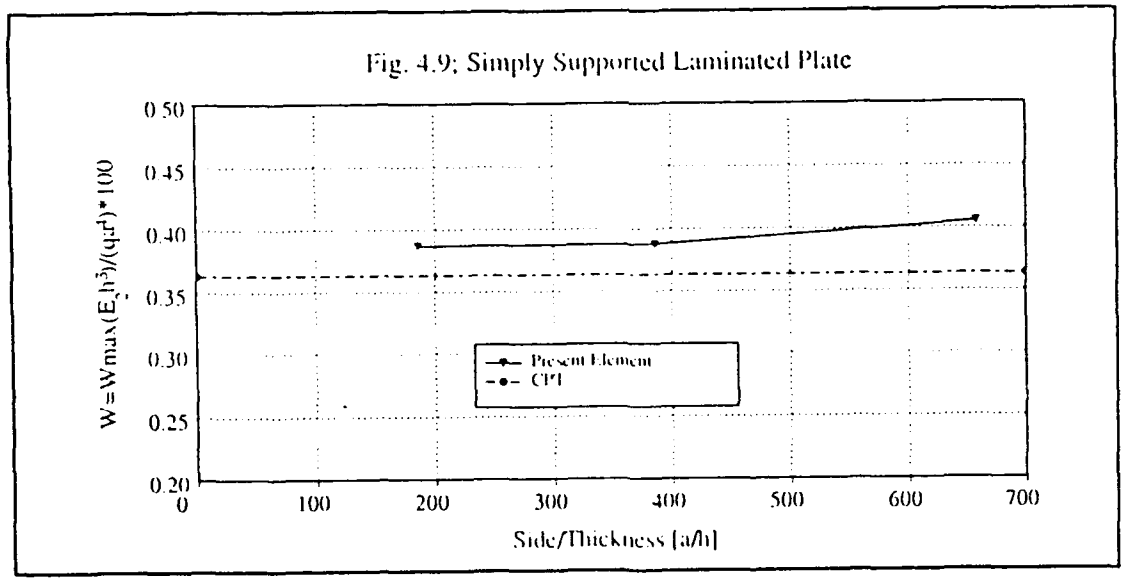

Figure 4.9: Simply Supported Laminated Plate

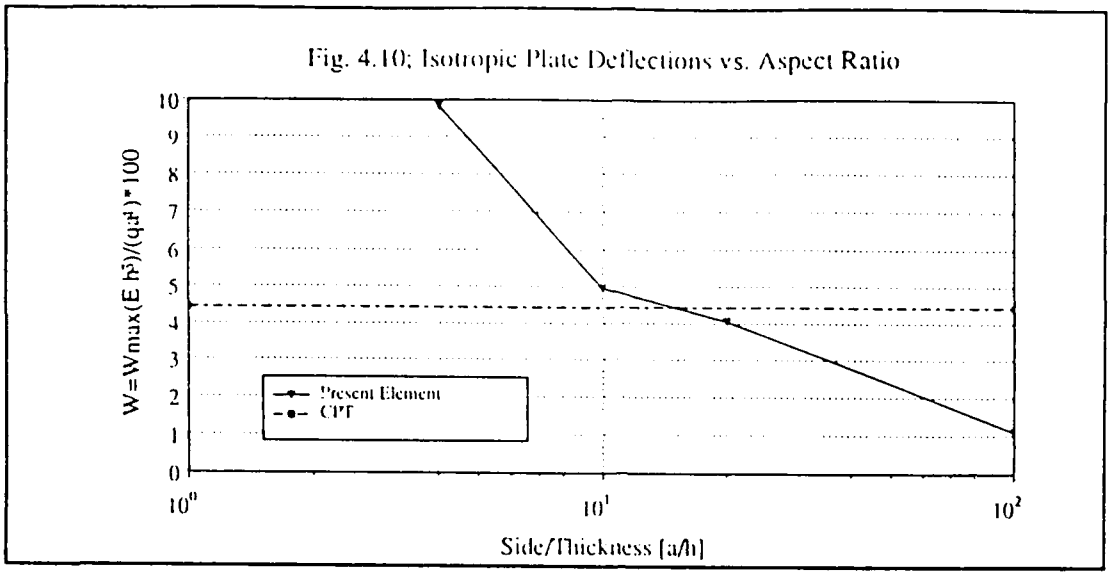

Figure 4.10: Isotropic Plate Deflections vs. Aspect Ratio

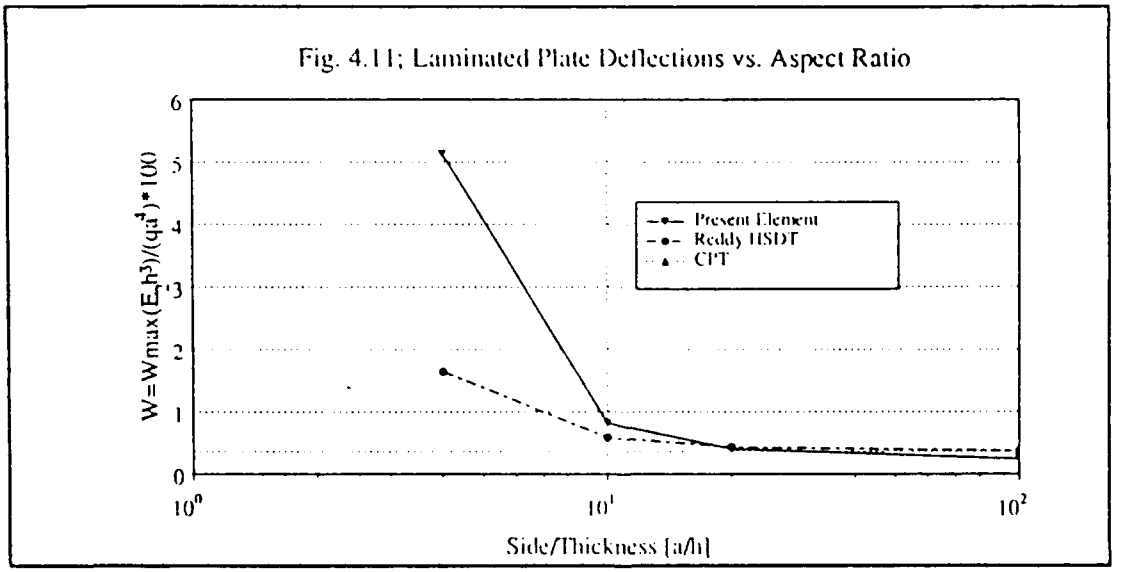

Figure 4.11: Laminated Plate Deflection vs. Aspect Ratio

V. CONCLUSIONS AND SCOPE FOR FUTURE RESEARCH

A. CONCLUSIONS

This study suggests a three-dimensional higher-order finite element to be incorporated in the analysis of thick plates composed of both isotropic and laminated composites. By using a tri-quadratic Lagrangian twenty seven noded solid element, no assumptions on transverse shear strains are introduced in the formulation. The formulation, based on the principle of virtual work, is presented for both linear and nonlinear analysis. The material constitutive relations for linear isotropic and composite materials are presented. For composites, both laminate theory and three dimensional anisotropic adaptations are described.

Several numerical examples using linear analysis are given for bars/beams and plates using both isotropic and composite materials. Three dimensional anisotropic relations are adapted for composites. The results show that the present element is effective for analysis of thick beams and plates, but exhibits shear locking for thin beam and plates.

Spurious modes are revealed for single element usage in plate modeling, as is the case for some other finite elements.

Reduced Integration in the thickness direction for beams and plates gives satisfactory results. An interesting outcome is that one element is sufficient to capture transverse deformation for thick laminated structures and mesh refinement in the other two directions yields convergent solutions.

B. SCOPE FOR FUTURE RESEARCH

More numerical experiments need to be performed to compare the present solution to closed-form solutions [Pagano, 1969] to evaluate the efficacy of this element.

Implementation of buckling analysis using the nonlinear element matrices presented herein is another task that may prove useful in predicting buckling response of thick composite cylinders subject to external pressure. By incorporating the centrifugal force in the external virtual work done by body forces, this element may be used in modeling rotor blades.

APPENDIX A
Shape Functions and Derivatives for Solid Element

Shape Functions for Solid Element

Mid-edge nodes:

$$
\begin{aligned}
N_2 &= \tfrac{1}{4} r\,(1+r)\,(1-s^2)\,t\,(1+t) \\
N_4 &= \tfrac{1}{4}\,(1-r^2)\,s\,(1+s)\,t\,(1+t) \\
N_6 &= -\tfrac{1}{4} r\,(1-r)\,(1-s^2)\,t\,(1+t) \\
N_8 &= -\tfrac{1}{4}\,(1-r^2)\,s\,(1-s)\,t\,(1+t) \\
N_{10} &= -\tfrac{1}{4} r\,(1+r)\,s\,(1-s)\,(1-t^2) \\
N_{12} &= \tfrac{1}{4} r\,(1+r)\,s\,(1+s)\,(1-t^2) \\
N_{14} &= -\tfrac{1}{4} r\,(1-r)\,s\,(1+s)\,(1-t^2) \\
N_{16} &= \tfrac{1}{4} r\,(1-r)\,s\,(1-s)\,(1-t^2) \\
N_{20} &= -\tfrac{1}{4} r\,(1+r)\,(1-s^2)\,t\,(1-t) \\
N_{22} &= -\tfrac{1}{4}\,(1-r^2)\,s\,(1+s)\,t\,(1-t) \\
N_{24} &= \tfrac{1}{4} r\,(1-r)\,(1-s^2)\,t\,(1-t) \\
N_{26} &= \tfrac{1}{4} r\,(1-r^2)\,s\,(1-s)\,t\,(1-t)
\end{aligned}
$$

Mid-plane nodes:

$$
\begin{aligned}
N_9 &= \tfrac{1}{2}\,(1-r^2)\,(1-s^2)\,t\,(1+t) \\
N_{27} &= -\tfrac{1}{2}\,(1-r^2)\,(1-s^2)\,t\,(1-t) \\
N_{11} &= \tfrac{1}{2} r\,(1+r)\,(1-s^2)\,(1-t^2) \\
N_{15} &= -\tfrac{1}{2} r\,(1-r)\,(1-s^2)\,(1-t^2) \\
N_{13} &= \tfrac{1}{2}\,(1-r^2)\,s\,(1+s)\,(1-t^2) \\
N_{17} &= -\tfrac{1}{2}\,(1-r^2)\,s\,(1-s)\,(1-t^2)
\end{aligned}
$$

Center node:

$$N_{18} = (1-r^2)\,(1-s^2)\,(1-t^2)$$

Corner nodes:

$$
\begin{aligned}
N_1 &= \frac{1}{8}(1+r)(1-s)(1+t) - \frac{1}{2}(N_2+N_8+N_{10}) - \frac{1}{4}(N_{11}+N_{17}+N_9) - \frac{1}{8}N_{18} \\
N_3 &= \frac{1}{8}(1+r)(1+s)(1+t) - \frac{1}{2}(N_2+N_4+N_{12}) - \frac{1}{4}(N_{11}+N_{13}+N_9) - \frac{1}{8}N_{18} \\
N_5 &= \frac{1}{8}(1-r)(1+s)(1+t) - \frac{1}{2}(N_4+N_6+N_{14}) - \frac{1}{4}(N_{13}+N_{15}+N_9) - \frac{1}{8}N_{18} \\
N_7 &= \frac{1}{8}(1-r)(1-s)(1+t) - \frac{1}{2}(N_6+N_8+N_{16}) - \frac{1}{4}(N_{15}+N_{17}+N_9) - \frac{1}{8}N_{18} \\
N_{19} &= \frac{1}{8}(1+r)(1-s)(1-t) - \frac{1}{2}(N_{20}+N_{26}+N_{10}) - \frac{1}{4}(N_{11}+N_{17}+N_{27}) - \frac{1}{8}N_{18} \\
N_{21} &= \frac{1}{8}(1+r)(1+s)(1-t) - \frac{1}{2}(N_{20}+N_{22}+N_{12}) - \frac{1}{4}(N_{11}+N_{13}+N_{27}) - \frac{1}{8}N_{18} \\
N_{23} &= \frac{1}{8}(1-r)(1+s)(1-t) - \frac{1}{2}(N_{22}+N_{24}+N_{14}) - \frac{1}{4}(N_{13}+N_{15}+N_{27}) - \frac{1}{8}N_{18} \\
N_{25} &= \frac{1}{8}(1-r)(1-s)(1-t) - \frac{1}{2}(N_{24}+N_{26}+N_{16}) - \frac{1}{4}(N_{15}+N_{17}+N_{27}) - \frac{1}{8}N_{18}
\end{aligned}
$$

Shape Function Derivatives for Solid Element - r direction

Mid-edge nodes:

$$
\begin{aligned}
N_{2,r} &= \tfrac{1}{4}t\,(1+2r)\,(1-s^2)\,(1+t) \\
N_{4,r} &= -\tfrac{1}{2}\,rst\,(1+s)\,(1+t) \\
N_{6,r} &= -\tfrac{1}{4}t\,(1-2r)\,(1-s^2)\,(1+t) \\
N_{8,r} &= \tfrac{1}{2}\,rst\,(1-s)\,(1+t) \\
N_{10,r} &= -\tfrac{1}{4}s\,(1+2r)\,(1-s)\,(1-t^2) \\
N_{12,r} &= \tfrac{1}{4}s\,(1+2r)\,(1+s)\,(1-t^2) \\
N_{14,r} &= -\tfrac{1}{4}s\,(1-2r)\,(1+s)\,(1-t^2) \\
N_{16,r} &= \tfrac{1}{4}s\,(1-2r)\,(1-s)\,(1-t^2) \\
N_{20,r} &= -\tfrac{1}{4}t\,(1+2r)\,(1-s^2)\,(1-t) \\
N_{22,r} &= -\tfrac{1}{2}rst\,(1+s)\,(1-t) \\
N_{24,r} &= \tfrac{1}{4}t\,(1-2r)\,(1-s^2)\,(1-t) \\
N_{26,r} &= -\tfrac{1}{2}rst\,(1-s)\,(1-t)
\end{aligned}
$$

Mid-plane nodes:

$$
\begin{aligned}
N_{9,r} &= -rt\,(1-s^2)\,(1+t) \\
N_{27,r} &= rt\,(1-s^2)\,(1-t) \\
N_{11,r} &= \tfrac{1}{2}\,(1+2r)\,(1-s^2)\,(1-t^2) \\
N_{15,r} &= -\tfrac{1}{2}\,(1-2r)\,(1-s^2)\,(1-t^2) \\
N_{13,r} &= -rs\,(1+s)\,(1-t^2) \\
N_{17,r} &= rs\,(1-s)\,(1-t^2)
\end{aligned}
$$

Center node:

$$N_{18,r} = -2r(1-s^2)\,(1-t^2)$$

Corner nodes:

$$
\begin{aligned}
N_{1,r} &= \frac{1}{8}\,(1-s)\,(1+t) - \frac{1}{2}\,(N_{2,r}+N_{8,r}+N_{10,r}) - \frac{1}{4}\,(N_{11,r}+N_{17,r}+N_{9,r}) - \frac{1}{8}N_{18,r} \\
N_{3,r} &= \frac{1}{8}\,(1+s)\,(1+t) - \frac{1}{2}\,(N_{2,r}+N_{4,r}+N_{12,r}) - \frac{1}{4}\,(N_{11,r}+N_{13,r}+N_{9,r}) - \frac{1}{8}N_{18,r} \\
N_{5,r} &= -\frac{1}{8}\,(1+s)\,(1+t) - \frac{1}{2}\,(N_{4,r}+N_{6,r}+N_{14,r}) - \frac{1}{4}\,(N_{13,r}+N_{15,r}+N_{9,r}) - \frac{1}{8}N_{18,r} \\
N_{7,r} &= -\frac{1}{8}\,(1-s)\,(1+t) - \frac{1}{2}\,(N_{6,r}+N_{8,r}+N_{16,r}) - \frac{1}{4}\,(N_{15,r}+N_{17,r}+N_{9,r}) - \frac{1}{8}N_{18,r} \\
N_{19,r} &= \frac{1}{8}\,(1-s)\,(1-t) - \frac{1}{2}\,(N_{20,r}+N_{26,r}+N_{10,r}) - \frac{1}{4}\,(N_{11,r}+N_{17,r}+N_{27,r}) - \frac{1}{8}N_{18,r} \\
N_{21,r} &= \frac{1}{8}\,(1+s)\,(1-t) - \frac{1}{2}\,(N_{20,r}+N_{22,r}+N_{12,r}) - \frac{1}{4}\,(N_{11,r}+N_{13,r}+N_{27,r}) - \frac{1}{8}N_{18,r} \\
N_{23,r} &= -\frac{1}{8}\,(1+s)\,(1-t) - \frac{1}{2}\,(N_{22,r}+N_{24,r}+N_{14,r}) - \frac{1}{4}\,(N_{13,r}+N_{15,r}+N_{27,r}) - \frac{1}{8}N_{18,r} \\
N_{25,r} &= -\frac{1}{8}\,(1-s)\,(1-t) - \frac{1}{2}\,(N_{24,r}+N_{26,r}+N_{16,r}) - \frac{1}{4}\,(N_{15,r}+N_{17,r}+N_{27,r}) - \frac{1}{8}N_{18,r}
\end{aligned}
$$

Shape Function Derivatives for Solid Element - s direction

Mid-edge nodes:

$$
\begin{aligned}
N_{2,s} &= -\tfrac{1}{2} rst\,(1+r)\,(1+t) \\
N_{4,s} &= \tfrac{1}{4} t\,(1-r^2)\,(1+2s)\,(1+t) \\
N_{6,s} &= \tfrac{1}{2} rst\,(1-r)\,(1+t) \\
N_{8,s} &= -\tfrac{1}{4} t\,(1-r^2)\,(1-2s)\,(1+t) \\
N_{10,s} &= -\tfrac{1}{4} r\,(1+r)\,(1-2s)\,(1-t^2) \\
N_{12,s} &= \tfrac{1}{4} r\,(1+r)\,(1+2s)\,(1-t^2) \\
N_{14,s} &= -\tfrac{1}{4} r\,(1-r)\,(1+2s)\,(1-t^2) \\
N_{16,s} &= \tfrac{1}{4} r\,(1-r)\,(1-2s)\,(1-t^2) \\
N_{20,s} &= \tfrac{1}{2} rst\,(1+r)\,(1-t) \\
N_{22,s} &= -\tfrac{1}{4} t\,(1-r^2)\,(1+2s)\,(1-t) \\
N_{24,s} &= -\tfrac{1}{2} rst\,(1-r)\,(1-t) \\
N_{26,r} &= \tfrac{1}{4} t\,(1-r^2)\,(1-2s)\,(1-t)
\end{aligned}
$$

Mid-plane nodes:

$$
\begin{aligned}
N_{9,s} &= -st\,(1-r^2)\,(1+t) \\
N_{27,s} &= st\,(1-r^2)\,(1-t) \\
N_{11,s} &= -rs\,(1+r)\,(1-t^2) \\
N_{15,s} &= rs\,(1-r)\,(1-t^2) \\
N_{13,s} &= \tfrac{1}{2}(1-r^2)\,(1+2s)\,(1-t^2) \\
N_{17,s} &= -\tfrac{1}{2}\,(1-r^2)\,(1-2s)\,(1-t^2)
\end{aligned}
$$

Center node:

$$N_{18,s} = -2s(1-r^2)\,(1-t^2)$$

Corner nodes:

$$
\begin{aligned}
N_{1,s} &= -\frac{1}{8}(1+r)\,(1+t) - \frac{1}{2}(N_{2,s}+N_{8,s}+N_{10,s}) - \frac{1}{4}(N_{11,s}+N_{17,s}+N_{9,s}) - \frac{1}{8}N_{18,s} \\
N_{3,s} &= \frac{1}{8}(1+r)\,(1+t) - \frac{1}{2}(N_{2,s}+N_{4,s}+N_{12,s}) - \frac{1}{4}(N_{11,s}+N_{13,s}+N_{9,s}) - \frac{1}{8}N_{18,s} \\
N_{5,s} &= \frac{1}{8}(1-r)\,(1+t) - \frac{1}{2}(N_{4,s}+N_{6,s}+N_{14,s}) - \frac{1}{4}(N_{13,s}+N_{15,s}+N_{9,s}) - \frac{1}{8}N_{18,s} \\
N_{7,s} &= -\frac{1}{8}(1-r)\,(1+t) - \frac{1}{2}(N_{6,s}+N_{8,s}+N_{16,s}) - \frac{1}{4}(N_{15,s}+N_{17,s}+N_{9,s}) - \frac{1}{8}N_{18,s} \\
N_{19,s} &= -\frac{1}{8}(1+r)\,(1-t) - \frac{1}{2}(N_{20,s}+N_{26,s}+N_{10,s}) - \frac{1}{4}(N_{11,s}+N_{17,s}+N_{27,s}) - \frac{1}{8}N_{18,s} \\
N_{21,s} &= \frac{1}{8}(1+r)\,(1-t) - \frac{1}{2}(N_{20,s}+N_{22,s}+N_{12,s}) - \frac{1}{4}(N_{11,s}+N_{13,s}+N_{27,s}) - \frac{1}{8}N_{18,s} \\
N_{23,s} &= \frac{1}{8}(1-r)\,(1-t) - \frac{1}{2}(N_{22,s}+N_{24,s}+N_{14,s}) - \frac{1}{4}(N_{13,s}+N_{15,s}+N_{27,s}) - \frac{1}{8}N_{18,s} \\
N_{25,s} &= -\frac{1}{8}(1-r)\,(1-t) - \frac{1}{2}(N_{24,s}+N_{26,s}+N_{16,s}) - \frac{1}{4}(N_{15,s}+N_{17,s}+N_{27,s}) - \frac{1}{8}N_{18,s}
\end{aligned}
$$

Shape Function Derivatives for Solid Element - t direction

Mid-edge nodes:

$$
\begin{aligned}
N_{2,t} &= \tfrac{1}{4}t\,(1+r)\,(1-s^2)\,(1+2t) \\
N_{4,t} &= \tfrac{1}{4}s\,(1-r^2)\,(1+s)\,(1+2t) \\
N_{6,t} &= -\tfrac{1}{4}r\,(1-r)\,(1-s^2)\,(1+2t) \\
N_{8,t} &= -\tfrac{1}{4}s\,(1-r^2)\,(1-s)\,(1+2t) \\
N_{10,t} &= \tfrac{1}{2}rst\,(1+r)\,(1-s) \\
N_{12,t} &= -\tfrac{1}{2}rst\,(1+r)\,(1+s) \\
N_{14,t} &= \tfrac{1}{2}rst\,(1-r)\,(1+s) \\
N_{16,t} &= -\tfrac{1}{2}rst\,(1-r)\,(1-s) \\
N_{20,t} &= -\tfrac{1}{4}r\,(1+r)\,(1-s^2)\,(1-2t) \\
N_{22,t} &= -\tfrac{1}{4}s\,(1-r^2)\,(1+s)\,(1-2t) \\
N_{24,t} &= \tfrac{1}{4}r\,(1-r)\,(1-s^2)\,(1-2t) \\
N_{26,t} &= \tfrac{1}{4}s\,(1-r^2)\,(1-s)\,(1-2t)
\end{aligned}
$$

Mid-plane nodes:

$$
\begin{aligned}
N_{9,r} &= \tfrac{1}{2}\,(1-r^2)\,(1-s^2)\,(1+2t) \\
N_{27,t} &= -\tfrac{1}{2}\,(1-r^2)\,(1-s^2)\,(1-2t) \\
N_{11,t} &= -rt\,(1+r)\,(1-s^2) \\
N_{15,t} &= rt\,(1-r)\,(1-s^2) \\
N_{13,t} &= -st\,(1-r^2)\,(1+s) \\
N_{17,t} &= st\,(1-r^2)\,(1-s)
\end{aligned}
$$

Center node:

$$N_{18,t} = -2t(1-r^2)\,(1-s^2)$$

Corner nodes:

$$
\begin{aligned}
N_{1,t} &= \frac{1}{8}(1+r)(1-s) - \frac{1}{2}(N_{2,t}+N_{8,t}+N_{10,t}) - \frac{1}{4}(N_{11,t}+N_{17,t}+N_{9,t}) - \frac{1}{8}N_{18,t} \\
N_{3,t} &= \frac{1}{8}(1+r)(1+s) - \frac{1}{2}(N_{2,t}+N_{4,t}+N_{12,t}) - \frac{1}{4}(N_{11,t}+N_{13,t}+N_{9,t}) - \frac{1}{8}N_{18,t} \\
N_{5,t} &= \frac{1}{8}(1-r)(1+s) - \frac{1}{2}(N_{4,t}+N_{6,t}+N_{14,t}) - \frac{1}{4}(N_{13,t}+N_{15,t}+N_{9,t}) - \frac{1}{8}N_{18,t} \\
N_{7,t} &= \frac{1}{8}(1-r)(1-s) - \frac{1}{2}(N_{6,t}+N_{8,t}+N_{16,t}) - \frac{1}{4}(N_{15,t}+N_{17,t}+N_{9,t}) - \frac{1}{8}N_{18,t} \\
N_{19,t} &= -\frac{1}{8}(1+r)(1-s) - \frac{1}{2}(N_{20,t}+N_{26,t}+N_{10,t}) - \frac{1}{4}(N_{11,t}+N_{17,t}+N_{27,t}) - \frac{1}{8}N_{18,t} \\
N_{21,t} &= -\frac{1}{8}(1+r)(1+s) - \frac{1}{2}(N_{20,t}+N_{22,t}+N_{12,t}) - \frac{1}{4}(N_{11,t}+N_{13,t}+N_{27,t}) - \frac{1}{8}N_{18,t} \\
N_{23,t} &= -\frac{1}{8}(1-r)(1+s) - \frac{1}{2}(N_{22,t}+N_{24,t}+N_{14,t}) - \frac{1}{4}(N_{13,t}+N_{15,t}+N_{27,t}) - \frac{1}{8}N_{18,t} \\
N_{25,t} &= -\frac{1}{8}(1-r)(1-s) - \frac{1}{2}(N_{24,t}+N_{26,t}+N_{16,t}) - \frac{1}{4}(N_{15,t}+N_{17,t}+N_{27,t}) - \frac{1}{8}N_{18,t}
\end{aligned}
$$

APPENDIX B
Jacobian Matrix

Jacobian matrix elements:

$$
\begin{aligned}
J_{11} = x_{,r} &= \sum_{i=1}^{27} N_{i,r}\, x_i \\
J_{12} = y_{,r} &= \sum_{i=1}^{27} N_{i,r}\, y_i \\
J_{13} = z_{,r} &= \sum_{i=1}^{27} N_{i,r}\, z_i \\
J_{21} = x_{,s} &= \sum_{i=1}^{27} N_{i,s}\, x_i \\
J_{22} = y_{,s} &= \sum_{i=1}^{27} N_{i,s}\, y_i \\
J_{23} = z_{,s} &= \sum_{i=1}^{27} N_{i,s}\, z_i \\
J_{31} = x_{,t} &= \sum_{i=1}^{27} N_{i,t}\, x_i \\
J_{32} = y_{,t} &= \sum_{i=1}^{27} N_{i,t}\, y_i \\
J_{33} = z_{,t} &= \sum_{i=1}^{27} N_{i,t}\, z_i
\end{aligned}
$$

Elements of the inverse Jacobian matrix:

$$
\begin{aligned}
\Gamma_{11} &= \frac{1}{J}\left(J_{22}\, J_{33} - J_{23}\, J_{32}\right) \\
\Gamma_{12} &= \frac{1}{J}\left(J_{13}\, J_{32} - J_{12}\, J_{33}\right) \\
\Gamma_{13} &= \frac{1}{J}\left(J_{12}\, J_{23} - J_{13}\, J_{22}\right) \\
\Gamma_{21} &= \frac{1}{J}\left(J_{23}\, J_{31} - J_{21}\, J_{33}\right)
\end{aligned}
$$

$$
\begin{aligned}
\Gamma_{22} &= \frac{1}{J}\left(J_{11}\, J_{33} - J_{13}\, J_{31}\right) \\
\Gamma_{23} &= \frac{1}{J}\left(J_{21}\, J_{13} - J_{11}\, J_{23}\right) \\
\Gamma_{31} &= \frac{1}{J}\left(J_{21}\, J_{32} - J_{22}\, J_{31}\right) \\
\Gamma_{32} &= \frac{1}{J}\left(J_{12}\, J_{31} - J_{11}\, J_{32}\right) \\
\Gamma_{33} &= \frac{1}{J}\left(J_{11}\, J_{22} - J_{21}\, J_{12}\right)
\end{aligned}
$$

Jacobian matrix determinant:

$$
\begin{aligned}
J = \det\left[J\right] &= J_{11}\left(J_{22}\, J_{33} - J_{23}\, J_{32}\right) \\
&- J_{12}\left(J_{21}\, J_{33} - J_{23}\, J_{31}\right) \\
&+ J_{13}\left(J_{21}\, J_{32} - J_{22}\, J_{31}\right)
\end{aligned}
$$

APPENDIX C

Theories

A. THEORY OF ELASTICITY SOLUTIONS

1. Cantilevered bar under traction

$$U_{max} = \frac{PL}{AE}$$

- P = Total load
- L = Bar length
- A = Cross section area
- E = Young modulus

2. Cantilevered Beam under end load

$$\begin{aligned} W_{max} &= \frac{PL^3}{3EI} + \frac{P\left(\frac{h}{2}\right)^2 l}{2IG} \\ &= \frac{PL^3}{3EI}\left[1 + \frac{3}{4}(1+V)\left(\frac{h}{L}\right)^2\right] \end{aligned}$$

Reference: Timoshenko, 1951.

B. CLASSICAL PLATE THEORY (CPT)

1. All edges clamped rectangular isotropic plate under central load

$$\begin{aligned} W_{max} &= \alpha\frac{Pa^2}{D} \\ D &= \frac{Eh^2}{12(1-\nu^2)} \\ \alpha &= 0.00560 \text{ for } \nu = 0.3 \end{aligned}$$

Reference: Timoshenko, 1959.

2. **All edges simply-supported, rectangular plate under uniformly distributed load**

$$W_{max} = \alpha \frac{qa^4}{D}$$

$$\alpha = 0\ 00406 \text{ for } \nu = 0.3$$

3. **Composite**

$$W_{max} = \frac{16}{\pi^6} qa^8 \prod_{m=1,3,5\ldots}^{\infty} \prod_{n=1,3,5\ldots}^{\infty} \frac{1}{mn\bar{D}}$$

$$\bar{D} = D_{11}m^4 + 2\left(D_{12} + 2D_{66}\right)(mn)^2 + D_{22}n^4$$

TABLE C-1

SAMPLE COMPOSITE MATERIAL DATA

Table C-1; Sample Composite Material Data

INPUT DATA ;

LAMINA	THKNES	THETA	E1	E2	V12	G12
8	0.12500	0.0	0.40000E+08	0.10000E+07	0.25	0.60000E+06
7	0.12500	45.0	0.40000E+08	0.10000E+07	0.25	0.60000E+06
6	0.12500	-45.0	0.40000E+08	0.10000E+07	0.25	0.60000E+06
5	0.12500	90.0	0.40000E+08	0.10000E+07	0.25	0.60000E+06
4	0.12500	90.0	0.40000E+08	0.10000E+07	0.25	0.60000E+06
3	0.12500	-45.0	0.40000E+08	0.10000E+07	0.25	0.60000E+06
2	0.12500	45.0	0.40000E+08	0.10000E+07	0.25	0.60000E+06
1	0.12500	0.0	0.40000E+08	0.10000E+07	0.25	0.60000E+06

OUTPUT DATA ;

A(i,j)-MATRIX

```
 0.12773E+08 0.55940E+07-0.81226E+06
 0.55940E+07 0.17603E+08-0.30995E+07
-0.81226E+06-0.30995E+07 0.59436E+07
```

B(i,j)-MATRIX

```
 0.00000E+00-0.27344E-01 0.00000E+00
-0.27344E-01-0.16406E+00 0.00000E+00
 0.00000E+00 0.00000E+00-0.62500E-01
```

D(i,j)-MATRIX

```
 0.20743E+07 0.28699E+06 0.72461E+05
 0.28699E+06 0.81544E+06 0.17998E+06
 0.72461E+05 0.17998E+06 0.31612E+06
```

Note; A,B and D matrices are evaluated ,neglecting Transverse Shear contribution i.e. G13=G23=0

Using Navier's solution with n=m=200, i.e. 100 terms for each direction, as given in the above, we have,

$$W_{max} = 0.052328$$

$$W = \frac{W_{max} * E * h^3}{q * a^4} * 100 = 0.3634$$

Where q=90 ; a=20

LIST OF REFERENCES

1. Allen, D. H. and Haisler, W. E., *Introduction to Aerospace Structural Analysis*, John Wiley & Sons, Inc., 1985.

2. Arnold, R. R., and Mayers, J., *Buckling, Postbuckling, and Crippling of Materially Nonlinear Laminated Composite Plates*, Stanford University, 1983.

3. Bathe, K. J., *Finite Element Procedures in Engineering Analysis*, Prentice-Hall, Inc., 1989.

4. CASA/GIFTS, Inc., *Computer Aided Structural Analysis/Graphical Interactive Finite Element Total System - Users Reference and Primer Manuals*, 1987.

5. Cook, M. P., *Concepts and Applications of Finite Element Analysis*, 3rd ed., John Wiley & Sons, Inc., 1989.

6. Eisley, J. G., *Mechanics of Elastic Structures*, Prentice-Hall, Inc., 1989.

7. Ford, B. W. R. and Stiemer, S. F., "Improved Arc Length Orthogonality Methods For Nonlinear Finite Element Analysis," *Journal of Computers & Structures*, Vol. 27, No. 5, pp. 345-353, 1987.

8. Gajbir, S. and Rao, S. Y. V. M., "Buckling of Composite Plates Using Simple Shear Flexible Finite Elements," *Composite Structures*, Vol. 11., #4, pp. 293-308, 1989.

9. Hoskin, B. C. and Baker, A. A., *Composite Materials for Aircraft Structures*, AIAA, 1986.

10. Hughes, T. J. R. and Cohen, M., "The 'Hetrosis' Finite Element For Plate Bending," *Journal of Computers & Structures*, Vol. 9, pp. 445-450, 1978.

11. Kolar, R. and Kamel, H. A., "On Some Efficient Solution Algorithms for Nonlinear Finite Element Analysis," International Conference on Nonlinear Mechanics, Trondheim, Norway, 1985.

12. Lo, K. H., Christensen, R. M. and Wu, E. M., "A High-Order Theory of Plate Deformation, Part 1: Homogeneous Plates," *Journal of Applied Mechanics*, Vol. 44, pp. 662-668, 1977.

13. Lo, K. H., Christensen, R. M. and Wu, E. M., "A High-Order Theory of Plate Deformation, Part 2: Laminated Plates," *Journal of Applied Mechanics*, Vol. 44, pp. 669-676, 1977.

14. Malvern, L. E., *Introduction to the Mechanics of a Continuous Medium*, Prentice-Hall, Inc., 1969.

15. Natsiavas, S., Babcock, C. D., and Knauss, W. G., *Postbuckling Delamination of a Stiffened Composite Panel Using Finite Element Methods*, NASA-CR-182803, August 1987.

16. Pagano, N. J., "Exact Solutions for Composites, Laminates in Cylindrical Bending," *Journal of Composite Materials*, Vol. 3, pp. 398-411, 1969.

17. Ramm, E. and Stegmuller, H., *The Displacement Finite Element Method in Nonlinear Buckling Analysis of Shells*, Springer, Berlin, Heidelberg, New York, 1982.

18. Reddy, J. N., "A Refined Nonlinear Theory of Plates With Transverse Shear Deformation," *International Journal Solids and Structures*, Vol. 20, pp. 293-301, 1984.

19. Reddy, J. N. and Chandrashekhara, K., *Nonlinear Analysis of Laminated Shells Including Transverse Shear Strains*, American Institute of Aeronautics and Astronautics, Inc., 1984.

20. Reddy, J. N. and Phan, N. D., "Analysis of Laminated Composite Plates Using A Higher-Order Shear Deformation Theory," *International Journal For Numerical Methods in Engineering*, Vol. 21, pp. 78-91, 1985.

21. Reddy, J. N., "A Generalization of Two-Dimensional Theories of Laminated Composite Plates," *Communication in Applied Numerical Methods*, Vol. 3, pp. 212-220, 1987.

22. Timoshenko, S. P. and Goodier, J. N., *Theory of Elasticity*, McGraw-Hill, Co., 1951.

23. Timoshenko, S. P. and Krieger, S. W., *Theory of Plates and Shells*, 2nd ed., McGraw-Hill, Co., 1959.

24. Tsai, S. W. and Pagano, N. J., "Invariant Properties of Composite Materials," Composite Materials Workshop, Tsai, S. W. et al., eds., Techonomic Publishing Co., Stanford, CT, pp. 233-253, 1968.

25. Vinson, J. R. and Sierakowski, R. L., *The Behavior of Structures Composed of Composite Materials*, Martinus Nighoff, 1987.

26. Yang, T. Y., *Finite Element Structural Analysis*, Prentice-Hall, Inc., 1986.

27. Zienkiewicz, O. C., Talor, R. L. and Too, J. M., "Reduced Integration Technique in General Analysis of Plates and Shells," *International Journal for Numerical Methods in Engineering*, Vol. 3, pp. 575-586, 1971.

INITIAL DISTRIBUTION LIST

		No. of Copies
1.	Defense Technical Information Center Cameron Station Alexandria, VA 22304-6145	2
2.	Library, Code 52 Naval Postgraduate School Monterey, CA 93943-5002	2
3.	Superintendent Naval Postgraduate School Chairman, Code AA Department of Aeronautics and Astronautics Monterey, CA 93943	1
4.	Superintendent Naval Postgraduate School Attn: Dr. Ramesh Kolar Code AA/Kj Monterey, CA 93943	6
5.	Dr. Rembert M. Jones Code 1823 David Taylor Research Center Bethesda, Maryland 20084	1
6.	Dr. Raymond Kvaternik Rotorcraft Structural Dynamics NASA Langley Research Center Hampton, VA 23665	1
7.	Captain Alon Yair Yerushalaim St. 44/B Apartment #5 BAT-YAM 59392 ISRAEL	2